JPRS L/10189

15 December 1981

USSR Report

PHYSICS AND MATHEMATICS

(FOUO 11/81)

FBIS FOREIGN BROADCAST INFORMATION SERVICE

NOTE

JPRS publications contain information primarily from foreign newspapers, periodicals and books, but also from news agency transmissions and broadcasts. Materials from foreign-language sources are translated; those from English-language sources are transcribed or reprinted, with the original phrasing and other characteristics retained.

Headlines, editorial reports, and material enclosed in brackets [] are supplied by JPRS. Processing indicators such as [Text] or [Excerpt] in the first line of each item, or following the last line of a brief, indicate how the original information was processed. Where no processing indicator is given, the information was summarized or extracted.

Unfamiliar names rendered phonetically or transliterated are enclosed in parentheses. Words or names preceded by a question mark and enclosed in parentheses were not clear in the original but have been supplied as appropriate in context. Other unattributed parenthetical notes within the body of an item originate with the source. Times within items are as given by source.

The contents of this publication in no way represent the policies, views or attitudes of the U.S. Government.

APPROVED FOR RELEASE: 2007/02/09: CIA-RDP82-00850R000400080043-2

JPRS L/10189

15 December 1981

USSR REPORT

PHYSICS AND MATHEMATICS

(FOUO 11/81)

CONTENTS

FLUID DYNAMICS

UDC 532.526.3

SYNTHESIZING METHOD OF CALCULATING PLANAR BOUNDARY LAYER IN WEAK POLYMER SOLUTIONS WITH LAMINAR, TRANSITIONAL AND TURBULENT FLOW ZONES

Moscow IZVESTIYA AKADEMII NAUK SSSR: MEKHANIKA ZHIDKOSTI I GAZA in Russian No 3, May-Jun 77 (manuscript received 10 Jun 76) pp 42-48

[Article by V. V. Droblenkov and G. I. Kanevskiy, Leningrad]

[Text] Investigation of the influence of small polymer additives on flow characteristics of viscous fluid is currently one of the most promising areas of research on friction drag reduction. One of the interesting problems here is the study of the influence that small polymer additives have on characteristics of the transition region of flow in the boundary layer, as well as on friction drag in the case of laminar, turbulent and transitional sections in the boundary layer. This article gives a possible method of calculating the planar boundary layer and friction drag for the case of motion of a solid in weak polymer solutions with constant concentration with consideration of the change in flow conditions in the layer, based on the use of integral relations. Problems associated with development of the boundary layer on the body as the polymer is fed in, and problems involving the influence of degradation or destruction of the polymer in the solution are not considered.

1. The laminar boundary layer is calculated by Pohlhausen's method with approximation of the velocity profile by a sixth-degree polynomial [Ref. 1], assuming that small polymer additives have practically no effect on its development. This assumption is confirmed by data of experiments done in tubes [Ref. 2]. In calculating the laminar boundary layer, the equation of momenta is integrated, the initial data being determined from the exact solution for the nieghborhood of the critical forebody point [Ref. 3].

The point of onset of laminar-to-turbulent transition is taken as the point of beginning of break-up of the laminar velocity profile, corresponding to the region of inception of turbulent spots. The point of loss of stability and the further development of perturbations beyond this point are determined by methods of linear stability theory. It is assumed that adding trace amounts of polymers to the flow has no effect on the position of the point of loss of stability nor on the development of small perturbations in the laminar boundary layer. This assumption is confirmed by the results of calculations of stability and development of

perturbations in a laminar boundary layer with trace polymer additives [Ref. 4]. The weak influence of polymer additives on development of perturbations in a laminar boundary layer means that the beginning point of transition can be taken as independent of the presence of polymer additives in the flow, which is confirmed by results of measurements in tubes and flat channels [Ref. 5].

In such assumptions, the following relation can be used to determine the point of loss of stability:

(1.1) $\mathrm{Re}_0^* = 4084 + 4000 \,\mathrm{th}\,[0.359(\lambda - 4.3)]$

Here Re_δ^* is the Reynolds number of loss of stability calculated with respect to thickness of displacement δ^* and velocity on the outer surface of the boundary layer U_δ, and λ is Pohlhausen's form factor. Formula (1.1) is derived by approximating the results of calculations of Re_δ^* with respect to linear stability theory.

Immediately beyond the point of loss of stability there is a build-up of the amplitudes of pulsation velocities with consideration of the existing distribution of pressures over the body [Ref. 3]

(1.2) $$\ln \frac{A}{A_0} = \int_{\mathrm{Re}_0^*}^{\mathrm{Re}^*} f(c_i, \mathrm{Re}^*, \lambda)\, d\,\mathrm{Re}^*$$

where Re* is the value of the Reynolds number at the given point, A is the amplitude of velocity pulsations at the same point, A_0 is the same quantity at the point of loss of stability, c_i is the rate of build-up of perturbations. The value of the integral in relation (1.2) is determined by using dependences $\ln (A/A_0)$ calculated from linear stability theory for constant values of λ, which can be approximated by the following relations:

(1.3) $$\ln \frac{A}{A_0} = a + b\,\mathrm{Re}^* + c\,\mathrm{Re}^{*2} \quad (\mathrm{Re}_0^* < \mathrm{Re}^* < \mathrm{Re}_1^*)$$

$$\ln \frac{A}{A_0} = \left(\ln \frac{A}{A_0}\right)_1 + e(\mathrm{Re}^* - \mathrm{Re}_1^*) \quad (\mathrm{Re}^* \geqslant \mathrm{Re}_1^*)$$

$$e = 0.00664 + 0.00424 \,\mathrm{th}\,[-0.41(1.5+\lambda)]$$

$$c = \left[e(\mathrm{Re}_1^* - \mathrm{Re}_0^*) - \left(\ln \frac{A}{A_0}\right)_1\right](\mathrm{Re}_1^* - \mathrm{Re}_0^*)^{-2}$$

$$b = e - 2c\,\mathrm{Re}_1^*, \quad a = -b\,\mathrm{Re}_0^* - c\,\mathrm{Re}_0^{*2}$$

$$\mathrm{Re}_1^* = 5000 + 3287 \,\mathrm{arc\,tg}\,(\lambda - 2.6) \quad (\lambda \leqslant 0)$$

$$\mathrm{Re}_1^* = 5000 + 4580 \,\mathrm{th}\,[0.506(\lambda - 2.6)] \quad (\lambda > 0)$$

$$\left(\ln \frac{A}{A_0}\right)_1 = 3.56 + 2.36 \,\mathrm{th}\,[0.458(\lambda - 2.6)]$$

It is assumed in the calculation that the point of onset of the laminar-to-turbulent transition is situated where the quantity $\ln (A/A_0)$ reaches a critical value defined by the formula

(1.4) $$\left(\ln \frac{A}{A_0}\right)_0 = 2.1 - 3.6 \ln e$$

Relation (1.4) is obtained on the basis of analysis of experimental data on the laminar-to-turbulent transition and is valid in the range of variation of the degree of turbulence of the external flow ε from 0.02 to 1.8%. The value of ε in formula (1.4) is in percent.

The influence of small polymer additives on characteristics of the turbulent boundary layer can be accounted for either by using rheological relations that describe the connection between the stress tensor and the strain-rate tensor in polymer flows, or by using semi-empirical methods in which the influence of polymer additives is accounted for by the change in universal turbulence constants. We will use the second approach, which was demonstrated in Ref. 6, 7 to be promising for calculating the characteristics of turbulent shear flows of weak polymer solutions.

By analogy with the description of the averaged velocity profile in pipe flow of weak polymer solutions, we propose using a logarithmic velocity profile with Cowles parameter and an additive constant B that is a function of the parameters of the dissolved polymer and the flow parameters

$$\frac{u}{v^*}=\frac{1}{\varkappa}\ln\frac{yv^*}{\nu}+\frac{\Pi}{\varkappa}\left(1-\cos\frac{\pi y}{\delta}\right)+B \tag{1.5}$$

In accordance with Meyer correlation [Ref. 8] it is assumed that the universal turbulence constant $\varkappa$ in weak polymer solutions does not change value, and is taken as equal to $\varkappa = 0.4$, and the parameter B is represented as follows:

$$B=B_0+\Delta B,\quad \Delta B=0,\quad v^*<v_0^*;\quad \Delta B=\alpha\lg\frac{v^*}{v_0^*},\quad v^*\geqslant v_0^* \tag{1.6}$$

Here y is the transverse coordinate, v* is dynamic velocity, Π is the Cowles parameter, δ is the thickness of the boundary layer, B_0 is a universal constant that retains its usual value $B_0 = 5.2$, α is a parameter that accounts for the properties of the dissolved polymer and its concentration in the solution, v_0^* is the value of dynamic velocity corresponding to the beginning of development of the Thoms effect. On the basis of experimental data it is assumed that the value of v_0^* is determined chiefly by the kind of dissolved polymer and its molecular weight. The numerical values of α and v_0^* are found on the basis of analyzing experimental data on flows of polymer solutions in tubes [Ref. 6-8] with consideration of the kind of polymer and its concentration in solution.

The characteristics of the turbulent boundary layer are calculated by the method of Ref. 9. In this calculation, the following are used: the equation of momenta, the equation of mass capture and the law of friction on the wall as found from relation (1.5) at $y = \delta$.

In determining the averaged velocity profile, the integral characteristics and the coefficient of local friction in the boundary layer in the region of laminar-to-turbulent transition, starting from the beginning point of the transition right up to the region of a completely developed turbulent boundary layer, the following assumptions are used that are based on analysis of experimental data. The region of inception of turbulent spots (beginning point of transition) coincides with the virtual beginning of the turbulent boundary layer. The thickness of loss of momentum of the laminar boundary layer calculated from the forebody critical point

coincides with the thickness of loss of momentum of the turbulent boundary layer reckoned from its virtual onset at a value of the intermittence coefficient γ equal to 0.5. Distribution of the coefficient of intermittence lengthwise of the transition region conforms to normal gaussian distribution.

Analysis of experimental data, and taking the transition layer as one in which the laminar velocity profile at a given point exists for a time interval proportional to $1-\gamma$, while the turbulent velocity profile exists for a time proportional to γ, enables us to represent the velocity in the transition region in the form [Ref. 10]

$$u(y)=(1-\gamma)u_L(y)+\gamma u_T(y) \tag{1.7}$$

Here $u_L(y)$ is the velocity profile in the laminar boundary layer reckoned from the forebody critical point, $u_T(y)$ is the velocity profile in the turbulent boundary layer reckoned from its virtual onset, and defined by relations (1.5) and (1.6).

The values of the intermittence coefficient at each point along the length of the transitional region that are necessary for calculations by formula (1.7) are determined from the condition of equality of the intermittence coefficient to 0.5 at the point where the thicknesses of loss of momentum of laminar and turbulent boundary layers coincide, and equality of the entire extent of the transition region to four standard deviations for gaussian normal distribution.

2. This method was used to do systematic calculations of boundary layer characteristics on a flat plate and wing sections over a wide range of Reynolds numbers and degrees of turbulence of the outer flow. Comparison of the results of calculations done in application to an ordinary liquid with experimental data of Ref. 10-12 shows satisfactory agreement [Ref. 13].

To analyze the influence of small polymer additives on the characteristics of flow in the transition zone, boundary layer calculations were done on a flat plate. The computations were done at Reynolds number Re calculated with respect to plate length L and plate velocity U_0 equal to $Re = 5\cdot10^6$, degree of free turbulence $\varepsilon = 0.5\%$, and $v_\infty^*/U_0 = 0.01$. The results of calculations of the coefficient of local friction c_f, dimensionless thickness of displacement δ^*/L and dimensionless thickness of loss of momentum δ^{**}/L as a function of dimensionless longitudinal coordinate $X = x/L$ are shown on Fig. 1. Curves 1 correspond to a value of $\alpha = 0$ (ordinary liquid), curves 2 and 3 correspond to values of $\alpha = 10$ and 20. These calculated parameters correspond approximately to motion in Polyox WSR-301™ ($v_\infty^* \sim 0.023$ m/s) with concentration $C \cong 0$, 10 and 30 ppm with velocity $U_0 = 2.3$ m/s. The arrows indicate the points of beginning and end of the laminar-to-turbulent transition on Fig. 1.

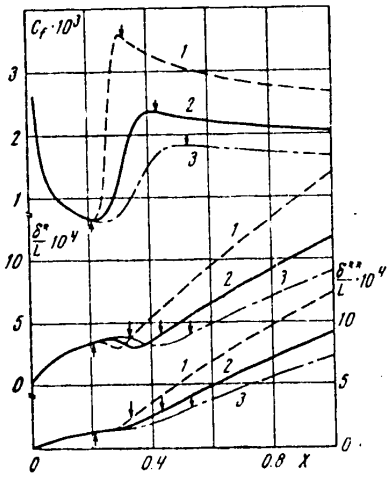

Fig. 1

Calculations show an appreciable increase in the length of the transition region when polymer additives are introduced into the flow. Their influence leads to a

reduction of the maximum value of the coefficient of local friction in the transitional flow region, and to downstream displacement of this maximum. Due to the influence of polymer additives, the position of the minimum thickness of displacement is shifted downstream, and the quantity δ^* decreases in the region of the developed turbulent layer. The thickness of loss of momentum δ^{**} under the effect of polymer additives decreases everywhere, beginning from the point of onset of the transition.

The results of calculations of the friction drag coefficient of a plate assuming purely turbulent flow at $\alpha = 10$, $v\delta/U_0 = 0.01$, $L = 0.9144$ m, are compared with data of experiments with towing of a plate in a solution of Polyox WSR-301™ at concentration of $C = 15$ ppm and plate length of $L = 0.9144$ m [Ref. 2] on Fig. 2. Here

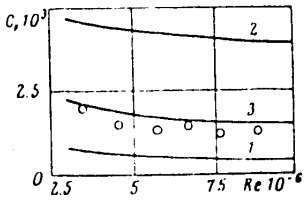

Fig. 2

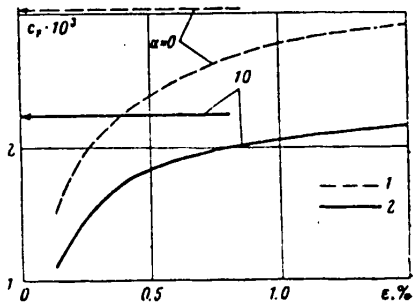

Fig. 3

curve 1 corresponds to laminar flow around the plate, curve 2 corresponds to turbulent flow of ordinary liquid, and curve 3 corresponds to turbulent flow of polymer solution. The results of the calculations are in satisfactory quantative and qualitative agreement with experimental data.

The influence of degree of turbulence on the coefficient of friction drag of the plate C_F when it is moving in a weak polymer solution (Polyox WSR-301™, $C \cong 10$ ppm) at $Re = 5 \cdot 10^6$ is illustrated by Fig. 3. Line 1 corresponds to flow of an ordinary liquid, and line 2 corresponds to flow of polymer solution. The arrows indicate friction drag in the case of purely turbulent flow. It can be seen that as the degree of turbulence increases, friction drag rises both for the case of motion in solvent and with motion in a polymer solution. However, the relative reduction of friction drag of a flat plate $\Delta C_F/C_{F_0}$ due to adding trace amounts of polymer to the flow changes weakly with a change in the degree of turbulence, and in the given case amounts to 25-28% (here C_{F_0} is the friction drag coefficient with motion in solvent, and ΔC_F is the absolute value of change in the friction drag coefficient).

The results of investigation of the influence of Reynolds number on friction drag of a plate in a flow of weak polymer solution are shown on Fig. 4. Curve 1 corresponds to purely turbulent flow of an ordinary viscous fluid around the plate, curve 2 corresponds to laminar flow around the plate, and curve 3 corresponds to flow of ordinary fluid around a plate at degree of free turbulence $\varepsilon = 0.5\%$. Curves 4-7 correspond to results of calculations of flow of a polymer solution around a plate at $\alpha = 10$ and $v^* = 0.023$ m/s, curves 4 and 5 being plotted on the assumption

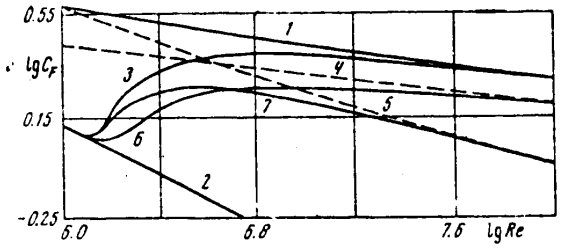

Fig. 4

of a purely turbulent flow mode in the boundary layer, while curves 6 and 7 were plotted in calculations at $\varepsilon = 0.5\%$.

In doing the calculations shown by curves 4 and 6, the Reynolds number was varied by changing the length of the plate at constant flow velocity of $U_0 = 2.3$ m/s ($v_\delta^* / U_0 = 0.01$). Curves 5 and 7 are the results of calculations as the Reynolds number is changed by varying the velocity of flow around the plate at a constant length of $L = 3$ m. The results confirm the fact that with flow of a polymer solution of the same concentration around the plate, the influence of the Reynolds number on C_F differs depending on whether it is varied by changing the length or changing the velocity.

When there are laminar and transitional sections present in the boundary layer on the plate, the curves for C_F as a function of Re deviate from the curve of laminar friction drag at a constant Reynolds number for the given degree of turbulence independent of the parameters of the dissolved polymer, and these curves asymptotically approach the corresponding dependence for the purely turbulent flow mode (curves 3, 6, 7 on Fig. 4).

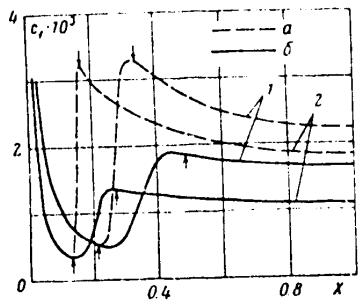

Fig. 5

Fig. 5 shows the results of calculations of the coefficient of local friction for a boundary layer on a 12% Zhukovskiy section at $Re = 5 \cdot 10^6$ and $2 \cdot 10^7$ and $\alpha = 0$ and 10. The calculations were done for a section with length $L = 2$ m. For the chosen Reynolds numbers the ratio v_δ^*/U_0 when using Polyox WSR-301™ ($v_\delta^* = 0.023$ m/s) is 0.00586 and 0.001465 respectively. The calculations used the experimentally measured velocity distribution on the outside surface of the boundary layer of the Zhukovskiy section at zero angle of attack [Ref. 12]. Curves *a* refer to flow of an ordinary fluid around the foil, while curves b are for flow of a polymer solution. Curves 1 correspond to a Reynolds number of $5 \cdot 10^6$, and curves 2 refer to a Reynolds number of $2 \cdot 10^7$. The arrows indicate the boundaries of transitional flow zones. Just as in the case of zero-gradient flow, the addition of trace amounts of polymer causes an appreciable increase in the length of the transitional flow region in the boundary layer.

	Re	Mixed boundary layer, $\varepsilon = 0.5\%$		Turbulent boundary layer	
		$5 \cdot 10^6$	$2 \cdot 10^7$	$5 \cdot 10^6$	$2 \cdot 10^7$
I		25.2	40.5	26.5	41.9
II		32.3	44.8	32.8	45.3

The values of relative drag reduction $\Delta C_F/C_{F_0}$ (in percent) for the Zhukovskiy section are compared with results of calculations for a flat plate in the Table. Here I is the plate and II is the 12% Zhukovskiy section.

The data of the Table show that the relative reduction of friction drag with introduction of polymer additives into the flow is somewhat greater on the foil than on the plate, other things being equal.

Just as in the case of zero-gradient flow, the presence of a laminar-to-turbulent transition on the Zhukovskiy section has little effect on the relative reduction of friction drag due to adding trace amounts of polymers to the flow.

REFERENCES

1. Schlichting, H., Ulrich, A., "Zur Berechnung des Umschlages laminar-turbulent", J. DTSCH. LUFTFAHRTFORSCHUNG, 1942.

2. "Gidrobionika v sudostroyenii" [Hydrobionics in Shipbuilding], TsNII TEIS, 1970.

3. Schlichting, H., "Teoriya pogranichnogo sloya" [Boundary Layer Theory], Moscow, "Nauka", 1969.

4. Droblenkov, V. V. Kanevskiy, G. I., "Laminar Boundary Layer and its Stability in Weak Polymer Solutions", IZVESTIYA AKADEMII NAUK SSSR: MEKHANIKA ZHIDKOSTI I GAZA, No 4, 1974.

5. Khabakhpasheva, Ye. M., Perepelitsa, B. V., "Fields of Velocities and Turbulent Pulsations When Trace Amounts of High-Polymer Substances are Added to Water", INZHENERNO-FIZICHESKIY ZHURNAL, Vol 14, No 4, 1968.

6. Vasetskaya, N. G., Ioselevich, V. A., "Constructing a Semiempirical Theory of Turbulence of Weak Polymer Solutions", IZVESTIYA AKADEMII NAUK SSSR: MEKHANIKA ZHIDKOSTI I GAZA, No 2, 1970.

7. Ioselevich, V. A., Pilipenko, V. N., "Turbulent Flow of Fluid With Polymer Additives in Boundary Layer With Longitudinal Pressure Gradient", DOKLADY AKADEMII NAUK SSSR, Vol 213, No 4, 1973.

8. Meyer, W. A., "A Correlation of Frictional Characteristics for Turbulent Flow of Dilute Viscoelastic Non-Newtonian Fluids in Pipes", A. I. Ch. E. JOURNAL, Vol 12, No 3, 1966.

9. Levkovich, Hodley, Horlock, Perkins, "Family of Integral Methods of Calculating a Turbulent Boundary Layer", RAKETNAYA TEKHNIKA I KOSMONAVTIKA, Vol 8, No 1, 1970.

10. Dhawan, S., Narasima, R., "Some Properties of Boundary Layer Flow During the Transition From Laminar to Turbulent Motion", J. FLUID MECH., Vol 3, No 4, 1958.

11. Schubauer, G. B., Klebanoff, P. S., "Contributions to the Mechanics of Boundary-Layer Transition", NAT. ADVIS. COMM. AERONAUT., Rept. No 1289, 1956.

12. Preston, J. H., Sweeting, N. E., "The Experimental Determination of the Boundary Layer and Wake Characteristics of a Simple Joukowski Aerofoil With Particular Reference to the Trailing Edge Region", AERONAUT. RES. COUNCIL, REP. AND MEM., No 1998, 1943.

13. Droblenkov, V. V., Kanevskiy, G. I., "Metod rascheta polozheniya i integral'nykh kharakteristik perekhodnogo pogranichnogo sloya" [Method of Calculating Position and Integral Characteristics of Transition Boundary Layer], manuscript deposited in All-Union Institute of Scientific and Technical Information No 1795-94 from 1 Jul 74.

6610
CSO: 8144/0203-B

UDC 532.526.2

LAMINAR BOUNDARY LAYER AND ITS STABILITY IN WEAK POLYMER SOLUTIONS

Moscow IZVESTIYA AKADEMII NAUK SSSR: MEKHANIKA ZHIDKOSTI I GAZA in Russian No 4, Jul-Aug 74 (manuscript received 1 Jun 73) pp 156-158

[Article by V. V. Droblenkov and G. I. Kanevskiy, Leningrad]

[Text] The article gives the results of a study of equations of a laminar boundary layer and its stability in weak polymer solutions. The mathematical model that describes the properties of flows of polymer solutions is a rheological model with consideration of the temporal relation between the stress tensor and the strain-rate tensor [Ref. 1]. Analysis of these equations shows that the relaxation properties of a liquid influence flow stability in large measure. The calculations show an increase in velocity profile stability in the boundary layer, and also a change in the nature of distribution of Reynolds stresses with consideration of the relaxation properties of the liquid.

With regard to relaxation properties, the equations of motion of a viscous incompressible fluid disregarding mass forces take the form [Ref. 1]

$$\frac{d\bar{V}}{dT} = -\frac{1}{\rho}\operatorname{grad} P + \nu\Delta\bar{V} + \frac{k}{\rho}\frac{d}{dT}(\Delta\bar{V}), \quad \operatorname{div}\bar{V} = 0 \tag{1}$$

Here T is time, k is relaxation viscosity, and the other symbols are conventional.

Let us assume that when trace amounts of polymers are added to the liquid, the basic concepts of boundary layer theory remain valid. Then the boundary layer thickness δ can be estimated as follows: $\delta \propto \sqrt{\nu}$ and $\delta \ll L$, where L is a characteristic linear dimension of the body.

Let us carry out the usual estimates in equations of motion (1) for the case of flow in a flat boundary layer [Ref. 2]. The ratio of relaxation terms to inertial terms will be characterized by the relaxation number $Rx = k/\rho L^2$.

Estimates show that the magnitude of terms that depend on relaxation properties of a liquid has the same order as the inertial terms and the terms that depend on ordinary viscosity only under condition

$$k/\rho \sim \delta^2 \tag{2}$$

In this case, we get the following system of boundary layer equations in dimensional variables:

$$(3)\qquad \frac{\partial U}{\partial T}+U\frac{\partial U}{\partial X}+V\frac{\partial U}{\partial Y}=-\frac{1}{\rho}\frac{\partial P}{\partial X}+\nu\frac{\partial^2 U}{\partial Y^2}+\frac{k}{\rho}\frac{d}{dT}\left(\frac{\partial^2 U}{\partial Y^2}\right),\quad \frac{\partial P}{\partial Y}=0$$

If the relaxation number Rx has order $(\delta/L)^n$ at $n>2$, the terms that account for the relaxation properties of the liquid can be disregarded as compared with the inertial terms and terms that depend on ordinary viscosity, and the boundary layer equations take their usual form. In the case where the relaxation number has order $(\delta/L)^n$ at $n<2$, we can disregard all terms in the boundary layer equation other than the term that contains pressure, and the terms that account for the relaxation properties of the liquid. The equations of the boundary layer in dimensional form then are written as follows:

$$(4)\qquad -\frac{\partial P}{\partial X}+k\frac{d}{dT}\left(\frac{\partial^2 U}{\partial Y^2}\right)=0,\quad \frac{d}{dT}\left(\frac{\partial^2 V}{\partial Y^2}\right)=0$$

Introducing the stream function of the main flow $\theta=\theta(Y)$ and the stream function of perturbing motion $\phi(X, Y, T)$ in equations of motion (1), and using conventional methods and assumptions of the linear theory of hydrodynamic stability [Ref. 3], we get the stability equation with consideration of relaxation properties of the liquid

$$(5)\qquad \frac{\partial(\Delta\varphi)}{\partial T}+\frac{\partial\theta}{\partial Y}\frac{\partial(\Delta\varphi)}{\partial X}-\frac{\partial\varphi}{\partial X}\frac{\partial^3\theta}{\partial Y^3}=\nu(\Delta\Delta\varphi)+\frac{k}{\rho}\left[\frac{\partial(\Delta\Delta\varphi)}{\partial T}+\frac{\partial\theta}{\partial Y}\frac{\partial(\Delta\Delta\varphi)}{\partial X}-\right.$$
$$\left.-\frac{\partial\varphi}{\partial X}\frac{\partial^3\theta}{\partial Y^3}+\left(\frac{\partial^4\varphi}{\partial X^3\partial Y}+\frac{\partial^4\varphi}{\partial X\partial Y^3}\right)\frac{\partial^2\theta}{\partial Y^2}-\frac{\partial^2\varphi}{\partial X\partial Y}\frac{\partial^4\theta}{\partial Y^4}\right]$$

Equation (5) is linear relative to function $\phi(X, Y, Z)$, and its solution can be sought in the form

$$(6)\qquad \varphi(X, Y, T)=\Phi(Y)\exp[i(\alpha X-\beta T)]$$

Here $\Phi(Y)$ is the amplitude of the stream function of the perturbing motion, α is a real quantity associated with perturbation wavelength λ by the relation $\lambda=2\pi/\alpha$, β is a complex quantity $\beta=\beta_r+i\beta_i$.

Let us use the notation $\beta/\alpha=C$ and convert to dimensionless quantities, taking as the characteristic velocity that on the boundary layer surface U_1, and taking δ as the characteristic linear dimension. We write the stability equation in dimensionless form

$$(7)\qquad (u_1-c)\left(\frac{d^2f}{dy_1^2}-\alpha f\right)-\frac{d^2u_1}{dy_1^2}f=-\frac{i}{\alpha R_1}\left(\frac{d^4f}{dy_1^4}-2\alpha^2\frac{d^2f}{dy_1^2}+\alpha^4 f\right)+$$
$$+\frac{k}{i\delta^2}\left[(u_1-c)\left(\frac{d^4f}{dy_1^4}-2\alpha^2\frac{d^2f}{dy_1^2}+\alpha^4 f\right)+\frac{du_1}{dy_1}\frac{d^3f}{dy_1^3}-\right.$$
$$\left.-\left(\frac{d^3u_1}{dy_1^3}+\alpha^2\frac{du_1}{dy_1}\right)\frac{df}{dy_1}-\frac{d^4u_1}{dy_1^4}f\right]$$

$$u_1=U/U_1,\quad c=C/U_1,\quad y_1=Y/\delta,\quad R_1=U_1\delta/\nu,\quad \mathrm{Rx}_1=k/\rho\delta^2$$

Here $\alpha = \alpha\delta$ is the wave number, $f = \phi/U_1\delta$ is the dimensionless amplitude of the stream function. The order of terms that account for the relaxation properties of the liquid coincide with the order of terms that account for ordinary viscosity when

(8) $$k/\rho \sim \delta^2\delta/L$$

Comparison of conditions (2) and (8) shows that the stability of liquid motion is more sensitive to its relaxation properties. Analysis shows the feasibility of using conventional velocity profiles of principal motion to study the influence that small polymer additives have on the stability of a laminar boundary layer.

To integrate equation (7) with boundary conditions of non-penetration and sticking on the wall ($y_1 = 0$) and matching of the solution with the "inviscid" solution on the outer surface of the boundary layer ($y_1 = 1$)

(9) $$f = df/dy_1 = 0 \quad (y_1 = 0)$$

(10) $$\alpha f + \frac{df}{dy_1} = 0, \quad \alpha\frac{df}{dy_1} + \frac{d^2f}{dy_1^2} = 0 \quad (y_1 = 1)$$

a sweep method was used [Ref. 4].

An investigation was made of the stability of the Blasius velocity profile approximated by a sixth-degree Pohlhausen polynomial at $Rx_1 = 0$, 0.0001, 0.001.

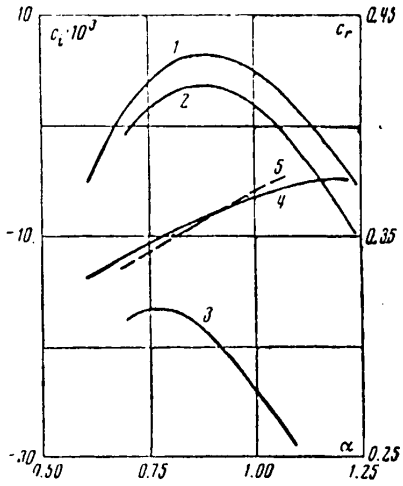

Fig. 1

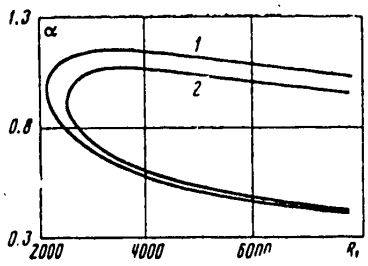

Fig. 2

The real and imaginary parts of the eigenvalues found in the calculations at a Reynolds number of $R_1 = 3100$ as a function of wave number are shown in Fig. 1. Curves 1-3 are dependences of the imaginary part of the eigenvalues (c_i) on wave number for Rx_1 equal to 0, 0.0001 and 0.001 respectively. Curves 4 and 5 correspond to the real part of the eigenvalues (c_r) at $Rx_1 = 0$ and $Rx_1 = 0.001$. The results show that the relaxation properties of the liquid have an insignificant effect on the rate of propagation of a perturbation (c_r) in the boundary layer, but appreciably reduce the rate of perturbation buildup (c_i).

Fig. 2 shows curves of neutral stability ($c_i = 0$) plotted from the results of calculations for values of $Rx_1 = 0$ (curve 1) and $Rx_1 = 0.0001$ (curve 2). The critical value of the Reynolds number corresponding to the point of loss of stability with transition from an ordinary viscous fluid to a fluid that has relaxation properties increases from $R_* = 2150$ to $R_* = 2520$ at a value of $Rx_1 = 0.0001$. This stability improvement is qualitatively confirmed by existing experimental data showing prolongation of the transition of the laminar flow mode to turbulent in weak polymer solutions [Ref. 5].

Our calculations show that the relaxation properties of a liquid have almost no influence on the distribution of rms values of pulsation velocities across the boundary layer, although they appreciably change the magnitude of Reynolds stresses.

REFERENCES

1. Pavlovskiy, V. A., "Theoretical Description of Weak Aqueous Polymer Solutions", DOKLADY AKADEMII NAUK SSSR, Vol 200, No 4, 1971.

2. Loytsyanskiy, L. G., "Mekhanika zhidkosti i gaza" [Mechanics of Liquid and Gas], Moscow, "Nauka", 1970.

3. Lin', Ts. Ts., "Teoriya gidrodinamicheskoy ustoychivosti" [Theory of Hydrodynamic Stability], Moscow, Izdateo'stvo inostrannoy literatury, 1958.

4. Sapozhnikov, V. A., Shtern, V. N., "Numerical Analysis of Stability of Plane Poiseuille Flow", ZHURNAL PRIKLADNOY MEKHANIKI I TEKHNICHESKOY FIZIKI, No 4, 1969.

5. White, V. D., McElligot, D. M., "Transition to Turbulence in Dilute Aqueous Solution of Polymer Mixture", TEORETICHESKIYE OSNOVY INZHENERNYKH RASCHETOV, No 3, 1970.

6610
CSO: 8144/0203-D

UDC 532.517.4

WALL TURBULENCE IN WEAK POLYMER SOLUTIONS

Moscow IZVESTIYA AKADEMII NAUK SSSR: MEKHANIKA ZHIDKOSTI I GAZA in Russian No 4, Jul-Aug 75 (manuscript received 13 Dec 74) pp 24-32

[Article by V. V. Droblenkov and L. S. Sitchenko, Leningrad]

[Text] An examination is made of problems of constructing a semiempirical method of determining the characteristics of wall turbulence, based on scaling theory and dimensional analysis, and application of the mixing-path hypothesis, and generalization of this method to the case of turbulent flow of weak polymer solutions close to smooth and rough surfaces.

1. Physical considerations that lead to formulation of a universal law of distribution of averaged velocity U close to a wall can be applied to the description of any single-point moments of the velocity field in this region, including for determination of the rms values of velocity pulsation components $\sqrt{\langle u_i^2\rangle}$ $(i = 1, 2, 3)$, Reynolds stresses $-\rho\langle u_1 u_2\rangle$ and correlation coefficient $K = -\langle u_1 u_2\rangle/\sqrt{\langle u_1^2\rangle\langle u_2^2\rangle}$ [Ref. 1]. Here the u_i are the components of pulsation velocity with respect to coordinate axes, subscript 1 corresponds to the longitudinal x-axis, subscript 2 corresponds to the transverse y-axis, and subscript 3 corresponds to the transversal z-axis.

All single-point moments within the limits of a layer with constant values of tangential stresses $\tau = \tau_0 = \text{const}$ may depend only on the transverse coordinate, the value of the tangential stress τ_0 at the wall, density ρ and the coefficient of kinematic viscosity ν, i. e. may be represented in the form of a product of some degree of dynamic velocity $v_* = \sqrt{\tau_0/\rho}$ multiplied by a universal function of dimensionless coordinate yv_*/ν that is unique to each of the moments and to given parameters of the polymer dissolved in the liquid

$$\sqrt{\langle u_i^2\rangle} = v_* f_i(y_*), \quad i=1, 2, 3; \quad -\langle u_1 u_2\rangle = v_*^2 f_4(y_*) \tag{1.1}$$

At sufficiently large values of y_*, the statistical state of turbulent pulsations should no longer depend on viscosity and the addition of polymers to the flow, and the functions $f_i(y_*)$ should approach certain constant values that are the same both for a flow of ordinary liquid and for a flow of weak polymer solutions:

$$f_i(\infty) = A_i, \quad i=1, 2, 3, 4 \tag{1.2}$$

To determine the form of functions $f_i(y_*)$ it is convenient to use the mixing-path hypothesis, according to which

$$(1.3)\qquad \sqrt{\overline{\langle u_i^2\rangle}}=l_i\frac{\partial U}{\partial y},\quad i=1,2,3;\quad -\langle u_1u_2\rangle=l^2\left(\frac{\partial U}{\partial y}\right)^2=l_1l_2K\left(\frac{\partial U}{\partial y}\right)^2$$

Here l and l_i are mixing lengths analogous to integral scales of turbulence. By introducing dimensionless velocities and using dimensionless coordinate y_*, we can write relations (1.3) in the form

$$(1.4)\qquad \begin{aligned}&\sqrt{\overline{\langle u_i^2\rangle}}=v_*l_{i*}\partial U_*/\partial y_*,\quad i=1,2,3\\ &-\langle u_1u_2\rangle=v_*^2l_*^2(\partial U_*/\partial y_*)^2=v_*^2l_{1*}l_{2*}K(\partial U_*/\partial y_*)^2\\ &l_{i*}=l_iv_*/\nu,\quad l_*=lv_*/\nu,\quad U_*=U/v_*\end{aligned}$$

Expressions (1.1) and (1.4) imply that

$$(1.5)\qquad f_i(y_*)=l_{i*}\partial U_*/\partial y_*\quad i=1,2,3;\quad f_4(y_*)=l_*^2(\partial U_*/\partial y_*)^2=l_{1*}l_{2*}K(\partial U_*/\partial y_*)^2$$

The value of l_* in a constant-stress layer can be determined from the formula [Ref. 2]

$$(1.6)\qquad l_*=\varkappa y_*[1-\exp(-y_*/a)]$$

In the case of an ordinary viscous liquid $\kappa = 0.4$, $a = 26$-27. Corresponding to expression (1.6) is the following value of the dimensionless derivative of averaged velocity:

$$(1.7)\qquad \frac{\partial U_*}{\partial y_*}=\frac{2}{1+\sqrt{1+4l_*^2}}=\frac{2}{1+\sqrt{1+4\varkappa^2y_*^2[1-\exp(-y_*/a)]^2}}$$

Relations (1.6) and (1.7) define the Reynolds stresses and the averaged velocity profile throughout the constant-stress layer, including the viscous sublayer, the buffer region and the zone of logarithmic velocity profile. The value of coefficient A_4 is identical to unity.

Dimensionless mixing lengths l_{i*} that determine the behavior of pulsation velocities in the wall region may be represented in a form analogous to (1.6)

$$(1.8)\qquad l_{i*}=A_i\varkappa y_*[1-B_i\exp(-C_iy_*/a)]$$

Coefficients A_i are determined from the rms values of pulsation velocity components in the region of the logarithmic velocity profile, where $y_*/a\gg 1$, and consequently $\exp(-y_*/a)\approx 0$. Viscous tangential stresses in this zone can be disregarded compared with turbulent stresses; then $\partial U_*/\partial y_*\cong 1/\kappa y_*$. With consideration of these arguments

$$(1.9)\qquad l_{i*}\approx A_i\varkappa y_*,\quad \sqrt{\overline{\langle u_i^2\rangle}}\approx v_*A_i \text{ when } y_*/a\gg 1$$

Analysis of experiments enables us to determine the values of coefficients A_i

$$(1.10)\qquad A_1=2,\quad A_2=1.1,\quad A_3=1.5$$

Coefficients B_i and C_i determine the behavior of l_{i*} and $f_i(y_*)$ in direct proximity to the wall, i. e. at low values of y_*, and can be found from representation of the functions $f_i(y_*)$ as Taylor series with respect to y_* in the neighborhood of point $y_* = 0$ and satisfaction of boundary conditions at $y_* = 0$

$$\left.\begin{aligned} f_3(y_*) &= a_3 y_* + b_3 y_*^2 + c_3 y_*^3 + \dots \\ f_2(y_*) &= b_2 y_*^2 + c_2 y_*^3 + \dots \\ f_1(y_*) &= a_1 y_* + b_1 y_*^2 + c_1 y_*^4 + \dots \end{aligned}\right\} \quad y_* \to 0 \tag{1.11}$$

At the same time, representation of l_{i*} in form (1.8), expansion of exponential function $\exp(-C\, y_*/\alpha)$ in a series as $y_* \to 0$ and the condition $\partial U_*/\partial y_* \cong 1$ implied by expression (1.7) as $y_* \to 0$ lead to the relation

$$f_1(y_*) = A_1 \varkappa (1 - B_1) y_* + A_1 B_1 C_1 \varkappa y_*^2/\alpha + \dots \tag{1.12}$$

Coefficients B_i and C_i are found from the condition of coincidence of values of $\sqrt{\langle u_i^2 \rangle}$ defined by relation (1.12) at $\kappa = 0.4$ and $\alpha = 26$, and experimental data on distribution of components of pulsation velocity within the confines of the viscous sublayer

$$B_1 = 0.625, \quad B_2 = 1, \quad B_3 = 0.99, \quad C_1 = 1, \quad C_2 = 0.5, \quad C_3 = 0.7 \tag{1.13}$$

Corresponding to these values of B_i and C_i are the following values of the first coefficients in series (1.11):

$$a_1 = 0.3, \quad b_1 = 0.01922, \quad b_2 = 0.00846, \quad a_3 = 0.006, \quad b_3 = 0.016 \tag{1.14}$$

Expressions (1.1), (1.4), (1.5), (1.7) and (1.8) at values of $\kappa = 0.4$ and $\alpha = 26$ and coefficients A_i, B_i, C_i defined by relations (1.10) and (1.13) completely determine the rms values of the components of pulsation velocity in the viscous sublayer, the buffer region and the zone of logarithmic velocity profile for flows of ordinary viscous liquid in a boundary layer, circular pipe and flat channel.

On Fig. 1, the results of calculations of functions f_i ($i = 1, 2, 3$) at $\kappa = 0.4$ and $\alpha = 26$ are compared with experimental data obtained in a circular pipe [Ref. 3] and in a flat channel [Ref. 4]. Curves 1, 2, 3 correspond to calculated values of f_i for a constant-stress layer. Points 4, 5, 6 designate experimental data [Ref. 3] at a Reynolds number of $Re = 5 \cdot 10^5$, 7, 8--at $Re = 5 \cdot 10^6$, 9, 10--data of Ref. 4. The Reynolds number $Re = U_0 d/\nu$ was calculated with respect to pipe diameter d and velocity on its axis U_0. Points 4, 7, 9 correspond to values of f_1, 5, 8, 9--to f_2, and points 6--to f_3. Agreement of calculated and experimental data can be taken as completely satisfactory.

2. The extent of the region in which tangential stresses can be considered constant and equal to their value at the wall is considerably dependent on the type of flow, and amounts to 10-15% of the characteristic transverse dimension of the turbulent flow, the boundary layer thickness δ, half-width of the channel b, or pipe radius r. In the external part of the boundary layer, or in the paraxial region of the flow in a pipe or channel, the pulsation characteristics are considerably influenced by the nature of the distribution of tangential stresses τ. Here the defining transverse scale is not the dimensionless coordinate y_*, but rather the ratio of

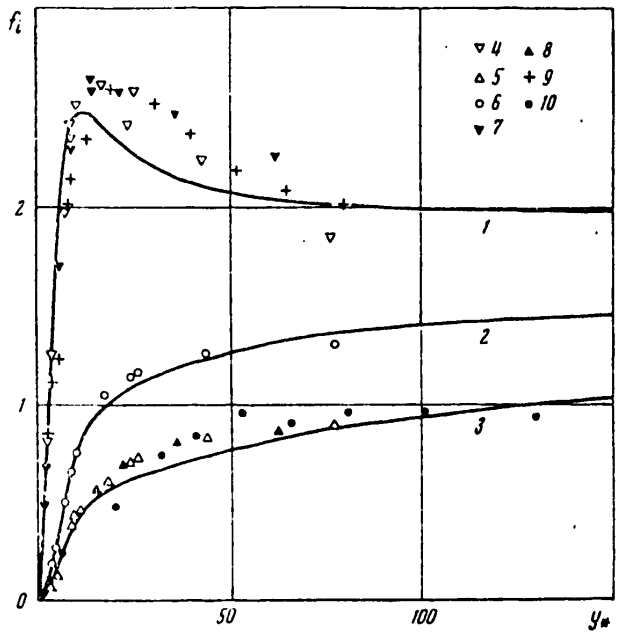

Fig. 1

the transverse coordinate y to the characteristic transverse dimension of the flow $\eta = y/b$ for a channel, $\eta = y/r$ for a pipe, and $\eta_1 = y/\delta$ for a boundary layer. The dimensionless derivative of the averaged velocity profile in the general case can be written as follows [Ref. 5]:

$$\frac{\partial U_*}{\partial y_*} = \frac{2\tau_*}{1+\sqrt{1+4l_*^2\tau_*}}, \qquad \tau_* = \frac{\tau}{\tau_0} \tag{2.1}$$

In the case of flow in a straight circular pipe or flat channel

$$\tau_* = 1-\eta \tag{2.2}$$

It is impossible to get the exact form of function $\tau_*(y)$ for a boundary layer. To describe the distribution of tangentional stresses across the turbulent boundary layer, we can use their approximation in the form of a polynomial with respect to powers of η_1 in which the coefficients are determined from the boundary conditions on the wall and on the outside boundary of the layer [Ref. 5]. In the case of an arbitrary longitudinal gradient of pressure p when two conditions are used on the wall and two on the outer boundary of the layer, the form of function $\tau_*(y)$ is determined by the relation

$$\tau_* = 1-3\eta_1^2+2\eta_1^3+\Phi\eta_1(1-\eta_1)^2 \tag{2.3}$$

Here $\Phi = \delta\partial p/\tau_0\partial x$ is a form factor that accounts for longitudinal pressure gradient and varies over a range of $-3 < \Phi < \infty$. The negative values of Φ correspond to

accelerated flow in the boundary layer, while positive values correspond to decelerated flow, and the value $\Phi = 0$ corresponds to a zero-gradient boundary layer.

In the outer part of the layer or the central region of flow in a pipe or channel, formula (1.6) for mixing-path length l_* becomes inapplicable. In these zones it is more correct to consider the mixing path approximately constant. According to the recommendations of Ref. 5,

(2.4) $l \approx 0.075\delta, \quad \eta_1 \to 1$

(2.5) $l \approx 0.14r, \quad l \approx 0.14b, \quad \eta \to 1$

in the case of a boundary layer and flow in a straight circular pipe and flat channel respectively. To retain the distribution of l_* in form (1.6) in the wall region and convert to expressions (2.4) or (2.5) in the external or paraxial part of the flow, it is convenient to use a modification of the interpolation formula proposed in Ref. 6. Then to describe l_* over the entire cross section of the flow, instead of (1.6) we can write

(2.6) $l_* = \varkappa y_* [1 - \exp(-y_*/a)] \exp(-D\eta_1)$

(2.7) $l_* = \varkappa y_* [1 - \exp(-y_*/a)] \exp(-E\eta)$

where $D = 1.65$ in the case of a boundary layer, which corresponds to the value $l_* = 0.0768\delta_*$ at $\eta_1 = 1$, $\delta_* = \delta v_*/\nu$; $E = 1.05$ in the case of flow in a circular pipe or flat channel, which assures a value of $l_* = 0.14r_*$ or $l_* = 0.14b_*$ at $\eta = 1$, $r_* = rv_*/\nu$; $b_* = bv_*/\nu$.

The rms values of pulsation velocities can be determined by using expressions (1.5), (2.1) and (2.2) or (2.3). In this connection, the formulas for mixing lengths l_{i*} derived for a constant-stress layer should be corrected analogously to the expression for l_*. A necessary auxiliary condition in constructing them is ensuring a correlation coefficient $K = 0$ on the outer surface of the boundary layer or on the axis of the pipe or channel. This condition is met by the expressions

(2.8) $l_{i*} = A_i \varkappa y_* [1 - B_i \exp(-C_i y_*/a)] \exp(-D_i \eta_1)/\sqrt{1-\eta_1}$

(2.9) $l_{i*} = A_i \varkappa y_* [1 - B_i \exp(-C_i y_*/a)] \exp(-E_i \eta)/\sqrt{1-\eta}$

Coefficients A_i, B_i, C_i retain the same values as in a constant-stress layer. Coefficients D_i and E_i were determined from the results of measurements of pulsation characteristics in the external part of the boundary layer and the paraxial region of flow in a pipe or channel:

(2.10) $D_1 = 2.6, \quad D_2 = 2.1, \quad D_3 = 2.4$

(2.11) $E_1 = 2.0, \quad E_2 = 1.5, \quad E_3 = 1.8$

Relations (1.5), (2.1), (2.3), (2.6), (2.8) at the values of coefficients (1.10), (1.13) and (2.10) define all three components of pulsation velocity in the boundary layer, while expressions (1.5), (2.1), (2.2), (2.7), (2.9) at the values of coefficients (1.10), (1.13) and (2.11) define the corresponding quantities for flow in a straight circular pipe or flat channel.

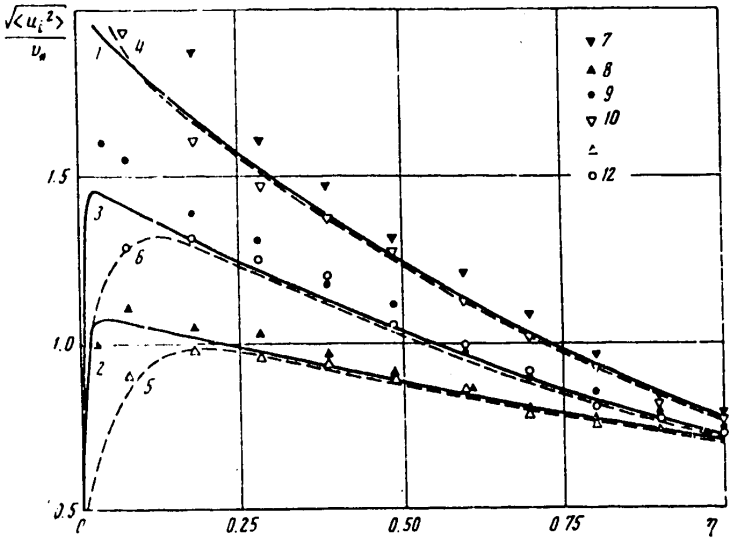

Fig. 2

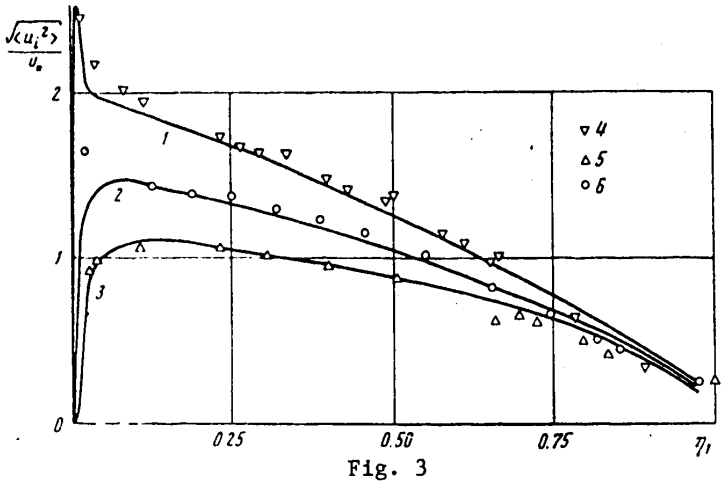

Fig. 3

Calculated and measured values of $\sqrt{\langle u_1^2\rangle}/v_*$ are compared on Fig. 2 for flow in a circular pipe, and on Fig. 3 for flow in a boundary layer on a flat plate. Solid curves 1, 2, 3 on Fig. 2 correspond to the calculated values of $\sqrt{\langle u_1^2\rangle}/v_*$ at $r_* = 8750$, and the broken curves 4, 5, 6--at $r_* = 1150$. Points 7, 8, 9 correspond to experimental data [Ref. 7] at $r_* = 8750$, while points 10, 11, 12 correspond to the data at $r_* = 1150$. Points 1, 4, 7, 10 correspond to values of $\sqrt{\langle u_1^2\rangle}/v_*$, points 2, 5, 8, 11--to values of $\sqrt{\langle u_2^2\rangle}/v_*$, and 3, 6, 9, 12--to $\sqrt{\langle u_3^2\rangle}/v_*$. On Fig. 3 the results of calculations of $\sqrt{\langle u_1\rangle}/v_*$ at $\delta_* = 2960$ and $\Phi = 0$ are shown by curves 1, 2, 3, while the corresponding experimental values obtained in Ref. 7 with measurements in a turbulent boundary layer of a flat plate at $\delta_* = 2960$ are shown by points

4, 5, 6. As can be seen from Fig. 2, 3, agreement between the calculated graphs and the experimental data is quite satisfactory.

The resultant relations can be considerably simplified in consideration of only the outer part of the flow in a boundary layer or the central region in a pipe or channel. In these cases we can disregard effects of molecular viscosity, which simplifies formula (2.1), that can then be written as

$$\partial U_*/\partial y_* = \sqrt{\tau_*}/l_* \tag{2.12}$$

At $y_*/a \gg 1$, formulas (2.6)-(2.9) are considerably simplified and transformed to

$$l_* = \kappa y_* \exp(-D\eta_1); \quad l_{i*} = A_i \kappa y_* \exp(-D_i\eta_1)/\sqrt{1-\eta_1} \tag{2.13}$$

$$l_* = \kappa y_* \exp(-E\eta), \quad l_{i*} = A_i \kappa y_* \exp(-E_i\eta)/\sqrt{1-\eta} \tag{2.14}$$

Relations (2.12)-(2.14) with consideration of distribution of τ_* in form (2.2) or (2.3) enable determination of the rms values of components of pulsation velocity in the case of a boundary layer and with flow in a pipe or channel in the following form:

$$\sqrt{\langle u_i^2 \rangle} = v_* A_i \exp[-(D_i - D)\eta_1] \sqrt{1+\eta_1 - 2\eta_1^2 + \Phi\eta_1(1-\eta_1)} \tag{2.15}$$

$$\sqrt{\langle u_i^2 \rangle} = v_* A_i \exp[-(E_i - E)\eta] \tag{2.16}$$

The values of A_i, D_i, E_i, D, E remain as before. Expressions (2.15) and (2.16) are valid for the case of developed steady-state turbulent flow of an ordinary viscous liquid at $\eta_1 > 0.1$, $\eta > 0.1$. It is noteworthy that in the case of analysis of the outer or central part of the flow the pulsation characteristics in developed turbulent flow are totally independent of the wall coordinate y_*, being determined only by the relative distance from the wall, η_1 or η.

3. The relations given in sections 1 and 2 can be extended to the case of turbulence with flow at surfaces with uniform grainy roughness. To do this we can use an expression for the mixing-path length in which an additional factor is introduced to account for roughness influence along with the smoothing factor [Ref. 2]

$$l_* = \kappa y_* [1 - \exp(y_*/a) + \exp(-60 y_*/a h_*)] \tag{3.1}$$

The numerical values of the coefficients in formula (3.1) are chosen from the condition of coincidence of experimental and calculated values of the coefficients of hydraulic drag of rough pipes. Here $h_* = hv_*/\nu$, h is the average height of the roughness bumps. At $h_* = 60$, effects of molecular nature and the influence of roughness cancel each other out and $l_* = \kappa y_*$. At $h_* > 60$ a mode of developed roughness obtains, and at $h_* < 60$ there is a transient state.

The influence of roughness shows up mainly in a narrow wall region. In the outer part of the layer or in the central part of the flow in the pipe and channel the turbulence characteristics are nearly independent of wall roughness. This means that the same correction factors as in the case of smooth walls can be used to describe the outer part of the flow for rough surfaces. Then throughout the flow cross section the mixing-path length l_* will be determined by the relations

$$l_* = \kappa y_* [1 - \exp(y_*/a) + \exp(-60 y_*/a h_*)] \exp(-D\eta_1) \tag{3.2}$$

$$l_* \kappa y_* [1 - \exp(-y_*/a) + \exp(-60 y_*/a h_*)] \exp(-E\eta_*) \tag{3.3}$$

Formulas (2.8) and (2.9) for mixing lengths that determine the rms values of the components of pulsation velocity must be corrected for the case of flow at rough surfaces in a similar way. Assuming that $h_* = 60$ is the limit in analysis of any single-point moments of the velocity field, we can get the following expressions for l_{i*} in the case of flow in a boundary layer or in a pipe and channel:

(3.4) $$l_{i*} = A_i \varkappa y_* [1 - B_i \exp(-C_i y_*/a) + B_i \exp(-C_i \cdot 60 y_*/a h_*)] \times \exp(-D_i \eta_i)/\sqrt{1-\eta_i}$$

(3.5) $$l_{i*} = A_i \varkappa y_* [1 - B_i \exp(-C_i y_*/a) + B_i \exp(-C_i \cdot 60 y_*/a h_*)] \times \exp(-E_i \eta)/\sqrt{1-\eta}$$

Coefficients D, E, A_i, B_i, C_i, D_i, E_i and the parameters κ and a retain their former values. At $h_* = 0$, formulas (3.2)-(3.5) are transformed to expressions (2.6)-(2.9) for flow at smooth surfaces. The components of pulsation velocity in the case of a boundary layer are determined by relations (1.5), (2.1), (2.3), (3.2), (3.4), (1.10), (1.13) and (2.10), and for flow in a pipe or channel--by expressions (1.5), (2.1), (2.2), (3.3), (3.5), (1.10), (1.13) and (2.11).

The results of calculations show that the influence of roughness is localized in the region immediately adjacent to the surface at a distance of the order of the height of the roughness bumps, leading to appreciable reduction of anisotropy of wall turbulence.

4. The computational relations that we have obtained, and that determine the pulsation characteristics of flow near a wall are also applicable to description of wall turbulence in weak polymer solutions. In this case it is sufficient to assume that the parameter a defining interaction of effects of molecular and molar nature is a nonlinear variable, and is associated with the kind of polymer, its concentration in solution, and some of its characteristics such as molecular weight. We can use the relations proposed in Ref. 8 as expressions that relate the value of a to polymer characteristics. The constant κ is assumed to be independent of the introduction of polymer additives to the flow, and it retains its usual value of $\kappa = 0.4$. Other things being equal, increasing concentration leads to an increase in the value of a, which corresponds to an increase in the lifetime of Klein vortices. This result is confirmed by studies done in Ref. 9 on flows of polymer solutions in a viscous sublayer region using a model of breakup of Klein vortices.

Available experimental and theoretical results lead us to assume that the influence of polymer additives on the characteristics of turbulent flows shows up primarily in the wall region of the flow. These results indicate the possibility of using relations obtained in our research at $a = \mathrm{var}(26 < a < \infty)$ to describe wall turbulence in shear flows of polymer solutions.

On Fig. 4, the results of calculations of components of pulsation velocity for a constant-stress layer at $a = 125$ are compared with data of measurements for flow of 0.012% solution of polyacrylamide in a flat channel [Ref. 4]. Curves 1, 2, 3 correspond to calculated values of $\sqrt{\langle u_1^2 \rangle}/v_*$, points 4 correspond to experimental values of $\sqrt{\langle u_1^2 \rangle}/v_*$, and points 5 correspond to experimental values of $\sqrt{\langle u_2^2 \rangle}/v_*$. In complete accord with experimental data, we observe a sharp rise in $\sqrt{\langle u_1^2 \rangle}/v_*$ at small values of y_*, and a reduction in quantities $\sqrt{\langle u_2^2 \rangle}/v_*$ and $\sqrt{\langle u_3^2 \rangle}/v_*$ in this region as compared with flow of ordinary viscous fluid. Introducing small polymer additives leads to an increase of anisotropy of velocity pulsations near the wall.

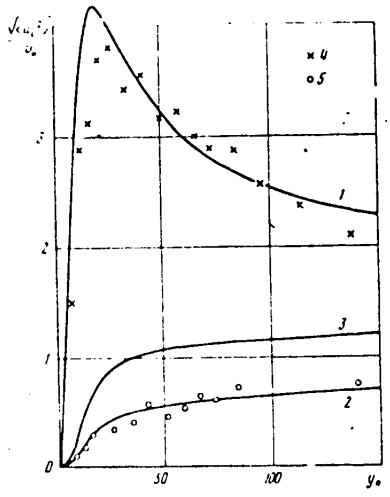

Fig. 4

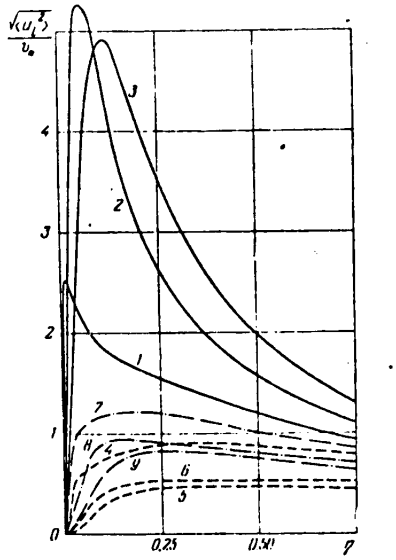

Fig. 5

Fig. 5 illustrates the combined effect that introducing polymer additives to the flow and varying the Reynolds number (changing r_*) have on the distribution of pulsation characteristics across the entire flow of liquid in a pipe. The calculations were done at $\alpha = 26$, $r_* = 500$--curves 1, 4, 7; $\alpha = 300$, $r_* = 500$--curves 2, 5, 8; $\alpha = 300$, $r_* = 250$--curves 3, 6, 9. Curves 1, 2, 3 correspond to calculated values of $\sqrt{\langle u_1^2 \rangle}/v_*$, curves 4, 5, 6--to $\sqrt{\langle u_2^2 \rangle}/v_*$, and curves 7, 8, 9--to $\sqrt{\langle u_3^2 \rangle}/v_*$.

The results of the calculations show that introducing polymer additives to the flow leads to an appreciable increase of the dimensionless longitudinal component of pulsation velocity and a considerable reduction in the transverse and transversal components throughout the pipe cross section. Maximum values of $\sqrt{\langle u_1^2 \rangle}/v_*$ with increasing α are shifted considerable distances away from the wall. At the same value of α, a reduction in r_* that corresponds to a reduction in Reynolds number leads to some reduction of maximum values of components of pulsation velocity, and a shift of the position of these maxima to considerable relative distances from the wall. With increasing α as r_* decreases, the maxima of $\sqrt{\langle u_2^2 \rangle}/v_*$ and $\sqrt{\langle u_3^2 \rangle}/v_*$ become more and more weakly expressed, and at large α and small r_* the transverse component of pulsation velocity remains nearly constant over a considerable part of the pipe cross section (curves 5, 6 on Fig. 5). The results can be attributed to an increase in relative thickness of the viscous sublayer and buffer region as the Reynolds number decreases or as trace amounts of polymers are added to the flow.

The results of the calculations and their comparison with experimental data show that the relations proposed in this paper are in total accord with known experimental facts and principal assumptions regarding averaged turbulent flow of an ordinary viscous liquid and weak polymer solutions in pipes, channels and a boundary layer throughout the entire range of possible Reynolds number variation.

The derived computational relations can be used to study the influence that surface roughness, Reynolds number, longitudinal pressure gradient and addition of trace amounts of polymers to the flow have on the characteristics of wall turbulence, and also in constructing integral and differential methods of calculating the boundary layer, using the equation of turbulent energy balance.

REFERENCES

1. Monin, A. S., Yaglom, A. M., "Statisticheskaya gidromekhanika" [Statistical Hydromechanics], Part 1, Moscow, "Nauka", 1965.

2. Van Driest, E. R., "On Turbulent Flow Near a Wall", J. AERO. SCI., Vol 23, No 11, 1956.

3. Laufer, J., "The Structure of Turbulence in Fully Developed Pipe Flow", NACA REPT., No 1174, 1954.

4. Khabakhpasheva, Ye. M., Perepelitsa, B. V., "Fields of Velocities and Turbulent Pulsations When Trace Amounts of High-Polymer Substances are Added to Water", INZHENERNO-FIZICHESKIY ZHURNAL, Vol 14, No 4, 1968.

5. Fedyayevskiy, K. K., Ginevskiy, A. S., Kolesnikov, A. V.. "Raschet turbulentnogo pogranichnogo sloya neszhimayemoy zhidkosti" [Calculating a Turbulent Boundary Layer of Incompressible Fluid], Leningrad, "Sudostroyeniye", 1973.

6. Szablewski, W., "Eine neue Konzeption für die Berechnung inkompressibler turbulenter Grenzschichten", IZVESTIYA AKADEMII NAUK SSSR: MEKHANIKA ZHIDKOSTI I GAZA, No 2, 1970.

7. Klebanoff, P. S., "Characteristics of Turbulence in a Boundary Layer With Zero Pressure Gradient", NACA REPT., No 1247, 1955.

8. Vasetskaya, N. G., Ioselevich, V. A., "Constructing a Semiempirical Theory of Turbulence of Weak Polymer Solutions", IZVESTIYA AKADEMII NAUK SSSR: MEKHANIKA ZHIDKOSTI I GAZA, No 2, 1970.

9. Black, T. J., "Viscous Drag Reduction Examined in the Light of a New Model of Wall Turbulence" in: "Viscous Drag Reduction", N. Y., Plenum Press, 1969.

6610
CSO: 8144/0203-C

UDC 532.526.2/4

VISCOUS DRAG OF TWO-DIMENSIONAL FOILS MOVING IN WEAK POLYMER SOLUTION

Moscow IZVESTIYA AKADEMII NAUK SSSR: MEKHANIKA ZHIDKOSTI I GAZA in Russian No 3, May-Jun 79 (manuscript received 13 Feb 78) pp 59-65

[Article by V. V. Droblenkov and G. I. Kanevskiy, Leningrad]

[Text] Determination of viscous drag of solids remains one of the major problems of applied hydroaerodynamics. Of particular interest is the study of how small polymer additives introduced into a flow can affect the parameters of flow of a viscous fluid around a body and its viscous drag. This article gives a possible method of solving this problem as applied to flow of a weak homogeneous polymer solution around a symmetric foil.

Viscous drag is comprised of friction drag and the pressure drag that arises due to redistribution of pressures over the surface of a body as a consequence of forces of viscosity. The entire flow region is divided up into a narrow zone of viscous fluid flow (the boundary layer and wake), and an external region of potential flow of inviscid fluid. The problem is solved by a method of successive approximations with consideration of the influence that the differentiated zones have on each other. The values of viscous drag found by direct integration of tangential stresses and pressures are compared with data of experiments and with quantities determined from the characteristics of the far wake.

Methods of calculating boundary layer characteristics when weak polymer solutions flow around solids, including with consideration of laminar, transitional and turbulent flow zones, have been fairly well covered in Ref. 1-5. Methods of determining the characteristics of a turbulent wake with consideration of the flow peculiarities in the near wake are proposed in Ref. 6 and 7. Methods of calculating the potential part of the flow have been quite thoroughly worked out. The nonviscous part of the flow influences the viscous region through pressure distribution over the outside of the boundary layer and the wake. The influence of the viscous region of flow on the characteristics of the potential flow zone shows up in the form of additional

velocities on the interface between the given regions. The theoretical possibility of accounting for this influence has been pointed out in Ref. 8 and 9.

1. An integral method is used to calculate the boundary layer with consideration of laminar, transitional and turbulent flow zones [Ref. 5]. The presence of trace polymer additives in the solution is accounted for by Meyer correlation for the profile of velocity u in a turbulent voundary layer [Ref. 10]

$$\frac{u}{v^*}=\frac{1}{\varkappa}\ln\frac{yv^*}{\nu}+\frac{\Pi}{\varkappa}\left(1-\cos\frac{\pi y}{\delta}\right)+B_0+\Delta B \tag{1.1}$$

$$\Delta B=0,\quad v^*<v_0^*;\quad \Delta B=\alpha\lg\frac{v^*}{v_0^*},\quad v^*\geqslant v_0^*$$

Here y is the transverse coordinate, v* is dynamic velocity, $\kappa = 0.4$ and $B_0 = 5.2$ are turbulence constants, Π is the Cowles parameter, δ is boundary layer thickness, α is a parameter that accounts for the properties of the polymer in solution and its concentration, v_0^* is the dynamic velocity corresponding to onset of the Thoms effect.

The characteristics of the nearby turbulent wake are determined by using the integral method of Ref. 7. The profile of velocity u and tangential stresses τ in the wake are approximated by the relations

$$\frac{u}{U_\delta}=1-\left(1-\frac{U_m}{U_\delta}\right)\left[(1-\gamma)\exp\left(-\frac{k^2y^2}{\delta^2}\right)+\frac{\gamma}{2}\left(1+\cos\frac{\pi y}{\delta}\right)\right] \tag{1.2}$$

$$\frac{\tau}{\rho U_\delta^2}=2\varkappa_1\left(1-\frac{U_m}{U_\delta}\right)^2(1-\gamma)k^2\frac{y}{\delta}\exp\left(-\frac{k^2y^2}{\delta^2}\right) \tag{1.3}$$

Here U_δ is the longitudinal velocity component on the outer boundary of the wake, U_m is the velocity on the axis of the wake, k and γ are lengthwise variable wake parameters, ρ is the density of the fluid, κ_1 is the coefficient of turbulent viscosity taken as variable with respect to the length of the wake. The turbulent wake parameters δ^*, k, γ, κ_1 and the dimensionless velocity defect $1 - U_m/U_\delta$ on the axis are determined in the process of integration of the following system of first-order differential equations: equations of momenta and energy, equations on the axis of the wake (discrete layer), equation of mass capture, equation relating turbulent viscosity to averaged velocity [Ref. 6].

It is assumed that the influence of small polymer additives on flow characteristics of a viscous fluid shows up in restructuring of turbulent exchange near the solid surface in the flow--in the viscous sublayer and buffer region [Ref. 1-5]--and has no direct influence on free turbulence, which includes the development of the turbulent wake behind the foil. In these assumptions, all peculiarities of the influence of polymer additives on flow characteristics in the wake should be accounted for in the change of initial data for flow calculation, and also in some change of characteristics of the potential part of the flow--in change of velocities and pressures on the outer boundary of the wake.

The initial values of the wake parameters are determined from the following conditions: continuity of thickness δ, thickness of displacement δ^*, and thickness of loss of momentum δ^{**} upon transition from boundary layer to wake; equality of tangential stresses on the trailing edge of the foil to maximum tangential stresses in the initial section of the wake; equality of velocity U_m on the axis in the initial section of the wake to velocity u_1 on the outer boundary of the viscous sublayer on the trailing edge of the profile. The latter condition is implied by the assumption that in direct proximity to the trailing edge at a distance of the order of the radius of the rear body round-off, the boundary layers that develop on the upper and lower surfaces merge with elimination of the viscous sublayer. Then

$$\frac{U_m}{U_0}=\frac{u_1}{U_0}=\frac{u_1}{v^*}\sqrt{\frac{c_f}{2}} \tag{1.4}$$

$$u_1/v^*=3.9+0.997(B_0+\Delta B)-0.00511(B_0+\Delta B)^2$$

where c_j is the local friction coefficient.

Conformal mapping theory is used to calculate potential flow around a flat contour. The function that maps the exterior of circle of radius a on the auxiliary plane onto the exterior of the investigated contour on the physical plane is found by the method of Ref. 9.

Effects of the reverse influence of the viscous part of the flow on the outer potential flow are modeled by introducing a system of sources and drains situated on the surface of the contour and on the axis of the wake, their intensity being determined in accordance with the Spence scheme as the derivative with respect to contour arc of the product of velocity on the outer boundary of the layer or wake multiplied by the thickness of displacement [Ref. 11].

The calculation was done by the method of successive approximations. On the initial approximation the characteristics of the boundary layer and wake are assigned, using either data on flow around a flat plate, or the results of calculations on a similar variant. To ensure convergence when carrying out successive approximations, a relaxation coefficient equal to 0.5 is introduced as in several papers using the method of iterations [Ref. 12]. The process of successive approximations is terminated upon attainment of a predetermined accuracy of the calculation; in the given method it is required that the velocities on the outside of the boundary layer on the trailing edge of the foil on two successive approximations must differ by no more than 1%.

The coefficients of friction drag C_F and pressure drag C_p are calculated by integrating tangential stresses and pressures over the surface of the contour

$$C_F=\frac{R_F}{0.5\rho U_0^2 L}=2\int_0^1 c_f\left(\frac{U_0}{U_0}\right)^2 d\left(\frac{x}{L}\right) \tag{1.5}$$

$$C_p=\frac{R_p}{0.5\rho U_0^2 L}=2\int_0^{l/2L}[(q-q_1)_+-(q-q_1)_-]d\left(\frac{z}{L}\right) \tag{1.6}$$

where U_0 is velocity of motion, L is profile length, t is profile thickness, q is the coefficient of pressure on the surface of the contour, q_i is the coefficient of pressure on the surface of the contour in an inviscid fluid, the subscripts "+" and "-" refer respectively to the the forebody and rear body parts of the profile, and z is the ordinate of the profile surface.

The distribution of pressures p_w over the surface of the contour is determined with consideration of the change in pressure across the boundary layer from the formula

$$(1.7) \qquad p_w = p_\delta + \rho \int_0^\delta \frac{u^2}{r}\, dn$$

where p_δ is pressure on the outside surface of the boundary layer determined with regard to velocities caused by the reverse influence of the viscous zone of flow; r is the radius of curvature of streamlines of the inviscid fluid calculated for the boundary layer region; n is the normal to the stream lines in the inviscid fluid; u is the velocity at the investigated point in the viscous fluid. Formula (1.7) is obtained from the condition of dynamic equilibrium of an element of the viscous fluid as it moves along a curvilinear trajectory [Ref. 11]. Use of formula (1.7) is based on the assumption that the stream lines inside the boundary layer in the viscous and inviscid fluids coincide. In this connection, its use is restricted by the dimensionless abscissa x/L = 0.95; hereafter the quantity $p_w - p_\delta$ will be taken as constant.

Viscous drag with respect to the characteristics of the far wake is determined by using the Squire-Young formula [Ref. 9], applicable to the cross section of the wake situated 20% of the length of the foil behind its trailing edge

$$(1.8) \qquad C_x = \frac{R_x}{0.5\rho U_0^2 L} = 2\frac{\delta^{**}}{L}\left(\frac{U_\delta}{U_0}\right)^{0.5(H+5)}$$

where δ^{**}, U_δ and $H = \delta^*/\delta^{**}$ are determined at x/L = 1.2.

2. In accordance with the proposed method, systematic calculations were done on characteristics of flow around symmetric wing profiles at zero angle of attack over a wide range of variation in the Reynolds numbers and degree of turbulence of the oncoming flow.

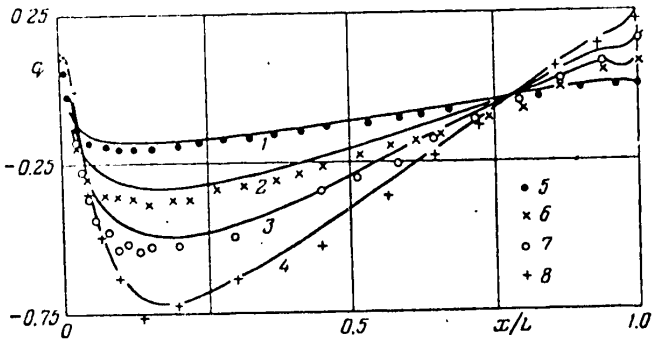

Fig. 1

t/L	Re·10⁻⁵	Experiment [Ref. 13]				Calculation		
		C_x (I)	C_x (II)	C_p	C_F	C_x	C_p	C_F
0.0550	6.124	6.50	--	1.22	5.28	9.31	1.35	7.96
0.0550	22.70	7.18	7.22	0.60	6.58	8.46	1.35	7.11
0.1040	10.67	8.52	9.02	1.98	6.54	9.16	1.96	7.20
0.1040	24.27	8.92	9.08	1.54	7.38	8.75	1.96	6.79
0.1506	10.45	9.90	9.74	2.14	7.76	9.84	2.43	7.41
0.1506	16.67	9.84	9.66	1.90	7.94	9.51	2.39	7.12
0.2069	3.281	13.16	--	4.80	8.36	12.55	3.79	8.76
0.2069	5.358	12.82	12.50	4.24	8.58	11.63	3.18	8.45

The results of calculations of the distribution of pressure over the surface and drag coefficients for a series of generalized Zhukovskiy foils are compared with data of experiment [Ref. 13] on Fig. 1 and in the Table. Omitted in the Table and hereafter for all coefficients of viscous drag is a factor of 10^{-3}. Curves 1-4 on Fig. 1, plotted in the calculations at a degree of turbulence $\varepsilon = 1.75\%$, and experimental points 5-8 refer respectively to foils with relative thickness t/L equal to 0.055, 0.104, 0.1506, 0.2069 tested at Reynolds numbers $Re = U_0 L/\nu$ of $2.27 \cdot 10^6$, $2.427 \cdot 10^6$, $1.667 \cdot 10^6$ and $3.281 \cdot 10^5$ respectively. The experimental values of viscous drag coefficients given in the Table were determined from data of dynamometric measurements (I) and from the results of measurements in a wake (II), while the friction drag coefficients were calculated as the difference between C_X and C_p [Ref. 13]. Comparison of the results of calculations with experimental data shows satisfactory agreement, which means that the proposed method can be used to analyze the influence of various factors on the characteristics of flow around flat symmetric foils.

To analyze the influence of small polymer additives on the characteristics of flow and viscous drag, calculations were done in application to a symmetric foil of 15% thickness. The computations were carried out for Reynolds numbers equal to 10^7 and 10^9 at a degree of free turbulence $\varepsilon = 0.5\%$. At both Reynolds numbers, the flow parameters were calculated in an ordinary viscous fluid ($\alpha = 0$), and in a weak polymer solution ($\alpha = 10$). At $Re = 10^7$, the velocity of foil motion was taken as equal to 1.15 m/s ($v_\infty/U_0 = 0.02$), and at $Re = 10^9$, $U_0 = 8$ m/s ($v_\infty/U_0 = 0.0029$). Such calculated parameters correspond approximately to motion in a solution of Polyox WSR-301™ ($v_\infty \approx 0.023$ m/s) with concentration $c = 0$ ($\alpha = 0$) and $c \cong 10$ ppm ($\alpha = 10$).

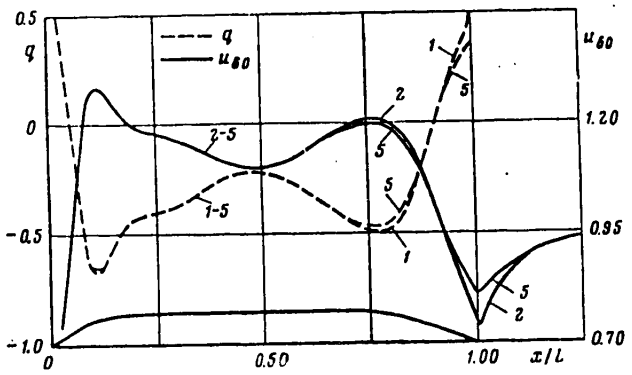

Fig. 2

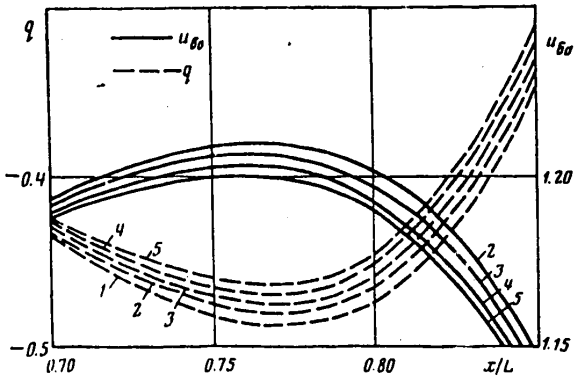

Fig. 3

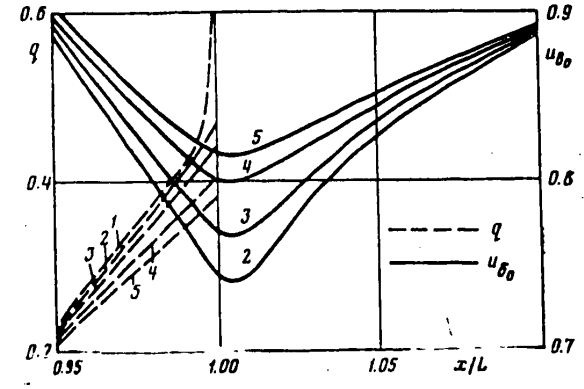

Fig. 4

The results of calculations of the coefficient of pressure q on a foil and the distribution of velocity on the outer surface of the boundary layer and wake $u_{\delta o}$ are shown in Fig. 2-4. Curves 1 correspond to pressure distribution with motion in an inviscid liquid, curves 2 and 3 correspond to motion at $Re = 10^7$, and curves 4 and 5 correspond to motion at $Re = 10^9$. Curves 2 and 4 are the distributions of velocities and pressures with motion in a polymer solution ($\alpha = 10$), and curves 3 and 5 are the distributions in an ordinary fluid ($\alpha = 0$). Fig. 5 shows the results of calculations of the thickness of the boundary layer and wake δ/L (curves 1-4), and the thickness of loss of momentum in the layer and wake δ^{**}/L (curves 5-8). Curves 1, 2, 5 and 6 correspond to $Re = 10^7$, and curves 3, 4, 7 and 8 correspond to $Re = 10^9$. Lines *a* correspond to flow of an ordinary liquid around the foil, and lines b correspond to flow of a polymer solution ($\alpha = 10$).

The results of calculations of viscous drag and its components for the investigated contour are summarized as follows:

Re	α	U_∞, m/s	C_F	C_p	C_x (I)	C_x (II)
10^7	0	1.15	5.876	1.642	7.519	7.23
10^7	10	1.15	5.082	1.413	6.495	6.11
10^8	0	8.00	3.488	1.071	4.558	4.25
10^8	10	8.00	2.376	0.867	3.243	2.82

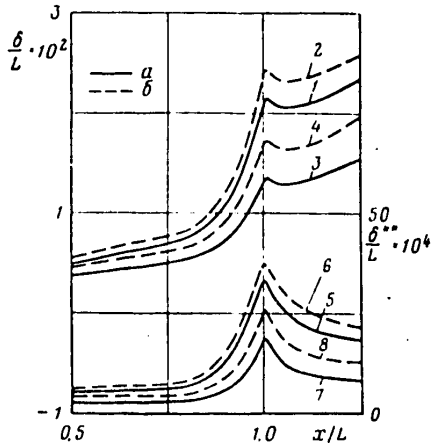

Fig. 5

Here (I) are the values of C_x as determined by integrating tangential stresses and pressures over the foil, (II) are the values of C_x calculated from the characteristics of the far wake.

Analysis of the given results of calculations leads us to the following major conclusions on the influence that trace polymer additives have on characteristics of the flow of a viscous liquid around a flat symmetric contour. A reduction in the integral thicknesses of the boundary layer and wake as a result of introducing polymer additives into the flow leads to a reduction of the reverse influence of the viscous flow zone on potential flow. As a consequence, there is a change of velocities on the outer surface of the layer and wake, and of pressures on the surface of the contour, bringing them more into line with the corresponding quantities in potential flow of an inviscid liquid around the body. The maximum influence of the viscous flow zone on the distribution of pressures over the contour, and of velocities and pressures over the outer surface of the boundary layer and wake will be observed in regions of the rear-body relief peak and on the trailing edge of the foil. On the whole, the influence that polymer additives have on flow characteristics of a viscous fluid is in some measure analogous to the effect of increasing the Reynolds number.

The data given above show that the values of viscous drag obtained by direct integration of pressures and tangential stresses agree satisfactorily with the corresponding quantities determined from the characteristics of the far wake. Introduction of trace polymer additives into the flow reduces viscous drag, the degree of reduction being about the same for friction drag and pressure drag.

REFERENCES

1. Ioselevich, V. A., Pilipenko, V. N., "Turbulent Flow of Liquid With Polymer Additives in Boundary Layer With Longitudinal Pressure Gradient", DOKLADY AKADEMII NAUK SSSR, Vol 213, No 4, 1973.

2. Ioselevich, V. A., Pilipenko, V. N., "Drag of Flat Plate in a Flow of Polymer Solution With Variable Concentration", IZVESTIYA AKADEMII NAUK SSSR: MEKHANIKA ZHIDKOSTI I GAZA, No 1, 1974.

3. Sedov, L. I., Vasetskaya, N. G., Ioselevich, V. A., "Calculation of Turbulent Boundary Layers With Polymer Additives", PROCEEDINGS OF INTERNATIONAL CONFERENCE ON DRAG REDUCTION, Cambridge, 1974, Cranfield, S. A., 1974.

4. Hassid, S., Poreh, M., "Boundary Layer Development of Polymer Solutions in Pressure Gradients", PROCEEDINGS OF INTERNATIONAL CONFERENCE ON DRAG REDUCTION, Cambridge, 1974, Cranfield, S. A., 1974.

5. Droblenkov, V. V., Kanevskiy, G. I., "Synthesizing a Method of Calculating a Planar Boundary Layer in Weak Polymer Solutions With Laminar, Transitional and Turbulent Flow Zones", IZVESTIYA AKADEMII NAUK SSSR: MEKHANIKA ZHIDKOŞTI I GAZA, No 3, 1977.

6. Sekundov, A. N., "Application of Differential Equations for Turbulent Viscosity to Analysis of Planar Non-Self-Similar Flows", IZVESTIYA AKADEMII NAUK SSSR: MEKHANIKA ZHIDKOSTI I GAZA, No 5, 1971.

7. Droblenko, V. V., Kanevskiy, G. I., "Calculation of Nearby Turbulent Planar Wake" in: "Gidrodinamika vysokikh skorostey" [High-Velocity Hydrodynamics], Leningrad, "Sudostroyeniye", 1974.

8. Prandtl, L., "Gidroaeromekhanika" [Hydroaeromechanics], Moscow, Izdatel'stvo inostrannoy literatury, 1949.

9. Loytsyanskiy, L. G., "Mekhanika zhidkosti i gaza" [Mechanics of Liauid and Gas], Moscow, "Nauka", 1970.

10. Meyer, W. A., "A Correlation of Frictional Characteristics for Turbulent Flow of Dilute Viscoelastic Non-Newtonian Fluids in Pipes", A. I. Ch. E. JOURNAL, Vol 12, No 3, 1966.

11. Spence, D. A., "Prediction of the Characteristics of Two-Dimensional Airfoils", J. AERO. SCI., Vol 21, No 9, 1954.

12, Nakayama, Neytel, Landveber, "Interaction of Flows at the End of a Body of Revolution, Part 2. Iteration Solution for Flows Within the Limits of the Boundary Layer and Wake and in the External Region", TEORETICHESKIYE OSNOVY INZHENERNYKH RASCHETOV, Mir, No 3, 1976.

13. Fage, A., Falkner, V. M., Walker, W. S., "Experiments on a Series of Symmetrical Joukowski Sections", AERONAUT. RES. COMM., REP. AND MEM., No 1241, 1929.

6610
CSO: 9144/0203-A

LASERS AND MASERS

UDC 621.311.6:621.375.826

ELECTRIC POWER SUPPLIES FOR LASERS

Moscow ISTOCHNIKI ELEKTROPITANIYA LAZEROV in Russian 1981 (signed to press 4 Jun 81) pp 2-8, 169

[Annotation, editor's foreword, introduction and table of contents from book "Electric Power Supplies for Lasers", by Konstantin Dmitriyevich Shmelev and Gennadiy Vasil'yevich Korolev, Energoizdat, 6000 copies, 169 pages]

[Text] An examination is made of electric power supply circuits for small-scale gas, solid-state and semiconductor lasers working in cw or pulsed modes. Principal methods and arrangements are given for igniting gas lasers and optical pumping lamps of solid-state lasers. A number of schemes are given for controlling emission parameters by acting on the output characteristics of the electric power supply.

For engineering and technical workers involved in developing electric power supplies for gas, solid-state and semiconductor lasers used in instrument making.

Editor's Foreword

In handling the tasks set before the Soviet people by the Twenty-Sixth Congress of the CPSU, of greatest significance are problems of increasing the efficiency of social production and improving the quality of goods produced. A leading role here goes to the latest advances in Soviet and worldwide science and engineering. It is generally acknowledged that one of the most outstanding phenomena in the field of physics over the past two decades has been the development of quantum electronics, and its component part--laser technology.

A distinguishing characteristic of laser technology is not only its revolutionizing role in many practical areas of human endeavor, but an unprecedented pace of introduction in the national economy. It was only a little more than three years from the time that the first lasers were made until they were being used under industrial conditions. A lot of the credit for this goes to engineers and workers who carried on the work started by the creators of this new field of physics--the eminent Soviet scientists, academicians N. G. Basov and A. M. Prokhorov.

Considerable credit for the rapid introduction of advances in laser technology into the national economy goes also to the specialists responsible for developing the electric power supplies for lasers. Important factors in this work were the searches for workable ways to match the current-voltage characteristics of laser emitters to the external (load) characteristic of the source of electric supply,

minimizing energy losses and meeting requirements on the range of control of the pumping parameters of active elements in lasers. It should be pointed out that there has not yet been much research on unifying the parameters of laser emission with the requirements for sources of electric supply for laser emitters.

This book will enable more complete formulation of requirements for electric power supplies for lasers and selection of circuitry with a view to maximizing efficiency and minimizing size and weight, which is very important for developing laser-based devices.

The book describes some original design features, presents engineering formulas for sources of electric supply for lasers, and makes recommendations on selecting the main functional elements of such sources.

Comments and suggestions should be addressed to 113114, Moscow, M-114, Shlyuzovaya nab., 10, Energoizdat.

V. M. Vakulenko,
USSR State Prize Laureate

Introduction

The development of lasers is a grand achievement of recent years by scientists and engineers in the Soviet Union and elsewhere. Gas, solid-state and semiconductor lasers have now found wide application in various devices and systems.

High coherence and monochromaticity of optical radiation of all kinds of lasers make them useful in a variety of communication systems, locating devices, range finders and altimeters, devices for measuring velocities and angles of turn, and interferometers.

Atomic helium-neon lasers have found wide application in instrument making. Thanks to frequency stability of emission, these lasers are used in interferometers, in optical communication lines as message-handling devices, as firing simulators on weaponry, and as a basis for ring gyroscopes. At cw emission power of up to 50-60 kW, helium-neon lasers consume no more than 50-60 W of power from the electric line.

Ion lasers differ appreciably from atomic lasers with respect to optical radiation power, reaching several watts per meter of the active element, and have found application in submarine lidar, as well as for control of chemical reactions.

Practically all molecular lasers use carbon dioxide as the active element with various additives of nitrogen and helium to raise efficiency to 30% and optical radiation power to tens of watts per meter of length. Carbon dioxide lasers are being successfully used in lidar and communications, and also as process lasers.

Direct current is ordinarily used for exciting cw operation of gas lasers. The power of the source of electric supply in this case is determined by the type of laser that is used and its linear dimensions. In cw gas lasers, the maximum radiation power per unit of length of the active element and the necessary power of the source of electric supply are as follows:

Types of lasers	Maximum emission power, W/m	Average efficiency, %	Power of sources of electric supply, W/m
Atomic	0.04-0.1	0.03 (0.1)	100
Ion	10-40	0.1 (0.2)	10,000-20,000
Molecular	50-1000	10 (30)	500-5000

In miniature devices (interferometers, gyroscopes), gas lasers are used in which the length of the active elements does not exceed a few dozen centimeters. In this connection, the power of the electric supply does not exceed tens or hundreds of watts. Pulsed operation is used to increase the power of optical radiation of all kinds of lasers (gas, solid-state and semiconductor). As compared with cw operation, pulsed operation for example of gas lasers enables an increase in optical power of the laser by a factor of about ten. Despite considerable powers of pulse radiation, the average consumption from the electric power supply remains small. By using Q-switching in the laser cavity, optical radiation can be increased by a factor of 10^3-10^4 as compared with power in the continuous mode.

Atomic gas lasers (He-Ne, He-Xe, He-Cd and others) in pulsed operation have not found any practical use. Among the pulsed gas lasers, the ones that have been extensively used are those based on gas ions (Ar, Kr, Xe, Ne) that emit in the ultraviolet and visible regions of the spectrum. These pulse lasers, working in the pulse mode, are being used in underwater navigation and signaling, in metrology and holography.

Nitrogen gas lasers in free emission radiate a pulse power of about 100 kW at pulse duration of 10 ns and recurrence rate of 1-100 Hz. These lasers are designed for use in photochemistry, high-speed photography and other scientific purposes.

Carbon dioxide molecular gas lasers in the free emission mode radiate a pulse power of 80-100 W, the pulse duration ranging from 1 to 10 μs, and the pulse recurrence rate is from 1 Hz to 1 kHz. In Q-switched operation, these same lasers can reach a radiation power of 1 kW with recurrence rate of up to 100 kHz, with cw pumping. Emission pulse duration in this case does not exceed 50 ns.

Rods of ruby, neodymium glass and YAG:Nd are used as the active element in solid-state lasers. The overall dimensions and mass of such active elements are considerably less than in gas lasers. Therefore, thanks to their compactness, solid-state lasers that operate in the pulsed mode have found application in airborne lidar systems, range finding and target illumination. These lasers are characterized by high pulse power at pulse duration of up to 100 ns. Solid-state YAG lasers that operate in the continuous mode are used in communications systems.

Semiconductor lasers (GaAs, InAs), thanks to relatively high efficiency (up to 40%), compactness, and a capability for optical frequency tuning have found application in pulsed altimeters, range finders and long-range communication systems (in both pulsed and cw operation). However, semiconductor lasers show a rather wide spectrum of the output signal and a greater angle of beam divergence.

Laser devices can be used both under stationary conditions (transmitting laser devices, lidars, beacons), and in a variety of mobile units: aerospace vehicles, satellites, surface transport. The primary source of electric power for such devices can be both industrial AC line voltage and DC supplies (batteries, accumulators). Therefore in developing sources of electric supply for lasers this is one of the decisive factors in choosing electric circuitry.

A characteristic feature of pulsed laser devices is the considerable level of output pulse power for a comparatively small average power consumed from the line. Minimum mass and overall dimensions, high efficiency and reliability are among the major requirements for sources of electric power for lasers.

At relatively low average laser radiation power, there is a considerable increase in requirements for stability of output parameters of optical emission in time, which depend on the output characteristics of the primary sources of electric power. It is known that accumulator voltages may vary over a range of ±20% of the rated value. Besides, the power of primary sources of electric supply (accumulators, converters) is limited and commensurate with the power required for excitation (supply) of the laser itself.

Contents page

6610
CSO: 1862/32

UDC 621.375.826

TUNABLE LASERS

Novosibirsk LAZERY S PERESTRAIVAYEMOY CHASTOTOY (SBORNIK NAUCHNYKH TRUDOV) in Russian 1980 (signed to press 2 Oct 80) pp 4, 121-125

[Annotation and abstracts of articles from book "Tunable Lasers (Collection of Scientific Papers)", edited by Doctor of Physical and Mathematical Sciences Veniamin Pavlovich Chebotayev, Institute of Thermal Physics, Siberian Department, USSR Academy of Sciences, 500 copies, 126 pages]

[Text] The collection contains the exposition of techniques and results of experimental research on a wide range of lasers with tunable frequency: dye lasers, color-center lasers, Landau-level magnetotunable laser, high-pressure pulsed gas lasers, optically pumped iodine laser, and line-tunable electrochemical HF laser.

Also described in the collection is a volume holographic grating recorded in a crystal of $LiNbO_3:Fe^{3+}$ for laser tuning.

The collection is intended for specialists in the field of nonlinear optics and laser spectroscopy.

UDC 621.375.826

LASERS USING F-CENTERS IN LiF AND NaF CRYSTALS

[Abstract of article by Gusev, Yu. L., Kirpichnikov, A. V., Konoplin, S. N. and Marenikov, S. I.]

[Text] A report on the results of research to develop pulsed lasers using color centers in LiF and NaF crystals.

The crystals were irradiated with different doses from a Co-60 source of gamma radiation to form F_2, F_2^+, F_2^- and F_3^- centers. An investigation is made of the emission characteristics of lasers on these color centers with pumping by dye laser, ruby laser, a YAG-neodymium laser and its second harmonic.

Overall tuning range is 0.62-1.4 μm. An investigation is made of questions of time stability of the color centers and their resistance to pumping radiation. It is found that F_3^- and F_3 centers are stable. A simple method is described for restoring F_2^+ centers by luminous radiation (ultraviolet or radiation of the second harmonic of the YAG:Nd laser).

An efficiency of 20% in the pulsed mode is attained on F_3^- centers in the NaF crystal. An estimation of the lasing threshold for cw operation gives 100 mW with focusing area of 10^{-5} cm^2 and intracavity losses of 10%. In principle, the band from 0.9 to 2.9 μm can be covered on F_3^- centers in different crystals. In conclusion, the field of application of color-center lasers is discussed. Figures 4, tables 4, references 10.

UDC 621.375.826

FREQUENCY DOUBLING OF TUNABLE CW F-CENTER LASER

[Abstract of article by Verbovskiy, V. I., Klement'yev, V. M. and Pecherskiy, Yu. Ya.]

[Text] The paper gives a brief description of a tunable cw laser on $F_A^{(II)}$ centers in the KCl:Li crystal, and presents the major characteristics of the laser. Frequency doubling is reported for emission of a color-center laser, as well as the He-Ne laser in a variety of nonlinear optical crystals. Converted radiation powers obtained for the $F_A^{(II)}$ laser are ~10^{-8} W in the $AgGaS_2$ crystal, and for the He-Ne laser ~10^{-7} W in the new nonlinear crystal $ZnGeP_2$. The given results can serve as a point of departure for developing the corresponding elements of frequency synthesis and measurement systems. Figures 2, references 8.

UDC 621.387.330.3

TUNABLE-FREQUENCY RADIATION SOURCES BASED ON PULSED GAS LASERS

[Abstract of article by Ishchenko, V. N., Kochubey, S. A., Lisitsyn, V. N. and Chapovskiy, P. L.]

[Text] The article gives the results of research aimed at developing pulsed wavelength-tunable lasers in the near ultraviolet, visible and near-infrared bands. Three versions of such devices are considered: high-pressure electric discharge lasers on atomic lines of inert gases, excimer lasers and dye lasers. Lasing wavelength regions, monochromaticity of emission and tuning characteristics are determined for each case. Operation in a master oscillator-amplifier scheme is studied on the excimer laser example. It is pointed out that such an arrangement has good prospects for practical use of tunable lasers. Attention is called to the importance of developing spectrometers required in scientific and applied problems. A pulsed laser spectrometer with high time resolution is described that is based on a high-pressure CO_2 laser, and used to study some of the transition characteristics of argon on the 0.912 μm line. Figures 17, references 42.

UDC 621.387.330.3

INVESTIGATION OF EMISSION PROPERTIES OF CW DYE LASER

[Abstract of article by Beterov, I. M., Vasilenko, L. S., Zakharov, M. I., Shishayev, A. V. and Yurshin B. Ya.]

[Text] The article gives an analysis of a method of obtaining a single-frequency lasing mode in a cw cye laser. This technique is based on the strong coupling that arises due to the effect of spatial saturation of gain when a selecting element

in the form of a thin absorbing film is introduced into the cavity. An experimental study of this method and of the causes that lead to broadening of the emission line of a single-frequency dye laser has enabled development of a cw dye laser with emission linewidth of 1 mHz, continuous tuning range of 3 GHz and maximum radiation power of 180 mW at pumping power of 3 W. Figures 9, references 20.

UDC 621.378.33

SINGLE-FREQUENCY EMISSION IN PULSED DYE LASER WITHOUT FABRY-PEROT ETALON

[Abstract of article by Lebedev, V. V. and Plyasulya, V. M.]

[Text] The paper gives the results of an experimental study of working conditions of a pulsed dye laser in which the spectrum is selected by a system of two flat diffraction gratings. A rhodamine-6G solution in ethanol was used as the active medium, and the second harmonic of a YAG-neodymium laser was the pumping source. With optimization of laser parameters, single-frequency emission was attained in a range of 551-567 nm. Frequency tuning was by simple rotation of a diffraction grating with spacing of 0.025 cm^{-1}. Figures 4, references 10.

UDC 772.773

VOLUME PHASE HOLOGRAPHIC GRATING IN $LiNbO_3$: SPACE-FREQUENCY SELECTOR OF TUNABLE LASER

[Abstract of article by Barkan, I. B., Lebedev, V. V. and Vorob'yev, A. V.]

[Text] An investigation is made of time, temperature and concentration dependences of processes of formation and relaxation ofa volume phase holographic grating [VPHG] in iron-doped $LiNbO_3$ crystals. The diffraction efficiency, dispersion, angular and spectral selectivity (resolution) are measured for VPHG's that have spatial frequency from 500 to 1500 lines/mm, and thickness from 3 to 14 mm. It is shown that there is a good outlook for using thick VPHG's as a space-frequency selector in making a tunable laser with short optical cavity, large aperture and high spectral and angular brightness of emission. Figures 10, table 1, references 19.

UDC 621.373.826

TUNABLE OPTICALLY PUMPED CW I_2 LASER

[Abstract of article by Matyugin, Yu. A. and Ustinov, G. N.]

[Text] A report on an experimental study of lasing on the electronic transition $B^3\Pi_{ou}^+ - X^1\Sigma_g^+$ of molecular iodine with pumping by emission of a cw 6G-rhodamine dye laser. Emission of the iodine laser was observed in the range of 0.67-1.24 μm. According to estimates, the total number of lasing in this band is of the order of 10^5. Threshold pumping power was on a level of 10-30 mW for a lasing band of 1.1-1.2 μm, and 30-100 mW beyond the limits of this band. An investigation was made of the shape of the laser emission line. Figures 7, references 20.

UDC 621.373.826

CW CHEMICAL HF LASER WITH LINE TUNING

[Abstract of article by Pecherskiy, Yu. Ya.]

[Text] The paper describes the design and characteristics of a cw chemical HF laser that is tuned by an intracavity prism. Lasing is achieved on 13 lines in a range of 2.64-3 μm. Maximum lasing power is 0.55 W. It is shown that amplitude noises in the laser radiation are concentrated mainly in the frequency region below 5 kHz. Amplitude stability of ±1% is attained in the noise-optimum mode. Lamb shift parameters are given. Frequency is stabilized with respect to its center. Figures 4, references 10.

UDC 621.375.826

MAGNETOTUNABLE CW SPIN-FLIP LASER

[Abstract of article by Gavrilov, V. P., Pestryakov, Ye. V. and Fedorov, S. A.]

[Text] The paper describes the construction of a cw magnetotunable spin-flip laser with pumping by different CO laser lines in the range of 5.2-5.6 μm. Lasing is achieved on the Stokes frequency in industrial specimens of a type with concentration from $5 \cdot 10^{14}$ to $2.2 \cdot 10^{15}$ cm^{-3}.

The authors discuss the outlook for using an external cavity to smooth the tuning characteristic and increase the output power of the spin-flip laser. Emission power of the spin-flip laser is increased with external mirrors on transmission-enhanced specimens with $C = 1.1 \cdot 10^{15}$ cm^{-3}. Figures 5, references 11.

UDC 621.378.33

PHASE SYNCHRONISM IN THREE-FREQUENCY COLLINEAR PARAMETRIC INTERACTION OF WAVES IN UNIAXIAL CRYSTALS

[Abstract of article by Barykinskiy, G. M.]

[Text] A simple algorithm is proposed for exact calculation of tuning curves that are required for making tunable parametric light generators and sum and difference frequency oscillators based on three-frequency parametric interaction of waves in optically uniaxial media with square-law nonlinearity. The given algorithm is also applicable to biaxial crystals in planes of principal cross sections, and is easily programmable.

The resultant algorithm is used for computer calculations of tuning curves for crystals. Figures 3, references 7.

UDC 621.375.826

INTRACAVITY LASER SPECTROMETER BASED ON LASER USING F_2^- CENTERS IN LiF CRYSTAL

[Abstract of article by Gusev, Yu. L., Ivanov, A. F., Marennikov, S. I. and Sinitsa, L. N.]

[Text] A report on development of an intracavity spectrometer using stable F_2^- centers in the LiF crystal. Stimulated emission of the color-center laser was excited in a longitudinal arrangement by neodymium laser pumping. Lasing in a range of 1.156-1.168 μm was achieved in a nonselective cavity.

The sensitivity of the intracavity spectrometer was $3 \cdot 10^{-5}$ cm^{-1} with color-center laser pulse duration of 1 μs. The spectrometer registered 19 absorption lines of atmospheric air in the IR band. Figures 2, references 4.

UDC 621.375.826

NONLINEAR LIGHT ABSORPTION BY COLOR CENTERS IN ALKALI HALIDE CRYSTALS

[Abstract of article by Gusev, Yu. L., Konoplin, S. N., Kirpichnikov, A. V. and Marennikov, S. I.]

[Text] A report on investigation of the effect of nonlinear dependence of absorption on light intensity in LiF crystals with F_2 centers. It is suggested that this effect can be explained by the change in population of electronic levels. Calculation agrees well with experiment.

A saturation effect was also observed in LiF crystals with F_2^+ centers under the action of ruby laser emission, and in a KCl crystal containing N centers under the action of YAG:Nd laser emission with $\lambda = 1.06$ μm.

Q-switched operation with frequency of up to 30 kHz is attained by using the nonlinear absorption effect in LiF crystals with F_2 centers. Figure 1, references 4.

6610
CSO: 1862/26

CHARACTERISTICS OF GASDYNAMIC LASERS USING COMBUSTION PRODUCTS WITH UNSTABLE CAVITIES

Novosibirsk FIZIKA GORENIYA I VZRYVA in Russian Vol 17, No 4, Jul-Aug 81 (manuscript received 21 May 80) pp 109-113

[Article by A. I. Didyukov, G. I. Kozlov and I. K. Selezneva, Moscow]

[Text] The use of unstable cavities in gasdynamic lasers enables emission with high directionality on large volumes of homogeneous active medium. The most extensively used unstable cavities in practical applications are telescopic cavities formed by two cylindrical or spherical mirrors.

In Ref. 1, numerical calculations on vibrational relaxation were done and power was optimized for gasdynamic lasers with planar cavities using mixtures of CO_2-N_2-CO-H_2O-H_2 produced by burning different fuels. In this paper we will study the optimization of characteristics of gasdynamic lasers with unstable cavities as well. The energy characteristics of gasdynamic lasers are analyzed on the basis of simultaneous solution of balance kinetic equation of vibrational relaxation in the combustion products [Ref. 1] and equations of radiation transfer in the geometric optics approximation [Ref. 2].

In accordance with Ref. 3, the intensity of radiation at an arbitrary point (x,y) of a cavity formed by cylindrical mirrors with common focus (x_0,y_0) is related to the intensity at a point of the same cross section located M times closer to the cavity axis (M is the magnification factor) by the expression

$$I(x, y) = F(x, y)\, I\left(x_0 - \frac{x_0 - x}{M}, y\right),$$
$$F(x, y) = \frac{R_1 R_2}{M} \exp\left[\int\limits_{s(x,y)} K_\nu(r)\, dr\right], \qquad (1)$$

where s(x,y) is the beam trajectory in the geometric approximation as waves travel in the positive and negative direction of the y-axis; R_1, R_2 are mirror reflectivities, K_ν is the gain of the medium.

The condition of existence of the solution of equation (1) is the condition of steady-state lasing

$$F(x_0, y) = 1. \qquad (2)$$

The quantity F(x,y) calculated for points in the plane of a large mirror (y = 0) may be represented as

$$F(x, 0) = \frac{R_1 R_2}{M} \exp\left\{\int_0^l \left[K_\nu\left(x_0 - \frac{x_0 - x}{M}, y\right) + K_\nu\left(x_0 + \frac{x_0 - x}{y_0} y, y\right)\right] dy\right\}. \quad (3)$$

Here l is the distance between cavity mirrors.

The transport equations imply that the intensity of waves propagating in the positive and negative directions of the y-axis are related to intensity near the concave mirror by the expressions

$$I^+(x, y) = I(x, 0) \exp\left[\int_0^y K_\nu(x, y')\, dy'\right], \quad (4)$$

$$I^-(x, y) = I\left(\frac{x, y_0 - x_0 y}{y_0 - y}, 0\right) \frac{y_0}{y_0 - y} \exp\left\{-\right.$$

$$\left. - \int_0^y K_\nu\left[\frac{x y_0 - x_0 y + y'(x_0 - x)}{y_0 - y}, y'\right] dy'\right\}. \quad (5)$$

A net-point method was used for simultaneous numerical solution of system (1)-(5), the equations of kinetics for vibrational degrees of freedom [Ref. 1] and the boundary conditions on the mirrors

$$I^+(x, 0) = R_1 I^-(x, 0), \; I^-(x, l) = R_2 I^+(x, l) \quad (6)$$

The axis of the cavity $x = x_0$ divides it into two parts: stimulated emission length l_1 and amplification length l_2. The solution for the stimulated emission part can be obtained only by an iteration method. The emission field is determined from the given distribution of gain and intensity on the axis of the cavity $I(x_0, 0) = I_0$ from (1), (4), (5). The resultant intensity distribution enables us to find a new distribution of gain in the volume of the cavity. Corrections are made to the initially arbitrary quantity I_0 until the systems of equations of distribution of the field and the gain obtained as a results of solution meet the condition of steady-state lasing (2). The solution in the right-hand part of the cavity can be found by using the same methods, but with assigned distribution of the field on the axis of the cavity $I(x_0, y)$.

Numerical calculations of the energy characteristics of a telescopic cavity have been done for a mixture of 10% CO_2 — 60% N_2 — 20% CO — 5% H_2O — 5% H_2 pre-expanded in a planar logarithmic nozzle with height of the critical cross section of 0.02 cm and degree of expansion of 50 [Ref. 1]. The stagnation temperature of the combustion products was taken as 2000 K, and the stagnation pressure was varied. Of greatest interest is the way that lasing power P and working efficiency of the cavity η depend on various parameters. Fig. 1 shows the function P(M) with laser parameters $l = 50$ cm, $l_1 = 5$ cm, $l_2 = 15$ cm for mixtures with stagnation pressure $p_0 = 20$ (1), 40 (2) and 60 atm (3) respectively. The broken curves show the efficiency dependences for the same mixtures.

Calculations show that for small values of M, efficiencies differ insignificantly. This shows that the main contribution to power in cavities with low magnification

is from the stimulated emission part, and consequently the energy losses due to vibrational relaxation are insignificant. As M increases, there is a drop in efficiency, and this drop is faster the greater the gas flux density. While the efficiency of the cavity falls with increasing pressure in the investigated range of variation of parameters, the power has an optimum value with respect to pressure that varies depending on the magnification of the cavity. Low-density mixtures are most advantageous (from the standpoint of power production) at high magnifications. The optimum values of p_0 decrease with decreasing M.

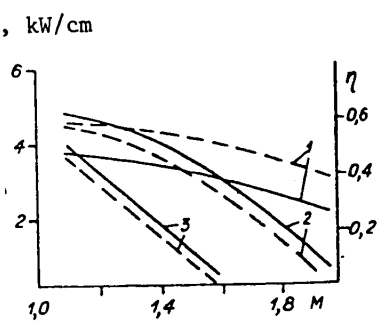

Fig. 1

Use of a telescopic cavity avoids the excessive constriction of emission at the input to the cavity that is observed when planar mirrors are used. Nonetheless, at small M there is considerable spatial inhomogeneity of the distribution of I. As calculations show, radiation denstiy in a cavity with small M under typical conditions of gasdynamic laser operation may vary by an order of magnitude along the flow. An increase in M leads to smoothing of the field distribution, although the efficiency falls at the same time.

Ref. 4 proposes using telescopic cavities based on triple-prisms with spherical faces or their two-dimensional analogs in the flow system. Such cavities are essentially telescopic cavities in which only the concave mirror, or both mirrors are replaced with internal-reflection prisms. As it travels through such prisms, the curvature of the light beams is transformed in the same way as with reflection from the mirrors that they replace, but the beam itself is reversed relative to the axis of the cavity.

For the sake of definiteness we will consider a cavity in which the concave mirror is replaced by a prism. As shown in Ref. 5, such a cavity has very little sensitivity to the presence of optical inhomogeneities. In the geometric optics approximation, self-consistent calculation reduces to simultaneous solution of equations of kinetics for vibrational degrees of freedom, and radiation transport equations (4) and (5) with boundary conditions on the mirrors

$$I^+(x, 0) = R_1^2 I^-(2x_0 - x, 0), \; I^-(x, 0) = R_2 I^+(x, 0). \qquad (7)$$

The distribution of field and gain is found by an iteration method. Used as the initial distribution was the distribution $I_0^+(x,0)$, constant with respect to the x-coordinate, and approximately corresponding in order of magnitude to the intensity on the axis of the analogous telescopic cavity with ordinary mirrors. The characteristic distribution of radiation intensity in plane $y = 0$ is shown in Fig. 2. The results refer to lasing in a mixture with $p_0 = 40$ atm, cavity parameters $l = 100$ cm, $l_1 = l_2 = 5$ cm and $M = 2$. The use of an internal-reflection prism instead of a mirror leads to practically uniform distribution of the overall intensity along the flow.

Comparison of the energy characteristics of the conventional cavity with those of the cavity in which one or both mirrors have been replaced with triple-prisms shows that they are similar over a wide range of variation in the flow parameters

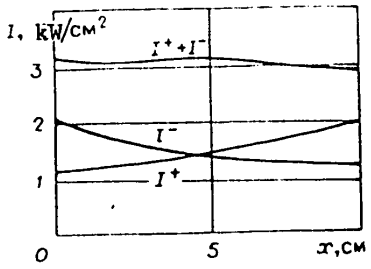

Fig. 2

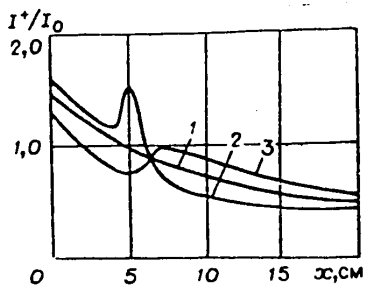

Fig. 3

and cavity dimensions. For example when M is changed from 2 to 5 for a mixture with $p_0 = 50$ atm, efficiency differences do not exceed 10%.

The energy characteristics of unstable resonators can be controlled by an external source as well. An unacceptable increase of angular divergence of radiation results from formation of a convergent wave in a telescopic cavity by adding a mirror or xome other reflective surface that partly covers the plane wave, or from introducing a convergent wave from an external source [Ref. 6]. The situation can be changed if a divergent external beam is used to control laser operation. One such arrangement, proposed by Yu. A. Anan'yev et al., consists in introducing radiation of given intensity from an external source into the central part of the telescopic cavity. In our work, a check was done on the effectiveness of this scheme for the telescopic cavity of a gasdynamic laser.

Typical distribution of relative intensity I^+/I_0 in the plane of a large mirror is shown in Fig. 3. The values of I^+ are normalized to the intensity in the center I_0 that arises when the telescopic cavity is working in the mode of stimulated emission. Curve 1 corresponds to distribution I^+/I_0 of a conventional telescopic cavity with parameters $l = 100$ cm, $l_1 = 5$ cm, $l_2 = 15$ cm and $M = 2$. The stagnation pressure of the mixture was $p_0 = 20$ atm. Curves 2 and 3 refer to distributions I^+/I_0 in the same cavity with a hole 0.2 cm wide in the large mirror through which radiation is injected with intensity of 1000 and 500 W/cm^2 respectively ($I_0 = 680$ W/cm^2).

Injection of radiation from the outside causes redistribution of the radiation density in the cavity. If the radiation density that is injected exceeds I_0, intensity distribution is set up in the cavity higher than the lasing emission level to the left of the axis, and lower than this level to the right of the axis of the cavity (see Fig. 3, curve 2). When the intensity of radiation injected from the outside is lower than I_0, steady-state distribution is formed with lower intensity in the stimulated emission part, and higher intensity in the amplification part of the cavity (see Fig. 3, curve 3).

Calculations have shown that injecting radiation from the outside does not improve the energy characteristics of the gasdynamic laser: power and efficiency. The most appreciable effect is on density distribution. Thus the telescopic cavity

arrangement with variable flux in the center is efficient from the standpoint of redistribution of the power of the outgoing radiation flux to the right and left of the axis and change in load on the mirrors.

REFERENCES

1. Kozlov, G. I., Ivanov, V. N., Selezneva, I. K., FIZIKA GORENIYA I VZRYVA, Vol 15, No 4, 1979, p 88.

2. Anan'yev, Yu. A., KVANTOVAYA ELEKTRONIKA, Vol 6, 1971, p 3.

3. Anan'yev, Yu. A., Koval'chuk, L. V. et al., KVANTOVAYA ELEKTRONIKA, Vol 1, 1974, p 5.

4. Virnik, Ya. Z., Gerasimov, V. B. et al., KRATKIYE SOOBSHCHENIYA PO FIZIKE, No 6, 1979.

5. Anan'yev, Yu. A., KVANTOVAYA ELEKTRONIKA, Vol Vol 1, 1973.

6. Anan'yev, Yu. A., Goryachkin, D. A. et al., KVANTOVAYA ELEKTRONIKA, Vol 6, 1979, p 8.

6610
CSO: 1862/12

UDC 621.375.826

CHARACTERISTIC FEATURES OF DRIVEN AMPLIFICATION OF FREE-RUNNING PHOTO-DISSOCIATION IODINE LASER PULSES: DURATION CONTROL

Moscow KVANTOVAYA ELEKTRONIKA in Russian Vol 8, No 5 (107), May 81
(manuscript received 6 Aug 80) pp 988-995

[Article by V. N. Kurzenkov]

[Text] Abstract: Results are presented from experimental studies of the process of nonlinear amplification of free-running photo-dissociation iodine laser pulses under conditions of synchronous or leading pumping of the amplifier. A sharp reduction in the pulse duration and an increase in peak power from 10^3 watts/cm^2 to a level exceeding 10^6 watts/cm^2 was demonstrated with input pulse delay times similar with respect to magnitude to the duration of the amplifier pumping pulse. Attenuation of a significant part of the trailing edge of the pulse was detected, which was caused by nonpyrolysis transition of the active medium of the amplifier to the absorbing state which is connected with the process of molecular iodine quenching of the excited atoms.

Figure 1 shows the experimental setup used to investigate the passage of light pulses emitted by a free-running photodissociation iodine laser (FL) through an amplifier. In contrast to the monopulse systems [1], in this case the interaction time of the radiation with the active medium of the amplifier is comparatively large, which permits the evolution of the pulse to be followed as the losses build up with time. As it turned out, these losses can be of a resonant nature.

The gain on the line $F = 3 \rightarrow F' = 4$ hfs of the $^2P_{1/2}$-$^2P_{3/2}$ transition of an I^{127} atom was studied in the experiment. A laser with two-tube pumping and compensated magnetic field provided an energy density at the amplifier input of 0.1-0.5 joule/cm^2 for a time of 50-70 microseconds. The amplifier was made from a cavity tube with active medium 50 cm long. Pure C_3F_7I or a mixture of it with SF_6, Xe was used as the filler. The measuring system permitted simultaneous recording of the shape of the pulses, energy, dynamic and static divergence at the amplifier input and output. The FL radiation was fed to the input of the amplifier either synchronously with pumping with a duration of τ_{pump} = 100 microseconds or with an adjustable delay

τ_{delay} = 0-250 microseconds. The measurement results demonstrated that the shape of the pulse and output power essentially depend on τ_{delay}. For τ_{delay} = 0 the duration and shape of the power-amplified pulse in practice did not change (Figure 2, a). With an increase in τ_{delay}, the pulse is shortened (Figure 2,b), and for $\tau_{delay} \geq \tau_{pump}$, it is shortened drastically (Figure 2, d), which is partially explained by the high gain at its front [2].

Attention is attracted not only by drastic shortening of the pulse on transition from synchronous pumping to driven amplification, but also the fact that in the latter case the intensity of the output signal decreases to zero, and not to the input signal level (Figure 2, c, e, f), that is, the main part of the input pulse passes through the active medium of the amplifier with amplitude attenuation. It must be noted that it is quite complicated to determine the magnitude of the attenuation in the recording system used as a result of the sharp difference of the amplitudes of the input and amplified signals. In the system shown in Figure 1, oscillographic observations of signals from photomultipliers 5, 16 recording the input and output pulses, time scans of the emission field in the far zone using image converters 10, 20 and also calorimetric measurements of the powers at the input and output of the amplifier (K_1 and K_2) were used. In Figure 2, c, e, f, oscillograms are presented which were obtained under conditions where the amplitudes of the input signal and amplified signal differ insignificantly, and with the same sensitivity of the measuring channels do not go beyond the limits of the dynamic range of the recording system. The amplitude of a lasing pulse with duration of ~100 microseconds passing through an unpumped amplifying stage is clearly visible (Figure 2, e). For the same level of input signal (Figure 2, c) the lasing pulse is not recorded at the amplifier output on completion of the amplification process in the C_3F_7I medium undergoing photolysis at a pressure of 15 mm Hg (Figure 2, f). The same picture was observed on the image converter in the time scans of the dynamics of the emission field in the far zone. The attenuation of the input signal at the time corresponding to the maximum of the lasing pulse can be $\geq$10 according to the experimental estimates. Thus, it was established experimentally that under defined conditions in the photodissociation iodine system consisting of a free-running laser and driven amplifier, the lasing pulse front nonlinear amplification stage is replaced by chopping this pulse.

The investigated system can be used without the application of additional modulators to reshape low-power pulses of arbitrary shape and duration emitted by a free-running dissociation FL laser into microsecond or shorter pulses having stable shape and maximum power at the front. The indicated method can be used in one amplifying stage to obtain pulses with a duration to 3 microseconds with respect to the base with gain of ~50 at the front with respect to the mean power level of the input signal. The front duration did not exceed 0.1 microsecond. By comparison with other methods of shaping analogous pulses used in iodine systems, for example, using magnetic fields [3, 4], this method, with its simplicity, is appreciably more efficient inasmuch as additional amplification of the pulse power is realized during the shaping process.

The energy characteristics of the output radiation with driven amplification and synchronous pumping of the stages, as the experiments demonstrated, differ significantly. With synchronous pumping (τ_{delay} = 0), when the lasing pulse is fed to

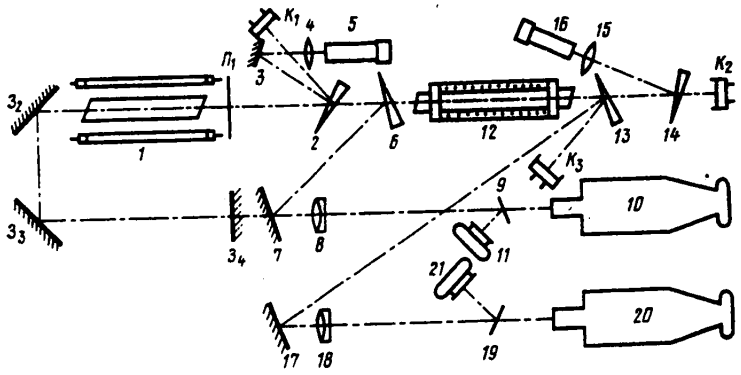

Figure 1. Diagram of the experimental setup: 1 -- FL [iodine photodissociation laser]; $П_1$ -- exposed plate with ρ = 4%; -- aluminum mirrors; 2, 6, 13, 14 -- light dividing wedges; 4, 15 -- focusing lenses; 5, 16 -- photomultipliers; 8, 18 -- projecting objectives measuring the emission divergence; 9, 19 -- glass plates; 10, 20 -- image converters; 21 -- cameras; 12 -- amplifying stage using a cavity tube; K_1-K_3 -- graphite calorimeters.

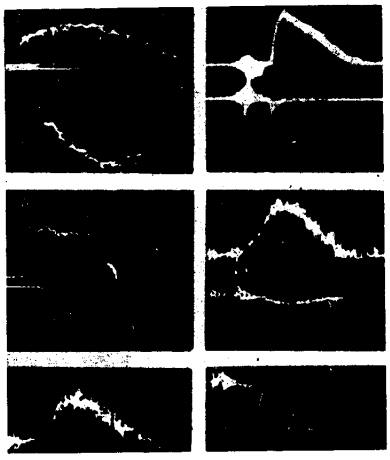

Figure 2. Oscillograms of pulses at the input (a, b, d, e -- upper signals, c) and output of the amplifier (a, b, d, e --lower signals, f). Scanning: a, b -- 10 microseconds/div; c-f -- 25 microseconds/div.

the amplifier simultaneously with the pumping pulse, additive summation of the energies of the input signal and the energy stored in the amplifier was observed. During driven amplification for $\tau_{delay} \geq \tau_{pump}$ and input signal power density of 2-7

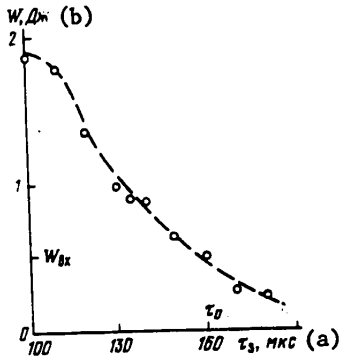

Figure 3. Power at the amplifier output W as a function of the delay time τ_{delay} for a driven amplifier.

Key: a. τ_{delay}, microseconds
b. W, joules

kilowatts/cm^2, the energy at the output corresponded to the energy stored in the amplifier, and the total energy of the long input pulse in practice had no influence on the magnitude of the output power which depended to a much greater degree on the delay time, decreasing as τ_{delay} increased. An example of this relation is presented in Figure 3. The power losses with long delays can be connected with inversion losses in the attenuation processes and, possibly, weak superluminescent (amplifier self-excitation did not occur). As follows from Figure 3, with a delay τ_0, the energy at the amplifier output becomes less than the energy of the input signal. At this time significant power gain is observed at the pulse front. The magnitude of τ_0 determined from the energy comparison, in the general case, obviously cannot characterize the time the inversion is maintained; determined by the intensity equalization time, this time was 100-400 microseconds in different series of experiments. With an increase in $\tau_{delay} > \tau_{pump}$, the output power decreased in practice to zero. The energy measurements show, therefore, that the inversion relaxation in the absence of emission is a comparatively slow process, with a characteristic time of $\gtrsim$0.1 millisecond. Here the effect of attenuation of the trailing part of the input pulse is manifested, which is expressed in the recorded energy equality in the presence of amplification at the front.

One of the causes of attenuation of the input pulse in the postamplification stage can be distributed linear losses on inhomogeneities in the active medium of the amplifier. The source of such inhomogeneities in the iodine system basically is the dynamic disturbance waves arising during pumping and leading to random deformations of the index of refraction of the medium [5, 6]. Actually, measurements of the radiation pattern demonstrated that the active medium of the amplifier is a complex dynamic lens sharply deforming the initial wave front. Depending on the delay time, the shape of the radiation pattern of the amplified emission, reflecting in practice the instantaneous pattern of the inhomogeneities, varied significantly, now acquiring the form of continuous distribution, now the form of

distribution with sharp maximum or minimum at the center. This indicates discontinuities in the radial distribtuion of the index of refraction gradient during collapse of the compression waves which is very intense under the cavity tube pumping conditions. In this case the pattern width increased from ~1 to ~10 mrad, but by estimates this is insufficient for the observed signal attenuation. The upper bound of the signal attenuation as a result of emission at inhomogeneities of the medium was determined by direct experimentation. For this purpose the amplifier was filled with a mixture of C_3F_7I (at ordinary experimental pressures) with air. As a result of collision quenching of the excited iodine atoms by oxygen molecules, the system was converted to the absorbing state. Additional amounts of an inert gas (Ar, Xe) or CO_2, SF_6, air to a total pressure of 200-600 mm Hg lowered the absorption cross section so much that the active medium became optically transparent on the transition frequency F = 3 to F' = 4. However, as is known [6], with an increase in the gas pressure the inhomogeneities do not decrease, but, on the contrary, increase. Under these conditions, for different pumping levels of the amplifier the relative reduction in the laser pulse power on passage through an optically inhomogeneous medium of a pumped amplifier did not exceed 10% together with the residual absorption. Thus, the radiation attenuation in the postamplifying stage is explained not by the losses at the inhomogeneities, but by absorption.

For analysis of the possible causes of transition of the active medium of the amplifier to the absorbing state let us consider the basic processes developed in an iodine system in the photolysis and postphotolysis stages:

$$RJ+h\nu_{н}\xrightarrow{(a)} R+J^{*}; \quad (1)$$

$$R+R\rightarrow R_2; \quad (2)$$

$$RJ \rightleftharpoons R+J; \quad (3)$$

$$J^{*}+h\nu_{с}\xrightarrow{(b)} J+2h\nu_{г}; \quad (4)$$

$$J+J+M\rightarrow J_2+M; \quad (5)$$

$$J^{*}+J_2\rightarrow J+J_2. \quad (6)$$

Key: a. pump b. l

The radicals $R = C_3F_7$ and their complexes $R_2 = C_6F_{14}$ formed under the effect of the pumping light $h\nu_{н}$ do not have absorption bands on the lasing frequency ν_l [7], and therefore they cannot lead to radiation absorption. Consequently, it is natural to assume that absorption is of a resonance nature and is realized in the $^2P_{3/2}-^2P_{1/2}$ transition of atomic iodine. It is obvious that for realization of this mechanism a large number of iodine atoms in the ground state and the presence of a process contradicting absorption saturation are required. The accumulation of iodine atoms in the ground state is realized by several channels, but the process of stimulated emission (4) itself is the basic process in the presence of the input signal. It must be noted that the transition of the medium to the absorbing state takes place in a time appreciably less than the lifetime of an atom in the excited state $T_1 \gtrsim 0.1$ millisecond and much greater than the transverse relaxation time $T_2 \lesssim 10$ nanoseconds; therefore emission cannot convert the medium to the absorbing state.

The inversion, as is easy to demonstrate on the basis of the balance equations which are valid in the given case, asymptotically approaches zero.

In parallel with process (4), a recombination process (5) develops which leads to accumulation of iodine molecules. Let us note that in the postphotolysis stage the reaction of inverse recombination of the iodine atoms with the radicals is not considered as a result of absence of radicals which are quickly bound into complexes in process (2). Molecular iodine, which is an extraordinarily effective quencher of the state $^2P_{1/2}$ leads to the occurrence of another channel for the accumulation of iodine atoms in the ground state in process (6).

As was demonstrated in [8], the process of thermal dissociation of the initial alkyl iodide (3) can take place independently, which also leads to an increase in the $I(^2P_{3/2})$ atom concentration. The rate of this process is determined by the temperature of the active medium and, according to the authors of reference [9], at temperatures close to critical (~1000 K), it can reach 10^{23} $cm^{-3} \times sec^{-1}$, which must lead to total decomposition of C_3F_7I into radicals and unexcited iodine in the time ~10 microseconds. Under the conditions of the investigated experiment, the process of intense thermal dissociation does not occur. First, this follows from the fact that amplification of the pumping pulse was observed in the slave mode. Secondly, on conversion of the amplifying stage to the lasing mode by installation of an additional resonator, a free-running pulse was recorded which lasts until the end of the pumping current pulse, which also indicates the absence of intense pyrolysis in the amplifying stage for the used pumping levels. With an increase in the pumping level, the amplifying and lasing characteristics of the stage were reproduced in the same form; therefore it is possible to assume that in the analyzed version the temperature of the active medium is far from critical. By estimates, for T = 700 K, the rate of the optical transitions exceeds by several orders the rate of thermal dissociation and, consequently, for investigation of driven amplification, it is sufficient to limit ourselves to consideration of the processes (4)-(6).

The amplifying medium can be represented in the form of a three-level system with populations of the lower and upper laser states N_1 and N_2 and the state corresponding to molecular iodine, N_3. The hfs levels can be ignored as a result of the single-frequency spectrum of the input signal (line F = 3 to F = 4 with fast relaxation between its halflevels [10]). The system of constitutive relations has the form

$$\dot{\Delta}=-\sigma/\Delta\ [1+(g_2/g_1)]-SN_3N_2\ [1+(g_2/g_1)]+2f;\ f=\dot{N}_3=kN_1^2N_0,$$

where $\Delta=N_2-g_2N_1/g_1$; σ is the amplification cross section; S is the quenching rate constant of the excited atoms by iodine molecules; k is the rate constant of the process (5); N_0 is the concentration of particles M in ternary collisions.

Let us consider the variation of the inversion with time at a fixed point of the amplifier, considering the intensity given in the form $I = I_0 \exp(-t/\tau)$, which with respect to the upper bound sufficiently reflects the shape of the pulse recorded experimentally. If we consider that after passage of the pulse front the variation of the concentration N_3 of molecular iodine in the time interval where $N_3 \ll N_1$ can be approximated by a linear function, assuming f to be a constant parameter which is varied in the calculation, then under the given assumptions, integration of the equation for the inversion gives

$$\Delta(t) = \left[\frac{g_2}{g_1} f \int_0^t e^{\xi(t)}\, \chi(t)\, dt + \Delta_0\right] e^{-\xi(t)},$$

where $\xi(t) = \sigma I_0 \tau [1 + (g_2/g_1)](1 - e^{-t/\tau}) + {}^1/_2 S f t^2$; $\chi(t) = 1 - (N - 2ft)St$; $N = N_1 + N_2 + 2N_3$.

The values of the parameters entering into the formulas are as follows: $g_2/g_1 = 1/2$; $\sigma I_0 = 10^5$ to 10^7 sec^{-1}; $k = (1\text{-}4)\cdot 10^{-31}$ cm^6/sec [11]; $S = 3.6\cdot 10^{-11}$ cm^3/sec [12]; $N_0 = 1.2\cdot 10^{18}$ cm^{-3}; $f = 10^{19}$-10^{21} $cm^{-3}\cdot sec^{-1}$; $N = 3\cdot 10^{16}$-$3\cdot 10^{17}$ cm^{-3}; τ = 5-25 microseconds.

In the investigated time interval where $N_3 << N_1$, N, the function $\chi(t)$ becomes negative, and the expression for the inversion assumes the form of a sum of a constant positive term and a negative term increasing with time, as a result of which for sufficiently large f transition of the active medium to the absorbing state is possible.

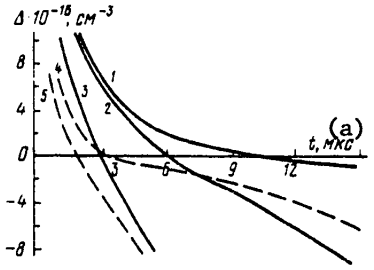

Key: a. t, microns

Figure 4. Time functions of the magnitude of the inversion for $B = (1 + g_2/g_1)\,\sigma I_0 = 6\cdot 10^5$ sec^{-1} and $f = 10^{19}$ (1), 10^{20} (2), 10^{21} $cm^{-3}\cdot sec^{-1}$ (3); $B = 1.4\cdot 10^6$ sec^{-1} and $f = 10^{20}$ $cm^{-3}\cdot sec^{-1}$ (4); $B = 10^6$ sec^{-1} and $f = 10^{21}$ $cm^{-3}\cdot sec$ (5).

The results are presented in Figure 4 from calculations of the time functions of the inversion for an initial value of $\Delta_0 = 3\cdot 10^{17}$ cm^{-3} for several values of I_0 and f. As was assumed, the functions have a sign-variable nature where the time of existence of the inversion decreases as the signal intensity increases (curves 2, 4 and 3, 5) and the rate of formation of the I_2 quencher molecules increases (curves 1-3).

As a result of stimulated transitions, the iodine atom concentration in the $^2P_{3/2}$ state reaches 10^{16} to 10^{17} cm^{-3} in ~1 microsecond, as a result $f = kN_1^2N_0$ is 10^{20} to 10^{21} $cm^{-3}\cdot sec^{-1}$ (curves 2-5). For $f = 10^{20}$ to 10^{21} $cm^{-3}\cdot sec^{-1}$ and t = 10 microseconds $N_3 \approx 10^{15}$ to 10^{16} cm^{-3}, which gives $SN_3 \approx 10^4$ to 10^5 sec^{-1}, at the same time as the signal decreasing to the level of the input signal, can give $\sigma I \approx 10^4$ to 10^5 sec^{-1}, that is, the induced transition rate is compensated by quenching of the

excited state. This fact explains the absence of absorption saturation by the emission of a free-running pulse, and the presence of absorption for the existing level of signal intensity gives grounds for assuming that $SN_3/\sigma I > 1$ for $\sigma\Delta_0 L > 2$.

The conclusion based on the determination of high efficiency of the process of recombination accumulation of molecular iodine is fully in accordance with the results of the experimental projects [7, 9] in which the formation of molecular iodine at rates of $\sim 10^{20}$ $cm^{-3} \cdot sec^{-1}$ was recorded directly for the pyrolysis mechanism of population of the state $^2P_{3/2}$ with a rate close to the rate of stimulated transitions in the amplification process. Thus, the deformation of a long laser pulse in the iodine system during nonlinear driven amplification can be explained within the framework of a model taking into account the interrelation of the collision processes of quenching the excited state of the iodine atom and recombination accumulation of molecular iodine.

Characteristic features of the amplification process in the investigated system permit its use to shape microsecond and, with additional amplification, even shorter radiation pulses. The possibility of further shortening of the pulse is easy to demonstrate in the example of an input pulse in the shape $I = I_0 \exp(-t/\tau)$. According to [13], the level 1/e output pulse duration is

$$\tau_{вых} = \tau e^{-\delta}/\sigma\eta, \quad (1)$$

Key: 1. output

where $\delta = \sigma\Delta_0 L$, and η is the total number of photons in the input pulse per unit area of beam cross section. For $\sigma\eta \sim 1$ and $\delta \sim 3$-4 the value of τ/τ_{out} will be 20-50 and, consequently, a pulse with a duration of ~10 microseconds easily shaped in a low-power preamplification stage, can be converted to a nanosecond pulse during subsequent amplification.

An experiment in successive pulse amplication in a multistage system was run on the previously used device after introducing an additional preamplifier into the system with an active medium 25 cm long, identical to the laser stage with respect to the remaining parameters. The final amplifier was a stage based on a cavity pumping tube. A laser with ring cavity and additional mirror [14] (reflection coefficient 4%) was used to suppress self-stress of the resonator mirror amplifiers of the laser. In experiments with filling the stages to a pressure of 15-30 mm Hg, the pulse power at the output was 1-3 joules. It is possible to determine the peak emission power by the burnup of a graphite calorimeter surface observed experimentally (under defined conditions and without preamplifier) under the effect of an unfocused beam. The power density required to form a flame on the graphite surface is ~5 Mwatts/cm^2 [15]. Hence it can be concluded that for a total beam power of ~20 Mwatts/cm^2 ($S = 5$ cm^2), the pulse obtained in the investigated system will have a length of ~100 nanoseconds. This conclusion agrees with the results of direct measurements of the pulse duration on a high-speed oscillograph: a halfheight pulse duration of 50-100 nanoseconds was recorded in individual experiments.

Thus, from the presented results it follows that the method of nonlinear amplification of free-running iodine laser pulses permits powerful emission pulses with

sufficient intensity, for example, for amplication in a nonlinear optical system and for the study of the interaction of radiation with matter, to be obtained simply and without additional modulators.

It is possible to formulate the basic results as follows:

1. An experimental study was made of the transmission of a free-running photodissociation laser emission pulse through a resonantly amplifying medium with synchronous or lead pumping of the amplifying stages. A sharp reduction in length of the pulse was demonstrated on transition to driven amplification.

2. It was shown that for driven amplification the laser pulse is chopped by non-pyrolysis transition of the medium to the absorbing state. This is connected with the presence of quenching collisions with I_2 molecules formed during recombination of atoms in the ground state. In this mode, even in the presence of pulse front amplification, the emission power at the amplifier output can be less than the input pulse power.

3. It is demonstrated that by optimizing the synchronization of the stages it is possible to shape emission pulses with intensity exceeding 1 Mwatt/cm^2 from low-power pulses emitted by a free-running photodissociation laser.

BIBLIOGRAPHY

1. E. Fill, K. Hohla, G. T. Schappert, R. Volk, APPL. PHYS. LETTS., No 29, 1976, p 805.

2. P. G. Kryukov, V. S. Letokhov, UFN (Progress in the Physical Sciences), No 99, 1969, p 1969.

3. I. M. Belousova, B.D. Bobrov, V. M. Kiselev, V. N. Kurzenkov, KVANTOVAYA ELEKTRONIKA (Quantum Electronics), No 1, 1974, p 1389.

4. B. V. Alekhin, B. V. Lazhintsev, V. A. Nor-Arevyan, N. N. Petrov, B. V. Sukhakov, KVANTOVAYA ELEKTRONIKA, No 3, 1976, p 2369.

5. L. Ye. Golubev, V. S. Zuyev, V. A. Katulin, V. Yu. Nosach, O. Yu. Nosach, KVANTOVAYA ELEKTRONIKA, No 6 (18), 1973, p 23.

6. L. I. Zykov, G. A. Kirillov, S. B. Kormer, S. M. Kulikov, V. A. Komarevskiy, S. A. Sukharev, KVANTOVAYA ELEKTRONIKA, No 2, 1975, p 123.

7. O. B. Danilov, V. G. Korolenko, I. L. Yachnev, PIS'MA V ZHTF (Letters to the Journal of Technical Physics), No 3, 1977, p 207.

8. V. Yu. Zalesskiy, ZHETF (Journal of Experimental and Theoretical Physics), No 62, 1971, p 892.

9. I. M. Belousova, O. B. Danilov, N. S. Kladovikova, I. L. Yachnev, PIS'MA V ZHTF, No 40, 1970, p 1562.

10. Ye. A. Yukov, KVANTOVAYA ELEKTRONIKA, No 2 (14), 1973, p 53.

11. L. S. Yershov, V. Yu. Zalesskiy, A. M. Kokushkin, KHIMIYA VYSOKIKH ENERGIY (High-Energy Chemistry), No 8, 1974, p 225.

12. C. C. Davis, R. J. Pirkle, R. A. Mcfarlane, G. J. Wolga, IEEE J., QE-12, 1976, p 334.

13. L. Frantz, J. Nodvik, J. APPL. PHYS., No 34, 1963, p 2346.

14. V. N. Kurzenkov, KVANTOVAYA ELEKTRONIKA, No 6, 1979, p 1705.

15. A. I. Barchukov, F. V. Bunkin, V. I. Konov, N. N. Kononov, G. P. Kuz'min, G. A. Mesyats, N. I. Chapliyev, KVANTOVAYA ELEKTRONIKA, No 3, 1976, p 1534.

10,845
CSO: 1862/220

UDC 662.613+535.339+533.601

CHARACTERISTICS OF EXPLOSION GAS DYNAMIC LASER UTILIZING ACETYLENE COMBUSTION PRODUCTS

Moscow KVANTOVAYA ELEKTRONIKA in Russian Vol 8, No 5 (107), May 81 (manuscript received 15 Aug 80) pp 1002-1011

[Article by A. B. Britan, V. A. Levin, S. A. Losev, G. D. Smekhov, A. M. Starik and A. N. Khmelevskiy, Mechanics Institute of Moscow State University imeni M. V. Lomonosov]

[Text]

Abstract: A study is made of the gain and specific stored energy of acetylene combustion products after the multi-nozzle grid of an explosion gas-dynamic laser (GDL). Nitrous oxide is used together with oxygen of the air as the oxidizing agent. The calculated gain is complared with the experimental data. An analysis is made of the gain and specific stored energy as functions of the composition of the mixture and flow stagnation parameters.

At this time, the creation of a highly efficient GDL and optimization of it with respect to all defining parameters are an urgent problem of laser engineering. An important characteristic of a laser system is the gain K_ν, which is related to the population of the laser levels, the inversion and, in the final analysis, defines the emission power generated by the laser. The results of comparing experimental values of K_ν with the calculated values permit determination of the possibilities and reliability of the calculation procedures [1]. In these studies the experiments in which the laser mixture is formed directly as a result of burning various fuels are of the greatest interest. Measurements performed on a laboratory setup have made it possible to obtain information under conditions approaching the conditions in a real GDL to the maximum, but the applicability of the results and the range of parameters obtained in this way are limited by the choice of a specific type of fuel [2-4].

Devices in which an additional energy source — shock waves [5, 6] or pulse discharge in a closed volume [7] -- is used, have broader possibilities. The composition and parameters of the working mixture in such experiments vary within broad limits, and this allows simulation of the flow conditions of the combustion products of a large class of laser fuels [1]. When analyzing GDL characteristics and also in experiments connected with more precise definition and checking of the calculation procedures, it appears expedient to combine several experimental setups of different types within the framework of one study. Gradual complication of the

gas composition from the simplest standard mixes investigated in a shock tube to complex multicomponent combustion products of real fuels allows significant expansion of the range of investigation and discovery of the effect of individual components on the characteristics of the GDL working media [8]. If a theoretical analysis is performed on the basis of a united calculation procedure and with a fixed set of constants, comparison of the calculation results with the experimental results permits sufficiently reliable checking of the validity of the mathematical model of the flow.

This paper is a continuation of previous shock tube studies [5, 8, 9], and it presents an analysis of inverse and energy characteristics of GDL utilizing acetylene-air fuel combustion products where nitrous oxide was investigated along with air oxygen as the oxidizing agent.

A GDL with multi-nozzle grid designed for limiting parameters p_0 = 200 atm, T_0 = 3000 K was used for the experiments. A general view of the gas dynamic module of the unit is depicted in Figure 1 in the plane of symmetry of the multinozzle grid. An explosion chamber 1 with blast cartridge 2 and connection 3 for connecting the vacuum line 4 is located on the upper end of the module. Gas escapes through the multi-nozzle grid 5 into a vacuum tank 6. The explosion chamber and nozzle grid are mounted on the upper flange of the unit 7. The explosion chamber and vacuum tank volumes are separated by a diaphragm 8. All of the connections between the subassemblies and parts of the device are sealed and permit evacuation of the system to less than 20 μm Hg. The explosion and pre-nozzle chamber volumes are in practice the same (~2 liters), and the vacuum tank 6 has a volume of 200 liters. The flow areas of the diaphragm s_1 and the holes in the upper flange 7 s_2 are of the same order (s_1/s_2 = 1.6), and they significantly exceed the flow area of the multinozzle grid (s_2/s^* = 720).

The nozzle length and its supersonic section were calculated unidimensionally [10] from the condition of maximum generated emission power for given mixture composition and stagnation parameters. The critical cross sectional height h^* = 0.35 mm was selected on the basis of calculating a two-dimensional flow, the parameters of which corresponded to optimal [11]. The nozzle expansion ratio ε = 140.

A standard system (see Figure 1) with the LG-22 continuous electric discharge CO_2-laser 9 equipped with an interrupter 10 was used to measure the gain. A capacitive filter in the electric circuit of the laser power pack made it possible to lower the level of emission intensity fluctuations of the laser to less than 3%. The amplified emission was fed through an IR filter 11 to a "Svod" type photoresistance 12.

Detonation of the mixture in the explosion chamber was initiated by detonating a constantan wire with a resistance of about 100 ohms. Measuring the pressure in the explosion chamber also permitted monitoring of the diaphragm rupture time and satisfaction of the condition of constancy of the volume during combustion of the mixture. This condition is necessary for reliable determination of the explosion product composition and parameters.

The experimental values of the pressure in the explosion chamber and before the entrance to the multi-nozzle grid measured at different initial pressures of the mix p_{init} are presented in Figure 2. The stagnating pressures obtained from the

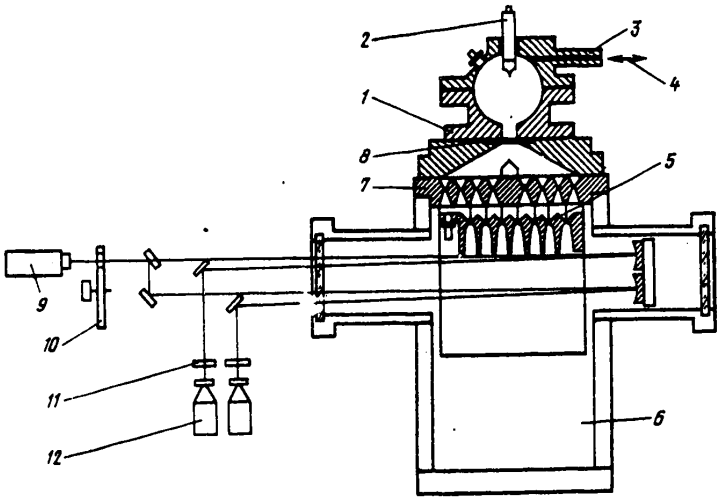

Figure 1. General view of the gas dynamic module of a pulsed GDL and gain measurement system.

thermodynamic calculation (the solid lines) [12] lie above the experimental points. Let us also note that the calculation overestimates the temperatures in the explosion products. This is indicated by a comparison of the calculated values of T_0 (see the table) with the results of the temperature measurements performed in [4]. Simple estimates permit explanation of this difference by incompleteness of combustion of the acetylene [13]. According to [4], for a mix containing 4% C_2H_2, T_0 = 1850 K, and for a mix containing 6.54% C_2H_2, T_0 = 1500 K. From the calculation it follows that combustion of the indicated mixes leads to insignificant variation (≤3%) of the total number of moles in the gas; therefore it is possible to calculate the increase in pressure in the products by using the experimental values of T_0 presented in [4]:

$$p_к/p_н = T_0\mu_н/(T_н\mu_к), \quad (1)$$
(a) (b)

Key: a. final b. initial

where μ is the molecular weight of the mix, the subscripts "H" and "K" correspond to the initial and final parameters of the mix. The values of p_{final} calculated in this way are presented in Figure 2 (the dotted line), and they agree with the experimental values within the limits of the experimental dispersion.

The range of investigated mix stagnation pressures characterizes the results of measuring the pressure ahead of the entrance to the multi-nozzle grid p_0 (see Figure 2). The increase in volume of the entire system at the time of rupture of the diaphragm and filling the prenozzle chamber lead to a pressure drop; therefore in the majority of experiments $P_0 = (0.5\text{-}0.7)P_{final}$, where P_{final} and P_0 are the maximum amplitudes of the signal from the pressure gage in the explosion chamber and ahead of the multinozzle grid, respectively.

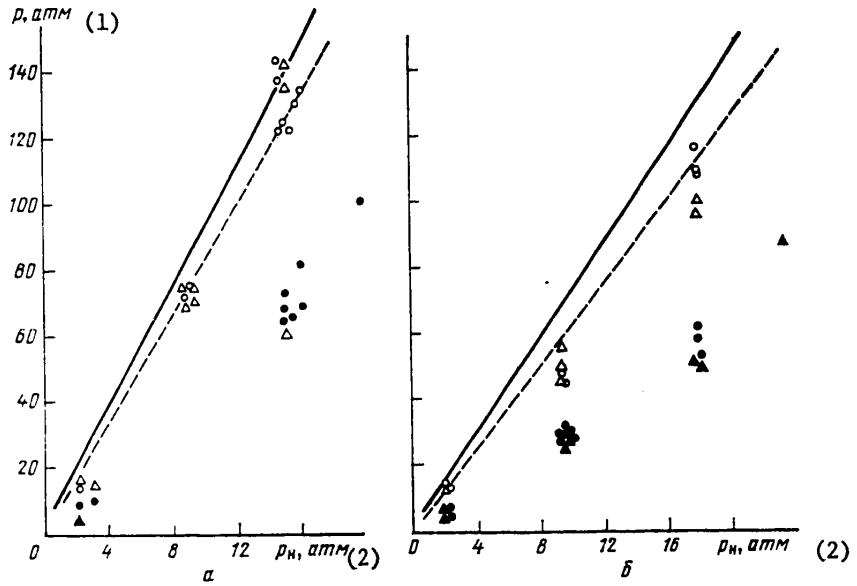

Figure 2. Pressure in the explosion products for different initial pressures of a mix of 4% C_2H_2 with air (a) and 6.54% C_2H_2 with air (b); the gain was measured along a multi-nozzle grid (○, ●) and in a single nozzle (△, ▲), and the pressure was measured in the explosion chamber (○, △) and before the entrance to the multinozzle grid (●, ▲)

Key: 1. p, atm 2. p_{init}, atm

The thermodynamic calculation data (see the table) show that in addition to the usual molecules for a CO_2-GDL (N_2, O_2, H_2O), the final products also include other components -- CO, NO, H_2, OH, O, H. Even a small amount of such admixtures leads to complication of the kinetics of the vibrational energy exchange by comparison with the model of the CO_2-N_2-O_2-H_2O mixture flow proposed in [5]. In this case, in addition to the energy exchange investigated in [5] it is necessary to consider new energy exchange channels [14-19]:

$$CO_2(00^01)+CO \rightleftarrows CO_2(00^00)+CO(v=1) \qquad W_{3,5}$$

$$CO_2(00^00)+CO \rightleftarrows \begin{cases} CO_2(11^10)+CO(v=0) \\ CO_2(03^10)+CO(v=0) \end{cases} \qquad \begin{matrix} W_{5,1,2} \\ W_{5,2} \end{matrix}$$

$$CO(v=1)+N_2 \rightleftarrows CO(v=0)+N_2(v=1) \qquad W_{4,5}$$

$$CO(v=1)+NO \rightleftarrows CO(v=0)+NO(v=1) \qquad W_{5,6}$$

$$CO(v=1)+H_2O \rightleftarrows CO(v=0)+H_2O(010) \qquad W_{5,8}$$

$$CO(v=1)+M \rightleftarrows CO(v=0)+M \qquad W^M_{5,0}$$

$$NO(v=1)+O_2(v=0) \rightleftarrows NO(v=0)+O_2(v=1) \qquad W_{6,7}$$

$$NO\ (v=1)+M \rightleftarrows NO\ (v=0)+M \qquad W^{M}_{6.0}$$

$$NO\ (v=1)+H_2O\ (000) \rightleftarrows NO\ (v=0)+H_2O\ (010) \qquad W_{6.8}$$

$$H_2\ (v=1)+M \rightleftarrows H_2\ (v=0)+M \qquad W^{M}_{11.0}$$

$$H_2\ (v=1)+H_2O\ (000) \rightleftarrows H_2\ (v=0)+H_2O\ (001) \qquad W_{11,10}$$

$$H_2\ (v=1)+OH\ (v=0) \rightleftarrows H_2\ (v=0)+OH\ (v=1) \qquad W_{11,12}$$

$$OH\ (v=1)+H_2O\ (000) \rightleftarrows OH\ (v=0)+H_2O\ (100) \qquad W_{12.9}$$

$$OH\ (v=1)+H_2O\ (000) \rightleftarrows OH\ (v=0)+H_2O\ (001) \qquad W_{12,10}$$

$$OH\ (v=1)+M \rightleftarrows OH\ (v=0)+M \qquad W^{M}_{12.0}$$

$$H_2O\ (001)+M \rightleftarrows H_2O\ (100)+M \qquad W^{M}_{10.9}$$

$$H_2O\ (100)+M \rightleftarrows H_2O\ (020)+M \qquad W^{M}_{9.8}$$

$$H_2O\ (001)+CO_2\ (00^00) \rightleftarrows CO_2\ (10^01)+H_2O\ (00^00) \qquad W_{10,1.3}$$

$$H_2O\ (100)+CO_2\ (00^00) \rightleftarrows CO_2\ (10^01)+H_2O\ (00^00) \qquad W_{9,1.3}$$

$$H_2O\ (001)+M \rightleftarrows H_2O\ (000)+M \qquad W^{M}_{10.0}$$

$$H_2O\ (100)+M \rightleftarrows H_2O\ (000)+M \qquad W^{M}_{9.0}$$

$p_н$, атм (b)	$p_к$, атм (c)	$T_р$, K	(a) Состав конечных продуктов, % CO_2	H_2O	N_2	O_2	CO	OH	O	H	H_2	NO
(d) Смесь 6,54 % C_2H_2—воздух												
4	37,1	2851	11,1	6,18	74,5	3,2	1,68	0,7	0,16	0,05	0,12	1,55
6	57,2	2875	11,77	6,19	76,6	3,2	1,65	0,7	0,157	0,05	0,12	1,58
8	76,8	2875	11,86	6,22	74,6	3,16	1,57	0,67	0,146	0,04	0,11	1,58
10	91,47	2750	12,57	6,4	75,06	3,07	0,92	0,47	0,08	0,088	0,067	1,31
(d) Смесь 4 % C_2H_2—воздух												
4	28,8	2157	8,21	4,06	76,9	9,84	0,092	0,096	0,01	$0,37\cdot10^{-2}$	$0,2\cdot10^{2}$	0,8
6	43,3	2157	8,21	4,06	76,9	9,85	0,017	0,087	$0,97\cdot10^{-2}$	$0,27\cdot10^{-3}$	$0,16\cdot10^{-2}$	0,8
8	57,7	2157	8,22	4,06	76,9	9,84	0,015	0,081	$0,84\cdot10^{-2}$	$0,22\cdot10^{-3}$	$0,15\cdot10^{-2}$	0,8
10	72,1	2157	8,21	4,07	76,9	9,85	0,014	0,077	$0,75\cdot10^{-2}$	$0,18\cdot10^{-3}$	$0,13\cdot10^{-2}$	0,8
(e) Смесь 6,67 % C_2H_2—33,33 % N_2O—60 % N_2												
1	12	3000	6,46	4,55	78,9	1,6	4,88	1,02	0,41	0,3	—	1,35
2	24,2	3039	6,95	4,73	79,1	1,43	4,48	0,92	0,31	0,22	—	1,34
4	49,1	3086	7,33	4,86	79,4	1,29	4,14	0,841	0,244	0,17	—	1,34
6	73,9	3101	7,63	4,96	79,6	1,19	3,86	0,775	0,2	0,14	—	1,31
10	124	3133	7,92	5,04	79,7	1,08	3,59	0,71	0,16	0,11	—	1,31

Key: a. end product composition, %
b. P_{init}, atm
c. P_{final}, atm
d. mix of ... with air
e. mix of ...

Here $W_{p,k}$ is the intermolecular energy exchange rate between p and k states of colliding molecules, and $W^{M}_{p,q}$ is the intramolecular exchange rate between the p and q states on collision with M(M = CO_2, N_2, CO, NO, O_2, H_2O, H_2, OH, H, O will be denoted by their numbers i = 1, 2, ..., 10, respectively); p, q, k can assume values from 0 to 12, where p = 1-3 correspond to symmetric, deformation and asymmetric

types of vibrations of the CO_2 molecule, p = 4-7 correspond to vibrations of the N_2, CO, NO and O_2 molecules, p = 8-10 correspond to deformation, symmetric and asymmetric types of vibrations of the H_2 molecule, p = 11, 12 correspond to vibrations of the H_2 and OH molecules; the combination states of the CO_2 molecule 11^10, 10^01 correspond to q = 1, 2; 1, 3. Isolating the exchange channels in the H_2O-H_2-OH system for the investigated layout and using the results of [19-21], it is possible to demonstrate that this system is described by three kinetic equations.

Actually, inasmuch as the VV'-process rates $W_{10,9}$, $W_{11,10}$, $W_{11,12}$, $W_{12,9}$, $W_{11,10}$ are approximately 10 to 100 times higher in the entire investigated temperature range of T = 200-3000 K than the process rates of VT-relaxation of the states 001 ($W^M_{10,0}$) and 100 ($W^M_{9,0}$) of the H_2O molecule, the vibrations of the H_2 molecule (v = 1, $W^M_{11,0}$) and the OH molecule (v = 1, $W^M_{12,0}$) [20, 21] and the intramolecular VV'-exchange process rate $W^M_{9,8}$, it is possible to consider that quasistationary distribution is established between symmetric and asymmetric types of vibrations of the H_2O molecule and also vibrations of H_2 and OH molecules.

The calculations performed in [21] demonstrated that during the flow of the indicated gases in a supersonic nozzle it is possible to set $T_9 = T_{10} = T_{11} = T_{12}$ for a broad range of variation of the discharge conditions and parameters. Thus, all the vibrational quantum exchange processes in the H_2O-H_2-OH mix can be described within the framework of a two-temperature model (T_8 and T_9). Let us also assume that as a result of the low concentrations of H_2O, H_2 and OH molecules in the mix (for the compositions investigated in this paper $\zeta_{H_2} \leqslant \zeta_{OH} < \zeta_{H_2O} \leq 0{,}06$, ζ_i is the mole fraction of the ith component in the mix), the variation of the population of the state 10^01 of the CO_2 molecule during nonresonant exchange with H_2O (001) and H_2O (100) is negligibly small by comparison with other processes leading to population variation of this state.

A system of kinetic equations was written in a form analogous to [15] considering the generally accepted assumptions regarding the presence of complete resonance between the states (10^00) and (02^00) of the CO_2 molecule. Joint integration of the gas dynamics and vibrational kinetics equations was performed in order to calculate the distribution of the nonequilibrium parameters of the medium. Details of the numerical integration and a description of the calculation procedure can be found in [5]. Temperature functions for $W_{p,q}$ were obtained on the basis of analyzing the results of [14, 17, 20-22].

A calculation was made in an approximation of a nonviscous nonheat-conducting gas; the flow was considered steady and linear. Studies performed in [9] show that this approximation insures sufficient accuracy when calculating the inverse flow characteristics after the tip of flat nozzles, the profile of which is shaped for attached flow with a uniform parameter field in the output cross section.

It was assumed that equilibrium dissociation of the mixture takes place at the entrance to the nozzle, and in a supersonic flow all of the chemical reactions are inhibited. For mixtures with ζ_{CO} and $\zeta_{NO} < 0{,}04$ it was assumed that $T_5 = T_4$ and $T_6 = T_7$ in the calculations.

The results of measuring p_0 were given as the initial conditions ahead of the entrance to the nozzle, and the value of T_0 was calculated according to (1) for values of p_k measured by a pressure gage installed in the explosion chamber. It was assumed that the combustion product composition corresponds to the calculated composition, and possible deviations from the calculated composition and uncontrolled admixtures have little influence on the gain.

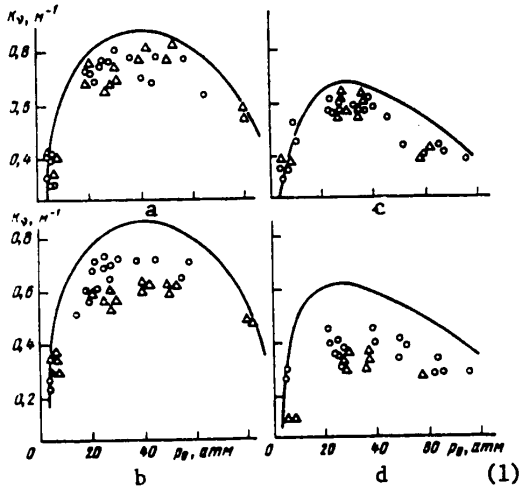

Figure 3. Gain as a function of stagnation pressure ahead of the entrance to a multi-nozzle grid: ○ — results of measurements along a multi-nozzle grid; Δ -- in a single nozzle; solid line -- calculated values; 4% C_2H_2 with air mix (a, b) and 6.54% C_2H_2 with air mix (c, d); measurements near the tip of a multinozzle grid (a, c) and down stream from the tip (b, d).

Key: 1. atm

The investigated mathematical model of the flow was used to calculate the inverse flow characteristics of acetylene combustion products. The calculated values of the gain were compared with the measurement results after the tip of the multinozzle grid which made it possible to check the applicability of the calculated model for analysis and prediction of the energy characteristics of high-temperature GDL.

Two series of experiments were run which differed with respect to composition of the acetylene-air mix. In each experiment the gain was recorded simultaneously near the tip of the multinozzle grid and 60 mm downstream from the tip. In addition, K_ν was measured for two positions of the grid with respect to the sounding plane. The measurement scheme in the plane of symmetry of the multi-nozzle grid is depicted in Figure 1. Measurements in a plane perpendicular to the plane of symmetry permitted determination of the gain in a single nozzle formed by two nozzle vanes.

The results of the first series of experiments (4% C_2H_2 with air) are presented in Figure 3, a, b. Near the tip of the nozzle (Figure 3, a) the experimental points obtained for different positions of the multi-nozzle grid agree with each other and

the calculation results within the limits of error. The maximum values of K_ν = 0.8 m^{-1} were reached for p_0 = 50 atm. In the stagnation pressure range from 20 to 55 atm, K_ν varied little, remaining within the limits of 0.7 to 0.8 m^{-1}. Close values of K_ν = 0.6-0.7 m^{-1} were obtained in [4] for a mix of 5.5% C_2H_2 with air (T_0 = 1800 K) in the pressure range of p_0 = 4-16 atm.

Satisfactory agreement of the calculated values of K_ν with the experimental values made it possible to analyze the nature of variation of K_ν with pressure. In particular, a calculation analysis of the nonequilibrium parameter distribution along the nozzle demonstrated that with an increase in p_0, deactivation of the upper laser level (00^01) and the fast, almost resonant VV'-process of the excited state (v = 1) of the N_2 molecule, increases. At the same time, the deformation vibrations of the CO_2 molecule at $p_0 \geq 30$ atm are in practice in equilibrium with the translational degrees of freedom ($T_2 \approx T$). In the p_0 = 30-60 atm range, a decrease in population of the upper laser level is compensated by an increase in the total number of inverse particles per unit volume (here the gain is maximal). With further rise in stagnation pressure, along with a decrease in population, intense broadening of the spectral line of the radiation begins as a result of more frequent molecular collisions, and the gain decreases. For $p_0 < 30$ atm, $T_2 > T$, quasistationary distribution between the asymmetric mode of CO_2 and vibration of N_2 still cannot be established, as occurs at higher values of p_0. Therefore with an increase in the stagnation pressure from 6 to 30 atm, the lower laser level begins to empty more sharply, which along with growth of the number of inverse particles per unit volume leads to growth of K_ν, in spite of a decrease in T_3 and, consequently, the population of the upper laser level. If the peak in the $K_\nu(x)$ distribution at $p_0 > 30$ atm is reached inside the nozzle, then at p_0 = 6 atm, K_ν continues to increase in the flow after the tip, that is, the maximum gain is not measured near the tip of the nozzle in either case.

Figure 3, b shows the results of measurements and calculation of $K_\nu = f(p_0)$ in another measuring cross section which is located 60 mm downstream from the nozzle tip. It is obvious that the experimental points lie below the calculated points. The maximum difference comes at pressures of p_0 = 30-50 atm, and it reaches 20%. Let us note that values of K_ν measured in a single nozzle lie below the corresponding gain measured along the grid. The indicated divergence between theoretical and experimental values obviously is explained by the peculiarities of the actual flow structure connected with the presence of shock waves and wakes beyond the edges of the nozzle vanes (the flow takeoff angle in the given grid $\theta = 11°$ is quite large). The noted divergence of the experimental values of K_ν obtained in a single nozzle and by measurements along a grid obviously is connected with stronger influence of the buildup of the boundary layer and possible separation of the flow from the parallel side walls of the channel by comparison with the effects caused by the final takeoff angle of the flow.

In order to study the possibility of obtaining coherent radiation of a medium with significantly greater vibrational energy reserve than in the preceding case, the gain was measured in the combustion products of an acetylene-air mix with high (6.54%) C_2H_2 content, combustion of which insures $T_0 \geq 2500$ K. The function $K_\nu = f(p_0)$ obtained by calculation and experimentally is presented in Figure 3, b. It is obvious that measurements at the tip of the multi-nozzle grid agree well with

the calculation results in the entire range of stagnation pressure variation p_0 = 5-100 atm. In this case the maximum of the function $K_\nu = f(p_0)$ is sharper than for a lower acetylene content in the mix. The maximum value of K_ν is reached when p_0 = 30 atm in this case. This fact is explained first of all by the fact that the combustion products contain more carbon dioxide and water vapor and somewhat less nitrogen (see the table) and, secondly, by an increase in the gas temperature in each cross section of the nozzle. On the one hand, the indicated factors lead to greater deactivation of the vibrations of the CO_2 and N_2 molecules, and, on the other hand, to a decrease in density and, consequently, the total number of particles per unit volume by comparison with the preceding case. Therefore the maximum value of K_ν is somewhat smaller and amounts to 0.65 m^{-1} (by comparison with 0.82 m^{-1} for 4% C_2H_2 in the mix).

Just as in the preceding case, the experimental values obtained in the second measuring cross section (Figure 3, d) are below the calculated ones. The maximum divergence reaches 40% in this case for p_0 = 20-40 atm. The increase in divergence between the experimental and calculated values compared to the 4% C_2H_2-air mix is explained by acceleration of the relaxation processes behind the oblique shock wave front with an increase in stagnation temperature.

Recently a great deal of attention has been given to combustion in gas dynamic lasers using nitrous oxide as the oxidizing agent [1, 23, 24]. This interest arises from the fact that the exothermal reaction of hydrocarbon combustion in an N_2O atmosphere takes place with significantly greater release of energy than when burning hydrocarbon-air mixtures. The high temperatures ($T_0 \geq 3000$ K) reached in these reactions make it possible to obtain a medium with significant energy reserve in the vibrational degrees of freedom of the molecules of the mixture and to raise the specific characteristics of the lasers.

In order to determine the possibility of raising the specific parameters of a combustion GDL, in this paper studies were made of the inverse characteristics of the medium obtained on combustion of acetylene in an atmosphere of N_2O and N_2 (6.57% C_2H_2 with 33.3% N_2O and 60% N_2), in the pressure range p_0 = 5-100 atm. The combustion products of the given mix (see the table) contain almost half as much CO_2 as the combustion products of the mixture of 6.57% C_2H_2 with air, and twice as much molecular hydrogen and CO. A calculation study of the function $K_\nu = f(p_0)$ demonstrated that in spite of high stagnation temperatures ($T_0 \approx 3100$ K) in such a mix significant gains are reached ($K_\nu \approx 0.5$ m^{-1}) in a broad range of variation of the stagnation pressure (p_0 = 25-80 atm). It is interesting that by comparison with the combustion products of acetylene-air mixes, the deactivation of the vibrations of the N_2 molecules and the asymmetric mode of CO_2 takes place appreciably less sharply than in the given case. This is caused first of all by the smaller proportions of CO_2 and H_2O and larger proportion of N_2 in the mix and, secondly, a decrease in the total number of particles per unit volume with an increase in T_0.

These factors predominate over the increase in the relaxation process rate as a result of the increased temperature. Comparison of the theoretical results and the measured values of the gain (Figure 4) demonstrated that the calculation procedure gives a correct representation of the kinetics of the physical processes in the given molecular system. The calculation results agree well with the experimental data of p_0 = 25 atm. Divergence of the experimental and calculated values of K_ν

at $p_0 > 30$ atm obviously is explained by the following causes. When using nitrous oxide as the oxidizing agent, the processes of ignition and combustion of the working mixture take place more rapidly than combustion of mixes based on air. As a result, the pressure in the explosion chamber builds up quickly, which complicates the selection of the corresponding diaphragms. In the majority of experiments for $p_{init} > 5$ atm the diaphragms ruptured appreciably before the maximum pressure was reached in the combustion products. This, in turn, led to indeterminacy in the value of p_{final} and in the combustion product composition. The possible presence of unreacted N_2O in the mixture can significantly increase the deactivation rate of the upper laser level of the CO_2 molecule (00^01), inasmuch as the 00^01 state of the N_2O molecule is energywise similar to the 00^01 state of CO_2 and (v = 1) N_2 (energy defects ΔE = 178 and 152 K, respectively). The VV'-process rates between these states are quite large ($\sim 10^{-13}$ cm^3/sec), and the relaxation processes in the N_2O itself take place at an appreciably higher rate than in CO_2 [17, 23].

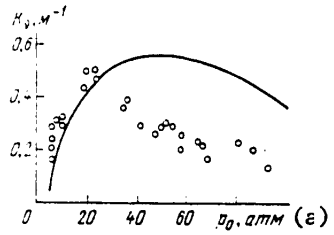

Figure 4. Gain as a function of stagnation pressure before the entrance to the multi-nozzle grid: mixture of 6.67% C_2H_2 with 33.33% N_2O and 60% N_2; -- measurements near the tip of the multi-nozzle grid; dotted line -- calculation results.

Key: a. atm

A detailed study of GDL based on acetylene combustion in an N_2O atmosphere requires more careful development of the experimental procedure and methods of calculating the combustion products of the indicated mixes.

For comparison of various fuels by efficiency it is necessary to consider the conditions which permit extraction of the energy stored in the CO_2 and N_2 molecular vibrations at the exit from the multi-nozzle grid. In the general case the problem consists in converting the maximum proportion of this energy to optical radiation before collision deactivation leads to pumping of this energy into translational and rotational degrees of freedom of the mixture molecules. Without giving specific examples of a resonator, the specific emission power stored per unit mass of the gas in the inverse transition can be determined by the expression [1, 10]

$$E_m^n = \frac{R}{\mu}\theta_{mn}\left(\mathcal{E}_3\zeta_{CO_2} + \mathcal{E}_4\zeta_{N_2} - \left[\mathcal{E}_3'\zeta_{CO_2} + \mathcal{E}_4'\zeta_{N_2}\right]_{K_{v=0}}\right), \qquad (2)$$

where $\mathcal{E}_j = r_j y_j/(1-y_j)$; $j = 3, 4$; r_j is the multiplicity of degeneration of the jth mode; θ_{mn} is the radiation frequency, K; the term $\left[\mathcal{E}_3'\zeta_{CO_2} + \mathcal{E}_4'\zeta_{N_2}\right]_{K_{v=0}}$ characterizes the mean number of quanta in the asymmetric CO_2 vibrations and the N_2 vibrations for zero

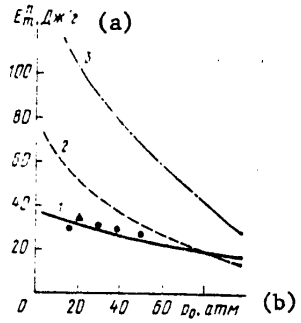

Figure 5. Specific stored energy as a function of stagnation pressure: 1 -- mixture of 4% C_2H_2 and air, T_0 = 1850 K; 2 -- mixture of 6.54% C_2H_2 and air, T_0 = 2500 K; 3 -- mixture of 6.67% C_2H_2, 33.33% N_2O and 60% N_2, T_0 = 3100 K; ● -- calculation [25]; ▲ -- calculation [2].

Key: a. joules/gram b. atmospheres

gain of the medium. The expression for $\mathcal{S}_3' = y_3'/(1-y_3')$ is easily obtained by equating the expression for the gain to zero [1, 10]. As a result, we have

$$y_3' = y_2^2 \exp\{[B_{00^01}j(j-1) - B_{10^00}j(j+1)]/T\} B_{10^00}/B_{00^01}. \quad (3)$$

For calculation of $\mathcal{S}_4' = y_4'/(1-y_4')$, we assume that $y_3' = y_4' \exp(-E_{3/4}/T)$.

The results of the calculations of E_m^n for the three investigated mixtures are presented in Figure 5. It is obvious that for each of the investigated mixes the value of E_m^n decreases with an increase in the stagnation pressure. This is explained by an increase in the relaxation rate of the energy stored in the vibrations of the gas molecules with an increase in p_0. The maximum values of the stored specific emission power are reached for low pressures of the active medium (p_0 = 6-10 atm), and for mixtures of 4% C_2H_2 with air and 6% C_2H_2 with air the maximum values are 35 and 70 joules/g, respectively, and for mixtures based on acetylene and nitrous oxide, even 125 joules/g, which is not less than the value of E_m^n for mixing lasers [23]. Inasmuch as the efficiency of the resonators with optimal parameters (transparency and flow length) can be quite high (η_p = 0.7 to 0.75) when using the indicated mixtures it is possible to obtain record high values of the specific emission power.

With respect to efficiency of acetylene-air fuels it is necessary to note that for small (~4%) acetylene contents the efficiency of such fuels is quite close to the efficiency of a benzene-air mixture. The calculated values of E_m^n obtained in [2, 25] for a benzene-air mix are shown in Figure 5 by the dots. The stagnation parameters and mixture compositions for the selected conditions compare.

Thus, the obtained results indicate the prospectiveness of using acetylene as a fuel in combustion CDL. Obviously the most prospective is use of three-component mixtures of C_2H_2-N_2O-N_2, the combustion of which makes it possible to obtain an active medium with high specific emission power ($E_m^n \simeq 120$ joules/g) for gains of $K_\nu \approx 0.4$-0.5 m^{-1}.

In conclusion, the authors express their appreciation to M. S. Dzhidzhoyev for useful discussions of the results of the paper, V. V. Lugovskiy for assistance in performing the experiments, and V. N. Makarov and Yu. V. Tunik for performing calculations when designing the nozzles.

BIBLIOGRAPHY

1. S. A. Losev, GASODINAMICHESKIYE LAZERY (Gas Dynamic Lasers), Moscow, Nauka, 1977.

2. M. G. Ktalkherman, V. M. Mal'kov, ISSLEDOVANIYE RABOCHEGO PROTSESSA GAZODINAMICHESKIKH LAZEROV (Study of the Working Process of Gas Dynamic Lasers), Edited by V. K. Bayev, Novosibirsk, ITPM, 1979.

3. N. V. Yevtyukhin, A. P. Genich, G. B. Manelis, FIZIKA GORENIYA I VZRYVA (Combustion and Explosion Physics), No 4, 1978, p 36.

4. V. N. Ivanov, "Candidates Dissertation," In-t problem mekhaniki AN SSSR, Moscow, 1978.

5. A. B. Britan, A. M. Starik, ZH. PRIKL. MEKH. I MEKHN. FIZ., (Journal of Applied Mechanics and Technical Physics), No 4, 1980, p 27.

6. A. Yu. Volkov, A. I. Demin, et al., TRUDY FIAN (Works of the Physics Institute of the USSR Academy of Sciences), No 113, 1979, p 150.

7. A. I. Odintsov, A. I. Fedoseyev, D. G. Bakanov, PIS'MA V ZHTF (Letters to the Journal of Technical Physics), No 2, 1976.

8. A. B. Britan, S. A. Losev, O. P. Shatalov, KVANTOVAYA ELEKTRONIKA (Quantum Electronics), No 1, 1974, p 2620.

9. A. B. Britan, R. I. Serikov, A. M. Starik, V. M. Khaylov, IZV. AN SSSR, SER. MEKHANIKA ZHIDKOSTEY I GAZOV (News of the USSR Academy of Sciences. Fluid and Gas Mechanics Series), No 1, 1980, p 203.

10. S. A. Losev, V. N. Makarov, KVANTOVAYA ELEKTRONIKA, No 3, 1976, p 960.

11. V. N. Makarov, Yu. V. Tunik, ZH. PRIKL. MEKH. I MEKHN. FIZ., No 5, 1978, p 23.

12. G. D. Smekhov, V. A. Fotiyev, ZH. VYCH. MATEM. N MAT. FIZ. (Journal of Computer Mathematics and Mathematical Physics), No 18, 1978, p 1284.

13. A. I. El'natanov, I. I. Srizhevskiy, ZH. FIZ. KHIMII (Physical Chemistry Journal), No 152, 1968, p 1294.

14. A. P. Genich, N. V. Yevtyukhin, S. V. Kulikov, et al., ZH. PRIKL. MEKH. I MEKHN. FIZ., No 1, 1979, p 34.

15. A. S. Biryukov, TRUDY FIAN, No 83, 1975, p 13.

16. V. V. Yegorov, V. N. Komarov, TRUDY TSAGI IM. N. YE. ZHUKOVSKOGO (Works of the Central Institute of Aerodynamics imeni N. Ye. Zhukovskiy), No 1959, 1975, p 35.

17. Yu. A. Kulagin, TRUDY FIAN, No 107, 1979, p 110.

18. G. I. Kozlov, V. N. Ivanov, I. K. Selezneva, FIZIKA GORENIYA I VZRYVA (Combustion and Explositon Physics), Vol 15, No 4, 1979, p 88.

19. V. A. Levin, A. M. Starik, IZV. AN SSSR. SER. MEKHANIKA ZHIDKOSTEY I GAZOV, No 2, 1980, p 102.

20. J. A. Blauer, G. R. Nickerson, AIAA Paper, 74-536, 1974.

21. V. A. Levin, A. M. Starik, NERAVNOVESNYYE TECHENIYA GAZA S FIZIKO-KHIMICHESKIMI PREVRASHCHENIYAMI (Nonequilibrium Gas Currents with Physical-Chemical Conversions), Moscow, Izd-vo MGU, 1980, p 25.

22. R. E. Center, J. CHEM. PHYS., No 59, 1973, p 3523.

23. A. E. Cassady, A. L. Pindro, J. F. Newton, RAKETNAYA TEKHIKA I KOSMONAVTIKA (Rocket Engineering and Astronautics), Vol 17, No 8, 1979, p 59.

24. J. Anderson, GAZODINAMICHESKIYE LAZERY. VVEDENIYE (Gas Dynamic Lasers. Introduction), Moscow, Mir, 1979.

25. R. J. Hill, N. T. Jewell, A. T. Jones, RAKETNAYA TEKHNIKA I KOSMONAVTIKA, Vol 16, No 3, 1978, p 119.

10,845
CSO: 1862/220

UDC 537.521.7

ATMOSPHERIC AIR BREAKDOWN BY NEODYMIUM LASER EMISSION FOR LARGE FOCAL POINT DIAMETERS

Moscow KVANTOVAYA ELEKTRONIKA in Russian Vol 8, No 5 (107), May 81
(manuscript received 4 Oct 80) pp 1122-1123

[Article by Ye. V. Zhuzhukalo, A. N. Kolomiyskiy, A. F. Nastoyashchiy and L. N. Plyashkevich]

[Text] Abstract: A study was made of the threshold power density w_π for large focal point diameters. A decrease in w_π from 70 to 2 GW/cm^2 was detected with an increase in d from 0.2 to 2.0 mm, which contradicts the avalanche breakdown theory, according to which for d > 100 microns w_π should be independent of d. Estimates are presented which indicate that the reduction in w_π can be explained by the effect of ion-molecular reactions.

1. Optical breakdown of air was investigated earlier in [1-5]. In the experiments of [1], a study was made of the threshold density w_π of the emission power of a neodymium laser as a function of the diffusion length Λ at an air pressure of p = 8.15 atm. It was found that in the interval of Λ = 15 to 70 microns the threshold varies approximately according to the law $w_\pi \sim \Lambda^{-3/2}$, in spite of the fact that for $\Lambda \gg \Lambda_{breakdown} \approx 5$ microns the diffusion losses of the electrons are insignificant and w_π theoretically [6] should not depend on Λ.

Efforts to explain this divergence with theory, for example, using the hypothesis of "diffusion-similar" losses [1] were unsuccessful [6]. Nevertheless, there was hope that for still larger values of Λ, in accordance with theory, the curve for w_π as a function of Λ would reach saturation. In order to check this proposition, measurements of w_π for large focal point dimensions were needed. The power of the lasers used in experiments [1-5] for this purpose was insufficient.

We performed studies of w_π on a powerful laser [7], which under unimodal conditions generated laser pulses $\tau \approx 200$ nanoseconds long (Figure 1). The radiation was focused in the air by lenses with focal lengths of f = 1.4 and 14.0 meters. The focal point diameters were d = 0.2 and 2.0 mm, respectively. Breakdown was observed for a pulse power $E \geq 4.5$ to 5 joules in the first case and $E \geq 12$ to 15 joules in the second case; the thresholds were 70 and 2GW/cm^2, respectively. A photograph of the laser spark near the threshold is shown in Figure 2, a. When the threshold was exceeded $w \gg w_\pi$, a long laser spark occurred consisting of individual

glowing centers (Figure 2, b), which resembled the spark observed by other authors (see the references in [8]).

Thus, a further reduction in w_π is detected with an increase in the size of the focal point to d = 2.0 mm. The law of variation of w_π is approximately the same as in [1]. The electron losses as a result of diffusion were insignificant in our experiments (with a "margin" of two or three orders); therefore it is natural to assume that for large focal point dimensions the breakdown mechanism is different than is proposed in avalanche theory.

Let us discuss the effect of ion-molecular reactions as one possible cause of divergence with theory [9]. The following reactions can take place in the air [10]

$$N_2^* + N_2 \longrightarrow N_4^+ + e, \; N_2^* + O_2 \longrightarrow N_2O_2^+ + e \text{ , and so on.} \tag{1}$$

The lifetime of the excited molecules depends on the optical thickness of the gas (for example, in the case of Lorentian or doppler contour of the line, the lifetime of a resonance photon $\tau^*_{eff} \sim d$ [11]); therefore an increase in size of the focal point should lead to a decrease in w_π.

Let us present some estimates. Neglecting electron diffusion, the ion multiplication rate [9]

$$\Gamma \approx (\nu_e^* \nu_i^*)^{1/2} - {}^1/_2 \tau^{*-1}_{s\phi_{(a)}}, \tag{2}$$

Key: a. eff

where ν_e^* is the molecule excitation frequency by electron impact; ν_i^* is the ionization rate according to (1). (Let us note that in the expression for ν_i^* it is possible also to consider a correction for ionization of N_2^* by laser emission; for CO_2-lasers [5] this ionization does not occur, but the effect of a reduction in w_π with size of the focal point is retained.)

Setting the reaction cross section (1) $\sigma_i^* \sim 10^{-16}$ cm^2 [10], we have $\nu_i^* \sim 10^8$ sec^{-1} and, consequently, for breakdown it is sufficient to insure that $\nu_e^* \sim 10^9$ sec, for which, in general, smaller w_π are required than in the case of direct ionization by electron impact. (Unfortunately, the performance of detailed calculations is complicated as a result of absence of reliable experimental cross sections). It is appropriate to note that the effect of ion-molecular reactions can explain deviations from Townsend's law at increased gas pressures [10] and high ionization in the glow discharge in molecular nitrogen [12].

In [13], the reduction of w_π for large d was explained by the presence of aerosol particles in the gas; unfortunately, this paper contains obvious errors (for example, the proposition of the supposed reduction in inelastic losses with excitation of resonance levels; see the criticism in [6]). Solid particles suspended in the air can produce a diffusion-like effect for long pulses $\tau \sim 1$ millisecond and relatively high particle concentration [9]. For short laser pulses it is ununderstandable how breakdown occurring, for example, near an aerosol particle, can encompass the entire

laser beam cross section, for the known mechanisms of propagation of the front (slow combustion, light detonation [6]) do not provide the required speed.

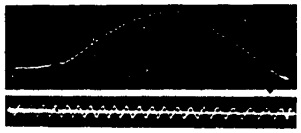

Figure 1. Shape of a laser pulse with time (sine period 20 nanoseconds).

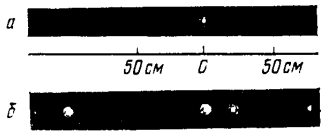

Figure 2. Photograph of a laser spark in the air (f = 14.0 m) near breakdown threshold (a) and on noticeably exceeding the threshold $w/w_{\pi} \approx 3$ (b).

The estimates made indicate that ion-molecular reactions can play an important role in optical breakdown of atmospheric air. At the same time, air breakdown under actual conditions, as follows from the accumulated facts, can have a highly complex nature, and it is impossible a priori to exclude the effect of other factors, including, for example, the presence of atmospheric aerosols.

The authors express their appreciation to N. G. Koval'skiy for his discussion.

BIBLIOGRAPHY

1. A. Hot, R. N. Yerand, D. Smith, DEYSTVIYE LAZERNOGO IZLUCHENIYA (Effect of Laser Emission), Moscow, Mir, 1968, p 42.

2. R. Tomlison, Ye. Damon, G. Busher; DEYSTVIYE LAZERNOGO IZLUCHENIYA (Effect of Laser Emission), Moscow, Mir, 1968, p 52.

3. S. Lencioni, APPL. PHYS. LETTS., 23, 12 (1973).

4. M. P. Vanyukov, et al., PIS'TA V ZhETF (Letters to the Journal of Experimental and Theoretical Physics), Vol 3, 1966, p 316.

5. D. C. Smith, APPL. PHYS. LETTS., Vol 19, 1971, p 405.

6. Yu. P. Rayzer, LAZERNAYA ISKRA (Laser Spark), Moscow, Nauka, 1974.

7. V. V. Alexandrov, et al., NUCLEAR FUSION. SUPPL., Vol 15, 1975, p 113.

8. V. A. Parfenov et al., PIS'TA V ZhETF, Vol 2, 1976, p 731.

9. A. F. Nastoyashchiy, KEANTOVAYA ELEKTRONIKA (Quantum Electronics), Vol 7, 1980, p 170.

10. E. D. Lozanskiy, O. B. Firsov, TEORIYA ISKRY (Spark Theory), Moscow, Nauka, 1975.

11. B. M. Smirnov, FIZIKA SLABOIONIZOVANNOGO GAZA (Physics of a Weakly Ionized Gas), Moscow, Nauka, 1978.

12. L. S. Smirnov, D. I. Slovetskiy, I. A. Sergeyev, TEPLOFIZ, VYS. TEMPER. (High-Temperature Thermophysics), No 15, 1977, p 15.

13. D. S. Smith, J. APPL. PHYS., No 48, 1977, p 2217.

10845
CSO: 1862/220

IN MEMORY OF EDUARD SERGEYEVICH VORONIN

Moscow KVANTOVAYA ELEKTRONIKA in Russian Vol 8, No 5 (107), May 81 p 1152

[Article by S. A. Akhmanov, N. G. Basov, F. V. Bunkin, V. S. Zuyev, Yu. A. Il'inskiy, I. N. Matveyev, V. V. Migulin, A. L. Mikaelyan, A. M. Prokhorov, V. S. Solomatin, M. F. Stel'makh, A. P. Sukhorukov and V. S. Fursov]

[Text]

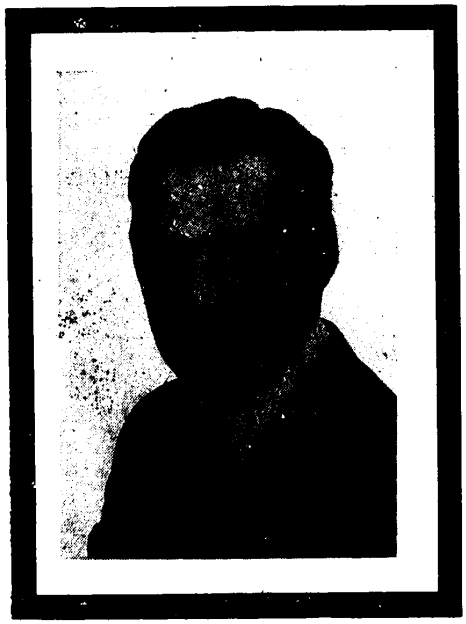

Soviet science suffered a severe loss on 12 March 1981, when a great scientist in the field of quantum electronics and nonlinear optics, doctor of physical and mathematical sciences, USSR State Prize Laureate Eduard Sergeyevich Voronin died at the age of 53.

E. S. Voronin devoted more than 30 years of his life to science, in particular, radio physics and nonlinear optics. He performed a number of important studies in the field of the physics of nonlinear oscillations, including pulse synchronization

of autooscillators. He obtained the brightest results in the field of coherent and nonlinear optics when studying the processes of the conversion of infrared radiation to the visible band using parametric interactions of light waves. Recently Eduard Sergeyevich conducted intense studies in the field of nonlinear adaptive optics.

E. S. Voronin was awarded the USSR State Prize in 1975 for his work in applied optics.

E. S. Voronin was an active member of the Board of Editors of the KVANTOVAYA ELEKTRONIKA (Quantum Electronics) Journal; he was on a number of scientific problem and coordination councils, and he participated in the organization of all-union conferences on quantum electronics and laser physics.

All of the scientific life of E. S. Voronin was continuously connected with Moscow State University. He was for a long time a co-worker with R. V. Khokhlov in the physics department of Moscow State University. A talented scientist and teacher, Eduard Sergeyevich educated many students.

E. S. Voronon, a member of the Communist Party, combined his scientific and pedagogical activity with a large amount of responsible social work.

Eduard Sergeyevich always distinguished himself by exceptional cheerfulness, warmth and responsiveness in his relations to people.

The bright memory of Eduard Sergeyevich Voronin will remain in our hearts forever.

10,845
CSO: 1862/220

UDC 621.378.33

CLOSED-CYCLE FAST-FLOW PULSED CO_2 LASER WITH CARBON DIOXIDE RECOVERY UNIT

Moscow KVANTOVAYA ELEKTRONIKA in Russian Vol 8, No 5 (107), May 81 (manuscript received 24 Oct 80) pp 1134-1136

[Article by A. V. Artamonov, A. G. Borkin, A. P. Dzisyak, S. V. Drobyazko, A. I. Lazurchenkov, A. A. Nekrasov and Yu. M. Senatorov]

[Text]

Abstract: The possibility of stabilizing the radiation power and mixture composition in a repetitively pulsed CO_2-laser by palladium-catalytic regeneration of carbon dioxide is demonstrated. The small-signal gain was measured in working mixtures of various compositions, and it was demonstrated that the decrease in gain with dissociation of CO_2 is connected both with a decrease in the CO_2 concentration and with an increase in the CO and O_2 concentrations.

1. In closed-cycle CO_2-lasers, the decrease in radiation power is primarily connected with dissociation of the carbon dioxide [1-5]. In order to prevent a decrease in power, the working medium of a CO_2-laser must be regenerated. One of the methods of stabilizing the chemical composition of the working mixture of the laser and, consequently, the output power of the emission is heterogeneous-catalytic oxidation of carbon monoxide [1, 6].

In this paper a study is made of the possibility of stabilizing the emission pulse power by palladium-catalytic regeneration of carbon dioxide, and the weak-signal gain is measured in laser mixtures of various compositions.

2. The experiments were run on a repetitively pulsed fast-flow laboratory CO_2-laser with transverse pumping of the gas [7]. The total volume of the gas channel was 1.5 m^3, the electrode gap volume was 0.8 liters. The gas was pumped by a 2DVN-1500 pump. All of the experiments were run on a mixture of CO_2: N_2: He = 10 : 45 : 45 with a total pressure of 80 mm Hg. The energy input to the discharge gap was 175 joules/liter-atmosphere, and the pulse repetition frequency was 200 hertz. The temperature of the gas and the catalyst was measured by chromel-copel thermocouples. The gas flow rate through the reactor was determined using a Pitot-Prandtl tube with MKM-250-0.02 differential micromanometer. The gas mixture composition was analyzed on the LKhM-8MD chromatograph. The pulse radiation power was measured by the TPI-1 graphite calorimeter in the monopulse mode. The gain was measured by the transmission method by a stable CO_2-laser using the procedure outlined in [8]. Palladium

black on a stainless steel carrier made in the form of grids with wire diameter of 0.25 mm and mesh size of 0.5 mm^2 was used as the catalyst. The palladium content was 0.3% by weight. The total weight of the catalyst was 0.5 kg, and the service life, more than 100 hours.

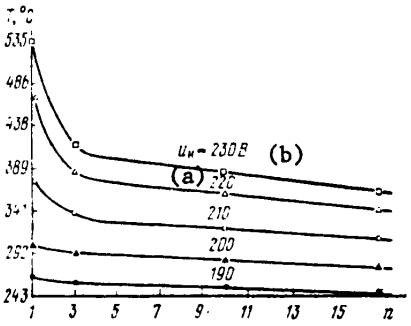

Figure 1. Variation of the grid temperature with respect to reactor length for various heating element voltages (n -- grid number).

Key: a. heating element b. volts

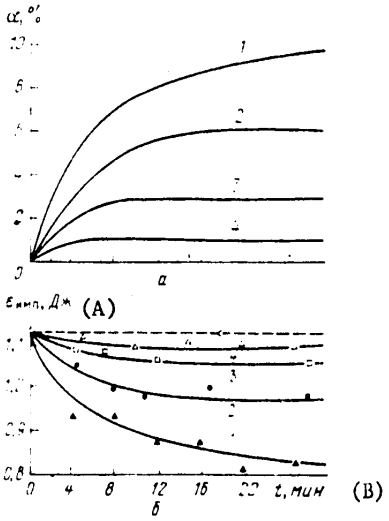

Figure 2. Degree of dissociation α (a) and pulse emission power ε_{pulse} (b) as a function of time without CO_2 recovery (1) and with recovery at various catalyst temperatures: T = 250 (2), 330 (3) and 400° C (4).

Key: A. ε_{pulse}, joules
B. t, minutes

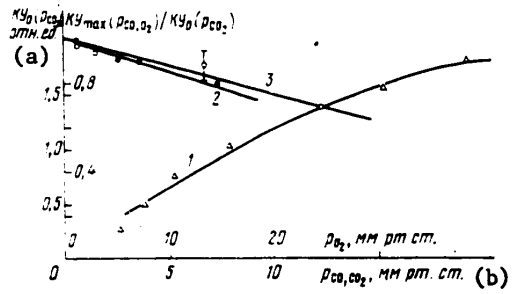

Figure 3. Gain at the peak as a function of CO_2 pressure (1) and CO (2) and O_2 (3) additive pressure at W = 105 joules/(liter-atmosphere), p = 150 mm Hg, N_2:He = 1:1.

Key: a. relative units
b. mm Hg

3. The catalytic reactor was a metal box with 5 kW adjustable-power coil heating element at the entrance. The reactor was installed in the gas loop channel (after the discnarge chamber) and covered part of its cross section. The grids with palladium black were installed across the flow with a spacing of 2 mm between them. The pressure drop on the cold catalytic reactor did not exceed ~10 mm H_2O for a gas velocity in the free channel of ~20 m/sec. The temperature variation of the catalyst grids with respect to reactor length (along the flow) is given in Figure 1. The temperature gradient is explained by radiant heating of the first grids. It was discovered that the given catalyst is unstable at temperatures above 500° C. This is probably connected with a sharp decrease in adhesion of the palladium black to the metal substrate.

4. Figure 2 shows the degree of dissociation of the CO_2 (α) and the pulse emission power as functions of time for a mixture of CO_2:N_2:He = 10:45:45. The curves 1 show the variation in the degree of dissociation and pulse power without carbon dioxide recovery. For a value of $\alpha \approx 10\%$, the decrease in the pulse emission power is ~27%. With palladium-catalytic recovery of the CO_2, the degree of dissociation decreases as its temperature rises (curves 2-4).

With a decrease in the degree of dissociation, the pulse power increases (curves 2-4) and for α = 1% it differs by ~3% from the initial power. Inasmuch as the emission power increases linearly as a function of the CO_2 content in the mixture only for a proportion of CO_2 < 15%, the results and the conclusions presented in this paper pertain to ternary mixtures with low CO_2 content [4].

When equilibrium is reached, the carbon monoxide formed as a result of CO_2 dissociation must be "burned" in the catalyst, that is,

$$\alpha_0 = a\beta(\alpha_0 + \alpha_n). \quad (1)$$

where α_0 is the degree of dissociation of the CO_2 in a single pass of the gas through the discharge chamber; α_n is the equilibrium degree of dissociation of CO_2; β is the degree of conversion of carbon monoxide in the catalytic reactor; a is the

proportion of the flow of gas through the catalytic reactor (considering the temperature in the reactor [9]).

As a rule, $\alpha_n \gg \alpha_0$, and it is possible to make the value of β equal to one, increasing the amount of catalyst and its temperature; therefore from (1)

$$\alpha_n = \alpha_0/a. \qquad (2)$$

Inasmuch as $\alpha_0 = k_1 n_e \tau$, where k_1 is the CO_2 dissociation rate constant for electron impact; n_e is the electron concentration; τ is the time the gases are in the discharge zone in a steady fast-flow laser or the pulse duration in a repetitively pulsed CO_2-laser, from (2) it follows that the equilibrium degree of dissociation increases with an increase in E/p and the specific energy input to the discharge W. For stabilization of α_n on the given level with an increase in α_0 it is necessary to increase the proportion of the gas flow passing through the recovery unit. The value of α_0 in a continuous-emission CO_2-laser with average power of 5 kilowatts reaches $\sim 2 \cdot 10^{-3}$. In this case 20% of the gas flow must be passed through the catalytic recovery unit with $\beta = 1$ to maintain α_n at a level of 1%.

5. On dissociation of CO_2, carbon monoxide and oxygen appear in the working gas mixture. The carbon monoxide and oxygen are the components which, according to the published data, have a negative influence on the radiation output power and gain [10-14]. In order to estimate the influence of the individual components on the decrease in pulse radiation power, the $gain_{max}$ was measured in gas mixtures of different chemical composition. The results presented in Figure 3 indicate that a decrease in CO_2 concentration, just as an increase in the CO and O_2 concentrations in the mixture, lead to a decrease in the gain. The primary contribution (~60%) to the decrease in gain is made by the change in carbon dioxide concentration, but when solving the problem of stabilizing the radiation output power, the appearance of carbon monoxide and oxygen cannot be neglected.

6. Thus, this paper allows the following conclusions to be drawn.

The application of a palladium catalyst permits stabilization of the chemical composition of the working medium and pulse radiation power of a closed-cycle CO_2-laser.

The decrease in $gain_{max}$ with an increase in CO and O_2 concentrations requires caution when using additives to stabilize the chemical composition (CO, O_2, and so on), for they can lead to a decrease in the radiation output power.

The equilibrium degree of dissociation of CO_2 is proportional to the specific energy input, it increases with an increase in E/p and is inversely proportional to the proportion of the gas flux fully recovered in the recovery unit.

BIBLIOGRAPHY

1. A. C. Eckbreth, P. R. Blaszuk, AIAA 5TH FLUID AND PLASMA DYNAMICS CONF., Boston, June 26-28, 1972.

2. S. S. Vorontsov, A. I. Ivanchenko, R. I. Soloukhin, A. A. Shepelenko, PRIK. MEKH. I MEKHN. FIZ. (Applied Mechanics and Technical Physics), No 3, 1977, p 6.

3. P. W. Pace, M. Lacombe, IEEE J. QE-14, 1978, p 263.

4. V. I. Garashchuk, I. A. Vasilets, KVANTOVAYA ELEKTRONIKA (Quantum Electronics), No 6, 1979, p 1783.

5. S. F. Balandin, V. A. Plastinin, et al., TEZISY DOKLADOV. II VSESOYUZ. SEMINARA PO FIZICHESKIM PROTSESSAM V GAZOVYKH OKG (Topics of Reports. Second All-Union Seminar on Physical Processes in Gas Lasers), Uzhgorod, 1978.

6. N. G. Basov, I. K. Babayev, V. A. Danilychev, et al., KVANTOVAYA ELEKTRONIKA, No 6, 1979, p 772.

7. A. A. Vedenov, S. V. Drobyazko, M. M. Korzinkin, KVANTOVAYA ELEKTRONIKA, No 7, 1980, p 1186.

8. R. R. Jacobs, REV. SCI. INSTR., No 44, 1973, p 1146.

9. G. N. Abramovich, PRIKLADNAYA GAZOVAYA DINAMIKA (Applied Gas Dynamics), Moscow, Nauka, 1976.

10. Ye. N. Lotkova, V. N. Ochkin, N. N. Sobolev, IEEE J. QE-7, 1971, p 396.

11. V. N. Ochkin, TRUDY FIAN (Works of the Physics Institute of the USSR Academy of Sciences), No 78, 1974, p 3.

12. S. S. Alimpiyev, N. V. Karlov, Yu. B. Konev, G. P. Kuz'min, R. P. Petrov, RADIOTEKHNIKA I ELEKTRONIKA (Radio Engineering and Electronics), No 15, 1970, p 2361.

13. P. Bletzinger, D. A. La Borde, W. E. Bailey, W. H. Long, P. D. Tannen, A. Garscadden, IEEE J. QE-11, 1975, p 317.

14. A. L. S. Smith, T. N. Bett, P. G. Browne, IEEE J. Q-11, 1975, p 335.

10,845
CSO: 1862/220

NUCLEAR PHYSICS

UDC 539.125.5.172

DIFFRACTION METHODS IN NEUTRON PHYSICS

Moscow DIFRAKTSIONNYYE METODY V NEYTRONNOY FIZIKE in Russian 1981 (signed to press 3 Jun 81) pp 2-4, 215-216

[Annotation, preface and table of contents of book "Diffraction Methods in Neutron Physics", by Yuriy Andreyevich Aleksandrov, Eduard Ivanovich Sharapov and Laslo Cher, Energoizdat, 1400 copies, 216 pages]

[Text] The principal content is a description of methods of doing diffraction experiments using both steady-state and pulsed neutron sources.

Intended primarily for experimental physicists who are not specialists on structural neutron diffraction studies, but require a text to acquaint themselves with modern methods of neutron diffraction. Also of use to students in advanced courses speicalizing in the field of neutron physics.

Tables 6, figures 137, references 284.

Preface

Recent years have witnessed considerable progress in methods and experimental equipment in neutron diffraction studies, and also an expansion of the use of neutron diffraction methods in the field of nuclear physics, solid state physics and biology. Therefore, in dealing with some problems that involve neutron physics, researchers who are not specialists in the area of neutron diffraction studies need to familiarize themselves with modern diffraction techniques. However, it is not easy to find a suitable overview that will introduce the non-specialist to the broad range of pertinent questions (an exception might be D. Bacon's well-known monograph "Neutron Diffraction" [Russian translation published by Izdatel'stvo inostrannoy literatury, Moscow, 1957]). This book is an attempt to fill the gap.

In addition to describing methods of doing diffraction experiments with steady-state and pulsed neutron sources, the authors give consideration to problems of exact determination of the integral intensity of diffraction reflection, and to the introduction of various corrections in experimental results.

The book deals mainly with problems relating to processes of elastic scattering of unpolarized neutrons, since it is the authors' feeling that problems of the dynamics of crystals, as well as problems relating to work with polarized neutrons, should be covered in separate monographs.

The book consists of eight chapters and an appendix. Chapter 1 contains minimum information on crystallography necessary for an understanding of the material presented later in the book. Chapters 2 and 3 examine the principal questions of the kinematic and dynamic theories of neutron diffraction. Currently there is intense development of research on neutron-optics effects based on the dynamic theory of neutron diffraction. The use of neutron-optics methods of research, in particular neutron interferometery is of promise in the study of neutrons, and also in solving some problems of nuclear and solid-state physics. Chapter 4 is devoted to the introduction of various corrections in experimental results (for extinction, absorption, diffuse scattering and the like). In doing research that involves the determination of the intensity of Bragg reflection of neutrons from single crystals and powders, it is very important to account for such corrections. Chapters 5-7 relate to techniques for doing diffraction experiments on steady-state reactors. They give descriptions of different kinds of neutron diffractometers (including existing facilities) and methods of working with them, examine such characteristics of these facilities as luminosity and resolution, and some other problems of neutron optics of diffraction systems, and give the latest advances in making and using crystal monochromators. Chapter 8 is devoted to a detailed description of diffraction experiments with the use of pulsed neutron sources. Work with pulsed neutron sources (pulsed reactors, accelerators with a target) has its own peculiarities. The material of this chapter is based mainly on experience accumulated in working with the IBR-30 pulsed reactor in Dubna. Recent years have seen an expansion of the use of methods of neutron diffraction not only in physics, but also in biology. Therefore we have considered it appropriate to give in the appendix some examples of the investigation of biological objects by the methods of neutron diffraction. To some extent these examples illustrate the use of the methods that we have considered. Other examples can be found in the recently published book "Strukturnaya neytronografiya" [Structural Neutronography] by Yu. Z. Nozik, R. P. Ozerov and K. Khennig, Moscow, Atomizdat, 1979.

The authors have assumed that the reader is familiar with the basics of techniques of neutron experiments, and therefore problems involving methods of neutron registration have not been brought up to any extent in the book.

The book uses customary units of measurement (eV, Å, b and so on). Their relation to the corresponding SI units is as follows: 1 Å = 10^{-10} m, 1 eV = $1.6 \cdot 10^{-19}$ J, 1 mm Hg = 133.3 Pa, 1 b = 10^{-28} m^2, 1 fm = 10^{-15} m, 1 atm = 101,325 Pa, 1 Oe = 79.6 A/m.

We are sincerely grateful to R. P. Ozerov, Yu. M. Ostanevich and A. B. Popov, who examined the manuscript of the book and made a number of important comments, and also to I. Gladkikh and L. A. Podgorova for considerable assistance with preparation of the manuscript.

Yu. Aleksandrov,
E. Sharapov,
L. Cher,
Dubna, December 1980

Contents

6610
CSO: 1862/28

OPTICS AND SPECTROSCOPY

UDC 621.373.826

USE OF DEGENERATE PARAMETRIC PROCESSES FOR WAVE FRONT CORRECTION (SURVEY)

Moscow KVANTOVAYA ELEKTRONIKA in Russian Vol 8, No 5 (107), May 81
(manuscript received 17 Dec 80) pp 917-935

[Article by E. S. Voronin (deceased), V. M. Petnikova and V. V. Shuvalov, Moscow State University imeni M. V. Lomonosov]

[Text]

Abstract: The results obtained by the authors when studying wave front reversal in degenerate parametric processes are reviewed. The problem of radiation signal transmission along an optically inhomogeneous path is investigated. A model of a phase distortion compensation system with wave front reversal in the parametric processes is constructed. The mathematical apparatus of the scattering coefficient was used to discover the limiting possibilities of the method. It is demonstrated that satisfactory compensation for the distortions takes place when the radiation converter resolves the effective size of the inhomogeneities. The possibilities of practical implementation of such systems are discussed.

1. Introduction

Recently, significant interest has been manifested in the use of the methods of nonlinear optics to compensate phase wave front distortions arising when light passes through an optically inhomogeneous medium [1-6]. The field complex-conjugate to the distorted field required for this purpose can be obtained for various types of stimulated scattering of light [2, 7, 8], and in degenerate parametric processes -- three-photon [3]

$$2\omega - \omega \rightarrow \omega \qquad (1)$$

and four-photon processes [1, 4]

$$\omega + \omega - \omega \rightarrow \omega. \qquad (2)$$

Along with equality of the frequencies of the incident and reversed fields amplification of the reflected signal is possible in the latter. It is this aspect of the matter that interests researchers.

First of all, it is necessary to discover the limiting possibilities of phase distortion compensation systems with wave front reversal (WFR) in degenerate parametric processes. For this purpose it is necessary to discover the factors determining the degree of reconstruction of the initial wave front and establish the criterion of satisfactory compensation of the distortions for specific physical problems.

In the first papers on WFR, the reversal system itself was assumed to be ideal. This meant that the reversed field was considered an exact complex-conjugate copy of the scattered field. In reality, any nonlinear process used for WFR filters the spatial signal radiation spectrum. Therefore for successful reconstruction of the initial wave front it is necessary to impose defined restrictions on the parameters of the inhomogeneous medium causing the distortions and the parametric converter. At the present time this approach is being used to study the possibilities of applying such systems in solving one of the basic problems of adaptive optics -- transmission of time and space-modulated signal radiation over an optically inhomogeneous path.

2. Calculation Procedure

Let a signal radiation plane wave with amplitude E_1 traveling through an optically inhomogeneous medium located in the plane $-z_0$ (Figure 1), acquire a phase lead $\phi(\rho)$, where ρ is the transverse component of the radius vector in a polar coordinate system. The radiation converter I will be considered to be a linear spatial filter [9]. In the simplest case it can be described either by the transmission coefficient $K(\kappa)$, where κ is the transverse projection of the wave vector, or by the scattering function $\Gamma(\rho)$. Let us remember that $K(\kappa)$ and $\Gamma(\rho)$ are related to each other by a Fourier transformation [9].

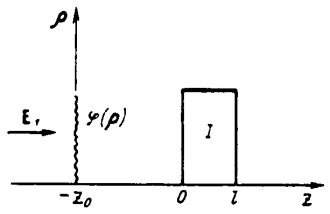

Figure 1. Model of a phase distortion compensation system

Using these values it is easy to define both the spectral and spatial field distribution after passing through the inhomogeneous medium a second time:

$$E_2(\rho, -z_0)=E_1^* \int \exp\{i\varphi(\rho)-i\varphi(\rho')\}\,\Gamma(\rho-\rho')\,d\rho'; \quad (3)$$

$$E_2(\varkappa, -z_0)=E_1^* \int K(\varkappa')\Phi(\varkappa-\varkappa')\Phi^*(-\varkappa')d\varkappa'. \quad (4)$$

Here $\Phi(\varkappa)=(2\pi)^{-2}\int \exp\{i\varphi(\rho)+i\varkappa\rho\}\,d\rho$ is the Fourier transform of the function $\exp\{i\varphi(\rho)\}$.

The degree of distortion compensation can be characterized by the ratio of the spectral amplitudes of the initial and reconstructed fields. However, inasmuch as this ratio depends on the efficiency of nonlinear interaction, normalization by the maximum value of the conversion factor K_0 is required:

$$\tau_1 = E_2(0, -z_0)/K_0 E_1^* \delta(\varkappa). \quad (5)$$

We shall consider the distortion compensation satisfactory if the reconstructed plane wave contains no less than 0.5 $|K_0|^2$ of the energy of the initial wave, that is,

$$|\tau_1|^2 \geqslant 1/2. \quad (6)$$

The degree of distortion compensation can also be characterized by the overlap integral [10]

$$I = |\int E_1(\rho, -z_0) E_2(\rho, -z_0) d\rho|^2 / \int |E_1(\rho, -z_0)|^2 d\rho \int |E_2(\rho, -z_0)|^2 d\rho.$$

However, this value is not so descriptive as the reconstruction coefficient (5) [11, 12] and, what is especially important, experimental determination of it turns out to be much more complicated.

The general expressions obtained (3)-(5) are valid both for three-photon and four-photon parametric radiation converters. A detailed calculation is possible considering the explicit form of the transmission coefficient and specific definition of the model of the distorting medium.

3. Models of a Thin Inhomogeneous Medium

1. Regular Phase Grating. Let us consider a model of a regular phase grating $\phi(\rho) = a \cos \gamma x$. The parameter a characterizes the fluctuation amplitude of the optical path, that is, the fluctuations of the index of refraction, the roughness of the medium, and so on. The transverse dimension of the inhomogeneities is defined by the value of γ^{-1}. For this model

$$\Phi(\varkappa) = \delta(\varkappa_y) \sum_{m=-\infty}^{\infty} i^m J_m(a) \delta(m\gamma + \varkappa_x), \quad (7)$$

where J_m is an mth-order Bessel function. The spectrum of a singly scattered field is equidistant. With an increase in a, a greater and greater proportion of the energy of the initial wave is pumped to the side peaks. It is obvious that reconstruction of the wave front takes place only when several peaks of the spatial spectrum containing the main part of the scattered field energy fall in the radiation converter band.

The compensation system can operate efficiently at $a \leq 1$ and with a transverse scale of the inhomogeneities $\gamma^{-1} \geq \Delta x_0$, where Δx_0 is the width of the scattering function of the radiation converter. With an increase in a restrictions must be imposed on the effective size of the inhomogeneities, which is determined by the width of the spatial spectrum (7).

2. Random Phase Grid. The phase lead in an optically inhomogeneous medium is a random function of the coordinates where the process $\xi = \exp\{i\varphi(\rho)\}$ is homogeneous, that is,

$$\langle \exp[i\varphi(\rho) - i\varphi(\rho')] \rangle = B(\rho - \rho'). \quad (8)$$

Here, averaging (4), we find

$$\tau_1 = K_0^{-1} \int K(\varkappa') S(-\varkappa')\, d\varkappa' = K_0^{-1} \int B(\rho)\, \Gamma(\rho)\, d\rho.$$

Here $S(\kappa)$ is the spectral density of the process ξ. Hereafter, we shall consider that $B(\rho) = \exp(-\rho^2/b^2)$ and $S(\varkappa) = 4\pi b^{-2} \exp(-\varkappa^2 b^2/4)$, where b characterizes the size of the inhomogeneities of the distorting medium.

The reconstruction effect is manifested more strongly the smaller the ratio of the width $\Delta_{\kappa\xi}$ of the spatial spectrum of the process ξ to the pass band of the converter $\Delta_{\kappa 0}$. For $\Delta\varkappa_\xi/\Delta\varkappa_0 \ll 1$ we obtain $\tau_1 \approx \int S(\varkappa)d\varkappa = 1$, , and on satisfaction of the opposite inequality distortion compersation does not occur.

It is easy to see that the preliminary qualitative conclusions obtained using the two models are analogous.

4. Radiation Converter Models

1. Three-photon Interaction. Degenerate three-photon interaction (1) has been studied quite well. Its basic advantage is comparatively high quantum efficiency, and its disadvantage is the presence of rigid conditions of phase synchrony, constricting the angular aperture of the converter. Nevertheless, the process can be used for WFR in cases where the distortions introduced by the inhomogeneous medium are comparatively small.

For low-efficiency three-photon interaction the conversion factor and the scattering function are well known [13, 14]:

$$K(\varkappa, \beta) = K_0 \frac{\sin \alpha\varkappa^2}{\alpha\varkappa^2} \exp(-i\beta\varkappa^2); \tag{9}$$

$$\Gamma(\rho, \beta) = \left\{ \operatorname{si}\frac{\rho^2}{4(\alpha+\beta)} + \operatorname{sign}(\alpha-\beta) \operatorname{si}\frac{\rho^2}{4(\alpha-\beta)} - \right.$$
$$\left. - i\left[\operatorname{ci}\frac{\rho^2}{4(\alpha+\beta)} - \operatorname{ci}\frac{\rho^2}{4(\alpha-\beta)}\right]\right\}. \tag{10}$$

Here $\beta(z) = (\lambda/4\pi)[z - 2z_k - l(2/n-1)]$ characterizes the detuning from the optimal focusing plane (that is, the plane in which $\beta = 0$), and the parameter $\alpha = \lambda l/4\pi n$ characterizes the width of the phase synchrony angle or the resolution of the converter; λ is the signal radiation wavelength; l is the nonlinear crystal length; n is the index of refraction; $-z_k$ is the longitudinal coordinate of the initial point.

Using (4), (5), (7) (9), it is possible to determine the reconstruction coefficient. Thus, for a regular model of the distorting medium

$$\tau_1 = \sum_{m=-\infty}^{\infty} J_m^2(a) \frac{\sin \alpha m^2\gamma^2}{\alpha m^2\gamma^2} \exp(i\beta m^2\gamma^2). \tag{11}$$

Figure 2 shows the reconstruction coefficient (11) as a function of the transverse dimension of the inhomogeneities and depth of fluctuations of the optical path for $\beta = 0$. For a random phase grid:

$$\varkappa_1 = \frac{2\pi}{b\alpha}\left[\operatorname{arctg}\frac{4b\alpha}{b^2+4(\beta^2-\alpha^2)} + \right. \tag{12}$$

$$\left. + s\pi - \frac{i}{2}\operatorname{sign}\beta \ln\frac{b^2+4(\alpha+\beta)^2}{b^2+4(\alpha-\beta)^2}\right];$$

$$s = \begin{cases} 1 & \text{for } b^2+4(\beta^2-\alpha^2)\geqslant 0; \\ 0 & \text{for } b^2+4(\beta^2-\alpha^2)<0. \end{cases}$$

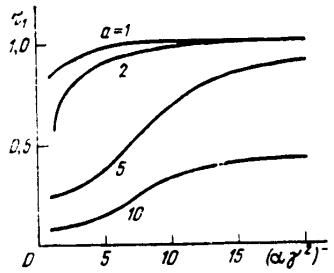

Figure 2. Reconstruction coefficient for a regular phase grating.

In practice, the phase distortion compensation system can be constructed as follows [11]. It is necessary to find the position of the optimal focusing plane, that is, the plane in which the scattering function (10) has the least width. In this plane the procedure for the determination of which can be analogous to the procedure in reference [14], the reversed field wave front is closest to the phase-conjugate front of the scattered field. It is necessary to use a special optical system to transfer the image from this plane to the plane $z = -z_0$ [11]. The inexactness of the image is characterized in (9), (10) by the parameter β and leads to the appearance of phase lead in the reconstructed plane wave which depends on the direction of propagation of the wave. Figure 3 shows the phase and modulus of the reconstruction coefficient (12) as functions of the effective size of the inhomogeneities and the parameter β.

Calculation by criterion (6) shows that the investigated compensation system can be used for the following ratios of the parameters of an inhomogeneous medium and radiation converter:

$$\begin{aligned} &\text{a) regular model } a\lesssim 1,\ \alpha\gamma^2\gtrsim 1; \\ &\text{b) random model } \beta\lesssim\alpha,\ b/2\,\alpha\gtrsim 1. \end{aligned} \tag{13}$$

The conditions (13) indicate that satisfactory distortion compensation is observed when the radiation converter used in the system resolves the effective size of the inhomogeneities.

Let us note that if the phase lead in (11), (12) is for any reason undesirable, more rigid restrictions must be imposed on the detuning β.

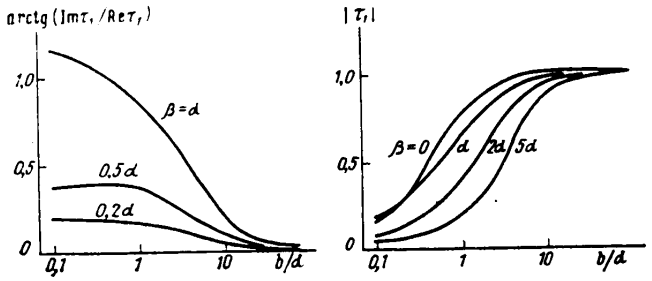

Figure 3. Reconstruction coefficient for a random phase grid.

2. Four-photon Interaction. The degenerate four-photon interaction (2) is in practice free of phase synchrony conditions [4]. In this case the resolution is determined by the aperture effects and can be much higher than for three-photon processes (1).

For four-proton interaction of plane waves in a nonlinear layer which is unlimited with respect to transverse coordinate, the reversed field can be written in the form [4]

$$E_2(\varkappa) = -i\,\mathrm{tg}(gl)\,E_1^*(\varkappa),$$

where $g=(2\pi\omega/cn)\chi E_3E_4$; χ is the cubic nonlinearity; $E_{3,4}$ are the amplitudes of the plane pumping waves. The scattering function or field of the converted image of a point [9] is defined by the expression

$$\Gamma(\rho) = -i\,\mathrm{tg}(gl)\,\delta(\rho).$$

The converted image is always in the same plane as the initial object, and it is an exact complex-conjugate copy. Total compensation for the phase distortions introduced by an arbitrary inhomogeous medium is insured here.

In practice, the volume of the interaction is always limited. Let us assume that in the plane z = 0 there is a gaussian diaphragm with transparency coefficient exp $(-\rho^2/\rho_D^2)$. Then the scattering function of the converter is not ideal. Moreover, the presence of the diaphragm disturbs its homogeneity

$$\Gamma(\rho, \rho_k, -z_k) = -i\frac{\mathrm{tg}(gl)}{\pi\Delta\rho^2}\exp\left[-\frac{(\rho-\rho_k)^2}{\Delta\rho^2} + i\frac{(\rho^2-\rho_k^2)k}{2z_k}\right].$$

Here $\Delta\rho = 2z_k/k\rho_D$ defines the resolution; ρ_k is the transverse coordinate of the initial point. It is obvious that the initial plane wave in this converter is converted to a field having a continuous spectrum which in the absence of inhomogeneities repeats the scattering spectrum at the input aperture.

The appearance of inhomogeneities on the path, for example, random inhomogeneities, leads to variation of the spectral composition of the reversed wave

$$\langle E_2(\varkappa, -z_0)\rangle = -i\pi\rho_A^2 \operatorname{tg}(gl) \exp\left[-\frac{\varkappa^2\rho_A^2}{4}\left(1+\frac{\Delta\rho^2}{b^2}\right) - i\frac{z_0\varkappa^2}{2k}\right]. \quad (14)$$

With a decrease in size of the inhomogeneities, the spectrum of the reconstructed field contracts; its total energy decreases $W = \int |\langle E_2(\varkappa, -z_0)\rangle|^2 d\varkappa$ and the energy of the scattered wave increases $W_p = W_0 - W$ (W_0 is the energy of the regenerated field in the absence of distortions). The mean amplitude of the scattered field for a randomly inhomogeneous medium is equal to zero. It is easy to see that the ratio $\tau_2 = W/W_0 = 1 + \Delta\rho^2/b^2$ permits determination of the degree of compensation of the distortions. Using a criterion analogous to (6), we require that

$$\tau_2 \geqslant 1/2. \quad (15)$$

Then it is possible to consider reconstruction of the wave front satisfactory if $b/\Delta\rho \gtrsim 1$. As before, the WFR scheme turns out to be effective when the radiation converter resolves the effective size of the inhomogeneities, which confirms equivalence of the values of τ_1 and τ_2.

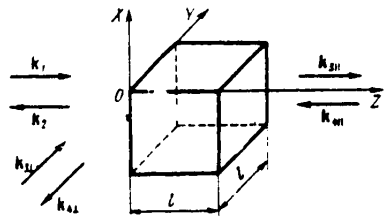

Figure 4. Collinear and perpendicular interaction configurations.

The next significant factor limiting the resolution of the four-photon parametric converter is angular divergence of the pumping beams. Here the scattering function is also inhomogeneous. Let us find the transformed image of the central point in the case of collinear and perpendicular interaction configurations (Figure 4). The solution of this problem will be used to construct a model of the four-photon converter taking into account both the aperture effects and the pumping beam divergence.

Collinear Wave Interaction. In the case where the pumping waves are plane waves, but $k_3 + k_4 \neq 0$, the mismatch of the wave vectors that occurs along the X and Y axes is compensated by $\varkappa_2 = \varkappa_3 + \varkappa_4 - \varkappa_1$ as a result of rotation of the vector k_2. Along the Z-axis the mismatch Δ is nonzero, and the process of wave interaction can be described by the reduced equations:

$$dE_2/dz = igE_1^* \exp(-i\Delta z);$$
$$dE_1^*/dz = igE_2 \exp(i\Delta z).$$

Hereafter we shall limit ourselves to the case of a comparatively low conversion efficiency $g\ell \ll 1$. For boundary conditions E_1 ($z = 0$) $\neq 0$ and E_2 ($z = \ell$) $= 0$, we obtain

$$E_2(\varkappa_2, -z_k) = -igl \exp(-i\Delta l/2) \operatorname{sinc}(\Delta l/2)\, E_1^*(\varkappa_4 + \varkappa_4 - \varkappa_2, -z_k). \quad (16)$$

Figure 5. Modulus of the scattering function of the converter considering divergence of the pumping during collinear interaction.

The rotation of the vector k_2 with respect to the direction $-k_1$ causes a shift of the image in the transverse direction. If pumping has a finite width of the angular spectrum $\kappa_i \leq \kappa_0$ (i = 3, 4), the initial target (point) blurs into a spot, the dimensions of which can be estimated using geometric optics $\Delta\rho = \kappa_0 z_k/k$. However, even in the case where the image of the target is formed on the front boundary of the nonlinear layer ($z_k = 0$), the radiation converter is already nonideal.

Let us consider two cases.

Let the pumping wave 4 be a plane wave, and wave 3 have a uniform finite angular spectrum:

$$E_3(\varkappa_3) = \begin{cases} E_3^0/\pi\varkappa_0^2 & \text{for } \varkappa_3 \leqslant \varkappa_0; \\ 0 & \text{for } \varkappa_3 > \varkappa_0; \end{cases}$$
$$E_4(\varkappa_4) = E_4^0\delta(\varkappa_4). \qquad (17)$$

Then from (16) it is easy to find the image of the point for an arbitrary plane pumping wave $E_3(\kappa_3)$. Integration with respect to κ_3 gives the resultant scattering function which in the paraxial approximation ($\varkappa_0/k \ll 1$, $\varkappa_1/k \ll 1$) is described by the expression

$$\Gamma(\rho) = \begin{cases} gl\,(e^{i\varkappa_0\rho^2/\Delta\rho_0} - e^{i\varkappa_0\rho})/\pi\varkappa_0\Delta\rho_0\rho^2 & \text{for } \rho \leqslant \Delta\rho_0 = l\varkappa_0/k; \\ 0 & \text{for } \rho > \Delta\rho_0. \end{cases} \qquad (18)$$

The modulus of the scattering function (18) is depicted in Figure 5.

Now let us propose that the pumping wave 3 is a plane wave, and the wave 4 has a finite angular spectrum analogous to (17). Then the scattering function of the converter

$$\Gamma(\rho)=\begin{cases} -igl\,(\Delta\rho_0/\rho_*-1)/\pi\Delta\rho_0^2 & \text{for } \rho\leqslant\Delta\rho_0=lx_0/k; \\ 0 & \text{for } \rho>\Delta\rho_0. \end{cases} \tag{19}$$

Its form is analogous to that shown in Figure 5.

Perpendicular Interaction of Waves. Let, just as in the preceding case, $k_3 + k_4 \neq 0$. As before the mismatch of the wave vectors with respect to the Z-axis is not compensated. In order to define the scattering function let us use the same method. It is easy to see that the divergence of the pumping waves in the planes XY and YZ have a different influence on the resolution. THus, if

$$E_{3,4}(x_{3,4})=\begin{cases} E^0_{3,4}\delta(x_{3,4x})/2x_0 & \text{for } |x_{3,4x}|\leqslant x_0; \\ 0 & \text{for } |x_{3,4x}|>x_0, \end{cases}$$

then $\Gamma(\rho)=-2igl\{[\cos(2x_0l)-1]/(2x_0l)^2+\mathrm{si}(2x_0l)/2x_0l\}\delta(\rho)$.

In the first approximation the divergence of the pumping wave in the YZ plane is felt only in the transformation efficiency. The resolution does not change, and the reconstruction coefficient remains equal to one.

If the pumping waves diverge in the XY plane, then then

$$\Gamma(\rho)=\begin{cases} -igl\left[\mathrm{Ei}(-ix_0x)-\mathrm{Ei}\left(\frac{-ix_0x^2}{\Delta x_0}\right)\right]\frac{\delta(y)}{2\Delta x_0} & \text{for } |x|\leqslant\Delta x_0=\frac{2x_0l}{k}; \\ 0 & \text{for } |x|>\Delta x_0. \end{cases} \tag{20}$$

Here Ei (x) is the integral exponent. The form of the scattering function is analogous to that presented in Figure 5.

Expressions (18)-(20) which were obtained permit the statement that both for collinear configuration and perpendicular configuration of the interaction, the resolution of the radiation converter in the plane of an inhomogeneous medium can be estimated as the sum

$$\Delta\rho_0+\Delta\rho=x_0(z_0+l)/k. \tag{21}$$

This approach also permits consideration of the influence of the aperture effects, since for a thin nonlinear layer ($\Delta\ell \ll 1$) it is equivalent to the divergence of the pumping beams, the spatial spectrum of which corresponds to the scattering spectrum on the wave aperture. Finally:

$$\Gamma(\rho,\ \rho_k,\ -z_k)=-igl\left(\frac{k}{z_k}\right)^2 T\left[\frac{k}{z_k}(\rho-\rho_k)\right]\exp\left[i\frac{k}{2z_k}(\rho^2-\rho_k^2)\right]. \tag{22}$$

Here T is the effective spatial pumping wave spectrum. In the case of gaussian beams which is important in practice,

$$E_j(x)=\frac{E_j^0}{\pi\Delta x_j^2}\exp\left(\frac{-x^2}{\Delta x_j^2}\right), \qquad j=3,4,$$

the scattering function has the form

$$\Gamma(\rho, \rho_k, -z_k) = -igl\frac{1}{\pi\Delta\rho}\exp\left[-(\rho-\rho_k)^2/\Delta\rho^2 + i\frac{k}{2z_k}(\rho^2-\rho_k^2)\right],$$

$$\text{where } \Delta\rho = z_k k^{-1}\sqrt{\Delta x_3^2 + \Delta x_4^2}.$$

For the constructed model, the criterion of satisfactory distortion compensation (15) is retained where $\Delta\rho$ must be understood as the resolution (21). Let us note that consideration of the divergence of the pumping beam for degenerate three-photon interaction would lead to analogous results. However, this only leads to significant broadening of the scattering function (10).

5. Models of an Extended Inhomogeneous Medium

The previously performed studies of the process of distortion compensation in volumetric inhomogeneous media [15, 16] do not permit confirmation that the diffraction of the scattered beam will succeed in developing at distances on the order of the length of the distorting medium itself. If such diffraction blurring is insignificant, as before it is possible to consider the distorting medium thin. In the general case the relation of the fields at the input $E_1(\rho)$ and output $E_1'(\rho)$ of an inhomogeneous medium is defined by the Green function $E_1'(\rho) = E_1(\rho')G(\rho, \rho')d\rho'$. After WFR by using the degenerate three-photon (10) or four-photon (22) transformation and secondary passage through the inhomogeneous medium, the regenerated field has the form

$$E_2(\rho) = \int G(\rho, \rho_1)\,\Gamma(\rho_1, \rho_2)\,G^*(\rho_2, \rho_3)\,E_1^*(\rho_3)\,d\rho_1 d\rho_2 d\rho_3. \qquad (23)$$

Although the distortion compensation system even in this case does not differ theoretically from those investigated above (item 2.3) for arbitrary extended inhomogeneities, the analysis is complicated by the necessity for defining the specific form of the Green function. This work was done for a cylindrical light guide and optical amplifier with induced thermal lens [17].

The following simple model has a more general nature. Let us consider a system of N thin phase grids spaced a distance of ℓ_j from each other (Figure 6). Each grid has a random transmission coefficient $\exp[i\phi_j(\rho)]$, and the correlation functions of these coefficients

$$B_{jj'}(\rho, \rho') = \exp\left[-(\rho-\rho')^2/b_j^2\right]\delta_{jj'}.$$

In a real physical medium the spacing between the plates is given by arbitrary distribution of the inhomogeneities. Their transverse dimension is determined as before by the value of b_j.

Let us propose that the WFR is realized by a four-photon radiation converter with scattering function (22). Then the reconstruction coefficient

$$\tau_2 = \left[1 + \sum_{j=1}^{N}\left(\frac{\Delta\rho_j}{b_j}\right)^2\right]^{-1}, \qquad (24)$$

where $\Delta\rho_j$ is the resolution of the converter in the plane of the jth phase grid. From (24) it follows that in the case of extended inhomogeneities the criterion (15)

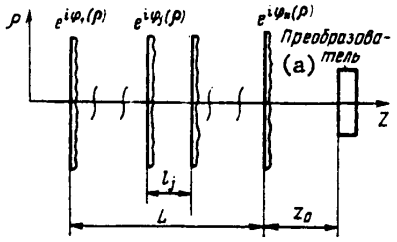

Figure 6. Model of an extended inhomogeneous medium.

Key: a. converter

imposes more rigid restrictions on the resolution:

$$\sum_{j=1}^{N} (\Delta\rho_j/b_j)^2 \leqslant 1.$$

The reconstruction coefficient (24) has a maximum value for optimal focusing of the scattered field:

$$z_{0\,\mathrm{opt}} = -\sum_{j=1}^{N} \frac{L_j}{b_j^2} \Big/ \sum_{j=1}^{N} b_j^{-2}, \tag{25}$$

where $L_j = \sum_{k=j}^{N-1} l_k$ is the distance from the jth phase plate to the Nth phase plate. It is possible to demonstrate that the plane $z_{0\,\mathrm{opt}}$ corresponds to the point of contraction of the gaussian beam scattered by an inhomogeneous medium. It is obvious that if the radiation converter is placed in this plane, then actually the maximum efficiency of the conversion and minimum broadening of the spectrum in the WFR process will be insured. Let us note that in the simplest case of two phase grids the plate with finer inhomogeneities must be resolved better — $\Delta\rho_1/\Delta\rho_2 = (b_1/b_2)^2$. If the size of the longitudinal and transverse inhomogeneities is constant, then $z_{0\,\mathrm{opt}} = -\frac{1}{2}\sum_{j=1}^{N-1} l_j$.

It is possible analogously to define the reconstruction coefficient also for other models of extended inhomogeneities, for example, periodic structures. For an inhomogeneous medium formed by two uniform phase gratings with transmission coefficients $\exp(ia_j\cos\gamma_j x)$ (j = 1, 2) at a distance L from each other:

$$\tau_2 = \sum_{m,m'\,p,p'=-\infty}^{\infty} J_m^2(a_1)\, J_{m'}^2(a_1)\, J_p^2(a_2)\, J_{p'}^2(a_2) \times$$
$$\times \exp\left\{-\frac{1}{2}[\alpha_1(m-m') + \alpha_2(p-p')]^2\right\}. \tag{26}$$

Here $\alpha_j = (1/2)\gamma_j\Delta x_j$; Δx_j is the one-dimensional resolution of the converter in the planes of arrangement of the gratings. Figure 7 shows the reconstruction coefficient

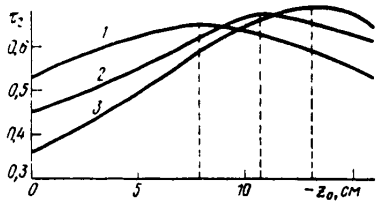

Figure 7. Reconstruction coefficient in different focusing planes ($a_1 = a_2 = 1.75$; L = 16 cm; equivalent angular divergence of the pumpings 0.3 mrad) for gratings with periods of $\gamma_1 = \gamma_2 = 0.187$ mm (1); $\gamma_1 = 0.15$ mm, $\gamma_2 = 0.225$ mm (2) and $\gamma_1 = 0.125$ mm, $\gamma_2 = 0.25$ mm (3).

(26) as a function of the position of the focusing plane. The presented graphs confirm the previously obtained conclusion (25). This comparison shows that the above investigated model of random inhomogeneities not only is more convenient, but quite completely reflects the general laws of the phenomenon. It permits analytical determination of the reconstruction coefficient considering both longitudinal and transverse inhomogeneities that vary along the path. The obtained expressions are simple and permit descriptive physical interpretation.

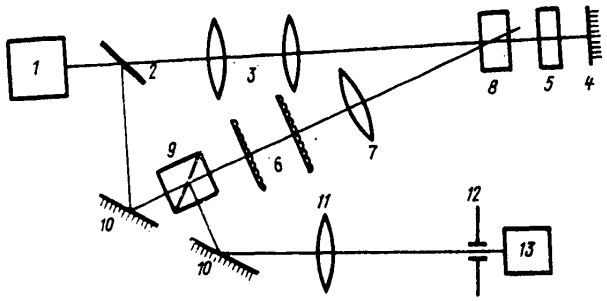

Figure 8. Diagram of the experimental setup.

In conclusion, let us present the results of experimental studies confirming conclusions from items 2-5. The studies were performed on a setup, the diagram of which is presented in Figure 8. An yttrium-aluminum garnet laser 1 ($\lambda = 1.064$ micron) which generates the basic transverse mode, was used as the radiation source. For a radiation pulse duration of 10 nanoseconds the output power of the laser was about 600 kilowatts.

The laser radiation with angular divergence of 0.7 mrad was divided into two beams by the plate 2. The higher power beam was used as the pumping wave, and the lower power beam was used to simulate the signal radiation. In order to improve the resolution of the converter, the pumping beam was also collimated by a telescopic system 3 to an angular divergence of 0.2 mrad. The second pumping wave was formed by a plane mirror 4, and it was polarized orthogonally to the first as a result of the application of a quarter-wave plate 5.

An inhomogeneous medium of finite thickness was simulated by a system of two identical phase gratings 6. The gratings were made by the method of etching thin glass substrates in hydrofluoric acid. Before etching, narrow strips of protective coating were applied to the substrates. The measurements of the energy distribution in an equidistant spectrum of radiation scattered by such a grating demonstrated the possibility of its approximation with accuracy of 10% by a sinusoidal grating with period of $\gamma_{1,2}^{-1} = 0.25$ mm and a phase modulation depth $a_{1,2} = 1.75$.

A beam scattered by the inhomogeneous medium was focused on the converter by a high-speed objective 7. The parametric converter 8 based on a gallium arsenide single crystal 0.55 cm thick generated a reverse wave polarized orthogonally to the incident wave [18]. The isolation of the reconstructed emission was provided by a polarization prism 9. The conversion efficiency reached 5 to 10%. The system for recording the reconstructed wave front included a rotating mirror 10, the objective 11, an iris diaphragm 12 placed in its focal plane and a co-axial photoelement 13.

The procedure for measuring the reconstruction coefficient consisted in the following. In the absence of phase gratings, the power of the generated radiation and conversion efficiency were determined. In this case the iris diaphragm 12 was closed to minimum size, still not irising the light beam. The introduction of phase gratings installed close up so that their images are constructed by the objective 7 in the middle of the nonlinear crystal 3 into the system decreased the power of the radiation by 25-30%. This decrease in power was connected with losses to reflection at the edges of the grating. Then this power P(0) was considered to correspond to the value of $\tau_2 = 1$. The gratings were moved apart so that their images were at a distance L from each other symmetrically on both sides of the crystal ($z_0 = -L/2$). This led to a decrease in power of the recorded radiation P(L). The ratio $\tau_2(L) = P(L)/P(0)$ was taken as the reconstruction coefficient.

The measurement results are presented in Figure 9. The theoretical dependence of τ_2 on the spacing between the gratings (26) is illustrated in the same figure (curve 1). The grating periods were recalculated for the plane of the images. The equivalent angular divergence of the pumping radiation is 0.3 mrad. An analogous function was also obtained for the model of two random phase grids (24) (curve 2) with effective size of the inhomogeneities of 34 microns. The approximation of the scattered radiation spectrum by the gaussian spectrum gives a value on the order of 26 microns. Some difference in estimates of this value obviously can be explained by the approximation error and deviation of the form of the gratings from sinusoidal.

The performed studies (items 2-5) demonstrate the possibility of simple estimation of the optimal parameters of the WFR required for satisfactory reconstruction of a plane wave front distorted by a real inhomogeneous medium.

6. Reconstruction of Space-Modulated Fields

During analysis of the process of reconstructing a space-modulated field it is necessary to define such generally accepted quality parameters of the image as resolution and contrast. In this section, this will be done by using the scattering function of a linear system made up of the inhomogeneous medium, parametric converter that reverses the wave front, inhomogeneous medium.

The analysis is performed for a regular phase grating and parametric converter with scattering function

$$\Gamma(x) = \sqrt{(\delta - i\tilde{\Delta})/\pi}\exp\left[-(\delta - i\tilde{\Delta})x^2\right]. \qquad (27)$$

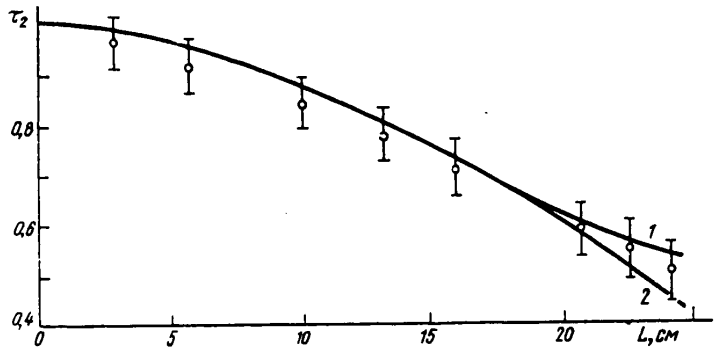

Figure 9. Reconstruction coefficient as a function of the thickness of an inhomogeneous medium.

The scattering function (27) approximates three (10) and four-photon (22) radiation converters quite well. For this model it is possible to show that the reconstructed image of the point -- the scattering function of the entire system -- is defined by the expression

$$F(x_1) = \frac{\gamma}{\sqrt{\pi}}\sqrt{\delta_1 - i\Delta_1}\sum_{m,\,p=-\infty}^{\infty} i^{p-m}J_m(a)\,J_p(a)\times$$
$$\times\exp\left\{-(\delta_1 - i\Delta_1)[z_1(m+p) - x_1]^2 + i\frac{z_1}{2}(m^2 - p^2) + ipx_1\right\}, \qquad (28)$$

where $\Delta_1 = \tilde{\Delta}/\gamma^2$; $\delta_1 = \delta/\gamma^2$; $x_1 = \gamma x$; $z_1 = (z_k - z_0)\gamma^2/k$. The form of the normalized scattering function $F(x_1 = F(x_1)/F(0)$ is shown in Figure 10 for different values of the parameters entering into (28). We shall determine the resolution of the system by the halfwidth of the central peak of the image of the point, and the contrast will be estimated by the energy included in the side peaks.

It is easy to see that the resolution is determined in practice by only one parameter δ -- the resolution of the radiation converter. The variation of the parameter δ_1 -- the relation between δ and the lattice period -- leads to variation of the contrast of the reconstructed image. For $\delta_1 \leq 1$, the efficiency of the compensation system drops sharply. The energy included in the side peaks of the scattering function will become appreciably greater than in the central function.

The variation of z_1 (Figure 10, c) has almost no influence on the halfwidth of the central peak, at the same time sharply changing the spatial location of the side peaks. Therefore for $\delta_1 \sim 1$ the regeneration can be considered satisfactory either in direct proximity to the inhomogeneous medium ($z_1 \ll 1$) or at distances corresponding to the far diffraction zone ($z_1 \gg 1$). The interpretation of this result is obvious if the field passing through the inhomogenous medium a second time is represented as a superposition of two components: the reconstructed one which in practice repeats the form of the scattering function of the radiation converter (27), and the unreconstructed one which diffracts on the grating inhomogeneities. In the near diffraction zone the peaks of the unreconstructed field

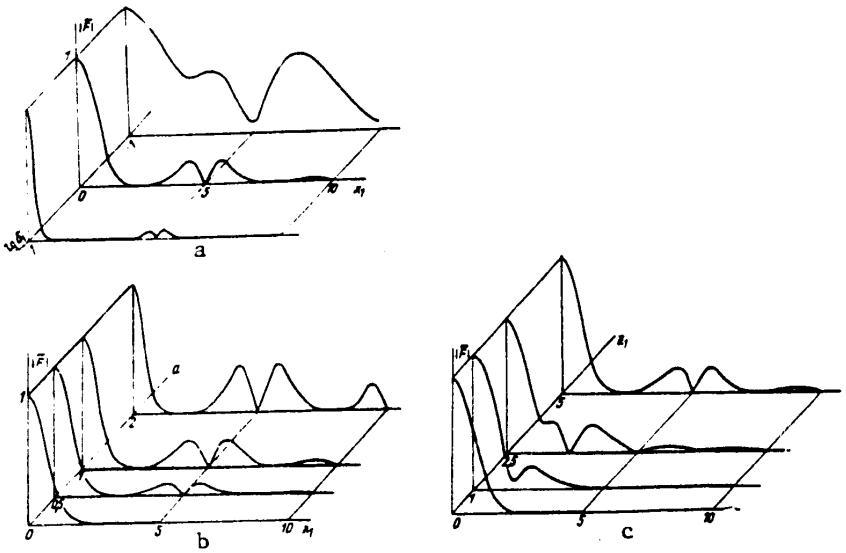

Figure 10. Scattering function of a system made up of the inhomogeneous medium, radiation converter, inhomogeneous medium.

broaden the central peak of the scattering function. With an increase in z_1 they are removed from the center of the field of view and can go beyond its limits at a defined distance. The energy efficiency of this system will drop sharply in this case.

Increasing the modulation depth of the optical path a leads to an increase in the side peaks (Figure 10, b), inasmuch as it is equivalent to worsening of the ratio between the resolution of the converter and the effective size of the inhomogeneity which can be determined by the width of the spatial spectrum of a singly scattered field. The phase of the scattering function also has a negative effect on the contrast of the reconstructed image which is sharply distorted. It is obviously possible to consider the condition $\Delta_1/\delta_1 \leq \pi$ the criterion of satisfactory reconstruction.

It is simpler to estimate the contrast of the reconstructed image in terms of the reconstruction coefficient of the plane wave τ_1. For the model selected by us

$$\tau_1(\varkappa_1) = \sum_{m=-\infty}^{\infty} J_m^2(a) \exp\left[-\frac{\delta_1 + i\Delta_1}{\delta_1^2 + \Delta_1^2} \frac{(m-\varkappa_1)^2}{4}\right], \qquad (29)$$

where $\varkappa_1 = \varkappa/\gamma$. The function $\tau_1(\varkappa_1)$ (29) is shown in Figure 11. A decrease in τ_1 with an increase in $\varkappa_1$ is caused by a decrease in the effective size of the inhomogeneities in the case of oblique incidence of the plane waves.

In the simplest case $\Delta_1 = 0$, which corresponds, for example, to a three-photon parametric conversion of the radiation $\beta = 0$; it is possible to characterize the contrast of the reconstructed image of the point by the ratio

$$C = \int_{-\infty}^{\infty} |\tau_1(\varkappa)|^2 d\varkappa \Big/ \int_{-\infty}^{\infty} |\tau_0(\varkappa)|^2 d\varkappa,$$

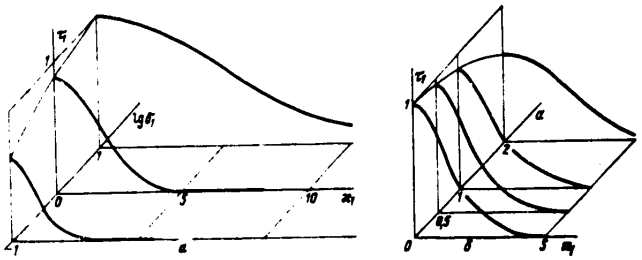

Figure 11. Plane wave reconstruction coefficient.

where $\tau_0(\varkappa)$ is the plane wave reconstruction coefficient in the absence of an inhomogeneous medium. For the models used

$$C = \sqrt{2\pi} \sum_{m,\,n=-\infty}^{\infty} J_m^2(a) J_n^2(a) \exp\left[-\frac{(m+n)^2}{8\delta_1}\right]. \qquad (30)$$

Figure 12 shows the contrast (30) as a function of the parameters δ_1 and a. The value of C is smaller the worse the radiation converter resolves the effective size of the inhomogeneities.

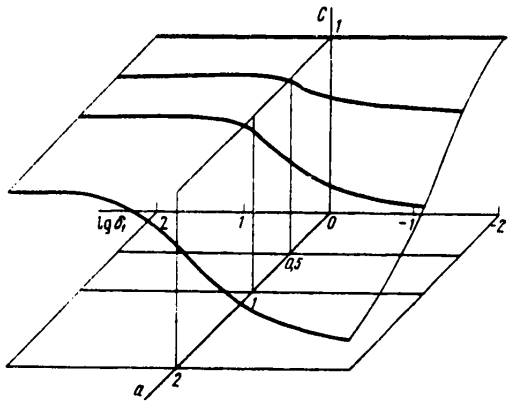

Figure 12. Contrast of a reconstructed image.

The results obtained depend slightly on the choice of the model of the distorting medium and have a quite general nature. For example, they agree well with the results of reference [19] for a model of a random phase grid. In both cases the reconstructed image of the point is an almost undistorted scattering function of the converter and the unreconstructed background, the peaks of which are located farther from the center of the field of view, the farther the initial target is from the inhomogeneous medium.

The experimental study of the process of reconstructing a space-modulated field was performed on a setup analogous to the one described in item 5. A metal slide was used as the target. The resolution was determined by photometric measurement of the edge of the image and, depending on the position of the objective 7, was from 30 to 8 lines/mm. Here the parameter δ_1 varied from 4 to 1. With optimal position of the objective, the image contrast was in practice ideal.

7. Possibilities for Utilizing Parametric Processes

The phase distortion compensation systems with parametric WFR have a number of deficiencies which restrict the region of their possible use. First, they are two-pass. The operating principle of the systems is based on WFR with subsequent passage of the reversed wave along the same inhomogeneous path. Secondly, the question of compensation of nonlinear distortions which can arise as a result of the self-stress processes. Finally, thirdly, the use of degenerate four-photon interaction in the WFR systems, in spite of high resolution, is not always possible as a result of comparatively low quantum efficiency. The discussion of measures to eliminate these difficulties is also a goal of this section.

1. Single-Pass Phase Distortion Compensation Systems. As before, we shall use a degenerate four-photon interaction (2) in the system, but one of the plane pumping waves E_3, just as the signal $E_1(\rho)$, will be passed through a thin distorting medium (Figure 13). The waves coming out of the homogeneous medium will have complex amplitudes $E_3'(\rho) = E_3 \times \exp[i\varphi(\rho)]$ and $E_1'(\rho) = E_1(\rho)\exp[i\varphi(\rho)]$. The second pumping wave E_4 remains plane. If the distance from the distorting medium to the radiation converter and thickness of the nonlinear layer are comparatively small, it is possible to neglect the diffraction diffusion of the waves $E_1'(\rho)$ and $E_3'(\rho)$. As a result of parametric interaction, a reconstructed wave will be produced $E_2(\rho) \sim E_1^*(\rho)$ [20, 21]. An analogous method of distortion compensation is used in holography for single passage of both a signal and a reference wave through an inhomogeneous medium [9, 22]. It must be noted that the restriction on thickness of the distorting medium is fundamental In a thick inhomogeneous medium phase distortions as a result of diffraction will become amplitude distortions, which cannot be compensated by the described method.

For the formation of waves E_3 and $E_1(\rho)$, it is possible to use one plane wave with circular polarization. The diagram of the experimental setup for this case is shown in Figure 14. The radiation of a YAG laser generating the basic transverse mode with angular divergence of 0.55 mrad was divided by a plate 1 into two beams of approximately the same power. Linear polarization of one of them using a quarter-wave plate 2 was converted to elliptic. One of the polarization components of this beam played the role of pumping, and the other the signal. The plane wave E_4 was formed by dielectric mirrors 3, 4 and the lens 5.

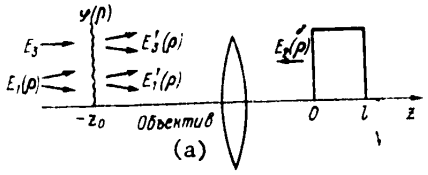

Figure 13. Single-pass phase distortion compensation system.

Key: a. objective

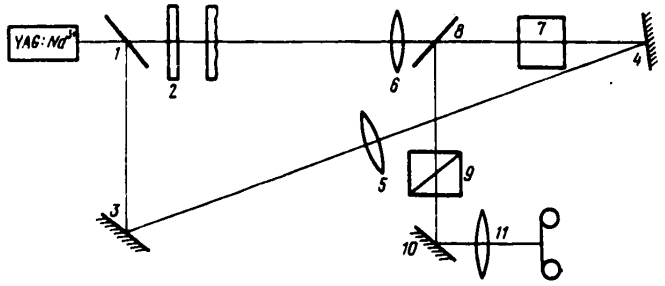

Figure 14. Diagram of the experimenal setup.

As the phase distorting medium we used either a glass plate with a layer of glass melt applied to it having a negative effect on the divergence of the beams by more than an order, or a plate made of gallium arsenide 5.5 mm thick in which self-stress effects were observed. The image of the exit edge of the distorting medium was formed by the objective 6 inside a cell 2 cm long filled with nitrobenzene 7. The radiation generated in the converter, isolated by a light-dividing plate 8, polaroid 9 and mirror 10, was recorded in the focal plane of the lens 11 on photographic film. Photometry of the image made it possible to determine the divergence of the investigated beam. The angular divergence of the reconstructed wave was 0.7 mrad, which was connected with complete identity of the amplitude profiles of one of the pumpings and the signal.

The method used can be developed further for a broader class of problems. In practice any modulation of at least one of the pumping waves — amplitude, phase, time — permits controlled variation of the operation of complex conjugation of the wave front, which in a number of problems of adaptive optics is not optimal. Let us demonstrate this possibility in a simple example having an analytical solution.

2. Compensation of Nonlinear Phase Distortions in a Two-Pass WFR System. As is known, the WFR method does not permit compensation for distortions of the wave front caused by self-stress of the fields with unequal intensities of the signal and reversed waves [23]. For total compensation of nonlinear distortions it is necessary to form the "reversed" wave front by varying the amplitude and phase profiles of the pumping beam so that the front will reconstruct the form of the wave front of the signal after secondary passage through the distorting nonlinear medium.

Let the signal radiation — a gaussian beam with spherical wave front — be distorted in a nonlinear medium I ($-z_0 \leq z \leq 0$):

$$E_1 = \frac{E_1^0}{f_1(z)} \exp\left[-\frac{\rho^2}{a_1^2 f_1^2(z)} - ik\frac{\rho^2 f_1(z)}{2f_1(z)} - i\varphi_1(z)\right]. \qquad (31)$$

Here E_1^0, a_1 are the initial beam amplitude and width; $f_1(z)$ is the dimensionless beam width ($f_1(-z_0) = 1$); $\phi_1(z)$ is the phase lead on the axis. In medium II ($0 \leq z \leq \ell$), degenerate four-photon interaction is realized, where the pumping waves are also gaussian:

$$E_{3,4} = E_{3,4}^0 \exp\left[-\rho^2 / a_{3,4}^2 \pm ik\rho^2 / 2R_{3,4}\right],$$

where $R_{3,4}$ are the radii of curvature of the wave front of the pumping beams.

We shall neglect the diffraction on the nonlinear interaction length $R_{3,4} \gg \ell$ and use an approximation of the given fields. Then the reversed wave is also a gaussian beam (31). Its parameters are subject to the boundary conditions:

$$E_2^0 = \eta E_1^{0*} \frac{f_2(0)}{f_1(0)}; \quad \frac{1}{a_2^2 f_2^2(0)} = \frac{1}{a_3^2} + \frac{1}{a_4^2} + \frac{1}{a_1^2 f_1^2(0)};$$

$$\varphi_2(0) = -\varphi_1(0) - \frac{\pi}{2}; \quad \frac{\dot{f}_2(0)}{f_2(0)} = \frac{1}{R_4} - \frac{1}{R_3} + \frac{\dot{f}_1(0)}{f_1(0)}.$$

The value of η is determined by the conversion efficiency. Let us consider the self-stress of a quite short signal pulse which does not encounter the returned radiation pulse in medium I. We shall consider that all of the nonlinear processes can be described by stationary equations. Then in the self-stress process the beam width varies as follows:

$$\ddot{f}_1 = \frac{1}{D_{1д}^2 f_1^3} - \frac{\nu}{D_{1нл}^2 f_1^3}; \quad \ddot{f}_2 = \frac{1}{D_{2д}^2 f_2^3} - \frac{\nu}{D_{2нл}^2 f_2^3}. \tag{32}$$

Here $D_{iд} = ka_i^2/2$; $D_{iнл} = (a_i/E_i^0)\sqrt{\varepsilon_0/|\varepsilon_2|}$; $\nu = \operatorname{sign}\varepsilon_2$; $\varepsilon = \varepsilon_0 + \varepsilon_2 |E|^2$ is the dielectric constant of medium I, which depends on the radiation intensity. The phase lead $\phi_2(-z_0)$ does not depend on ρ and does not influence the form of the reconstructed wave front. The solution of equations (32) permits us to find the constriction and curvature of the wavefront of the pumping beams insuring compensation of the nonlinear distortions:

$$\begin{cases} \dfrac{1}{a_3^2} + \dfrac{1}{a_4^2} = \dfrac{z_0^2 \nu (\eta^2 l - 1)}{a_1^2 D_{1нл}^2 \left[(1 + z_0/R_0)^2 + z_0^2/D_{1д}^2\right]\left[(1 + z_0/R_0)^2 + z_0^2 (1/D_{1д}^2 - \nu/D_{1нл}^2)\right]}; \\ \dfrac{1}{R_3} - \dfrac{1}{R_4} = \dfrac{a_1^2 (1 + z_0/R_0)}{z_0}\left(\dfrac{1}{a_3^2} + \dfrac{1}{a_4^2}\right). \end{cases} \tag{33}$$

(A) (A)

Key: A. nonlinear

Analogous results can also be obtained by the process of degenerate three-photon interaction. The proposed method of controlling the parameters of the reversed field can be more convenient than the application of adaptive mirrors.

3. Use of Ring Cavities. A significant increase in the quantum yield of systems with parametric WFR can be obtained by using positive feedback. It is known that in three-photon [24] and four-photon [25] parametric lasers the use of such feedback leads to a significant reduction of the lasing threshold.

Let us consider the possibility of the application of a ring cavity (Figure 15) to improve the efficiency of the WFR system with degenerate four-photon interaction. The signal radiation is fed to the cavity through a semitransparent mirror coupling 1 with reflection coefficient r_1. The spherical mirrors 2, 3 take the spatial field distribution from one end of the nonlinear medium 4 to the other, insuring positive feedback both with respect to the signal wave and with respect to the reversed wave.

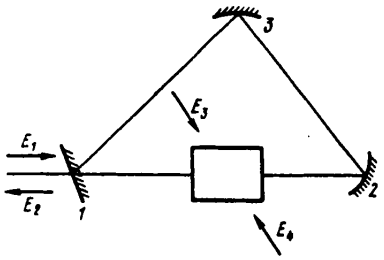

Figure 15. WFR system with ring cavity.

Let linearly polarized plane waves interact in an isotropic, unlimited nonlinear layer of thickness ℓ, where $E_1 \| E_2 \perp E_3 \| E_4$. The process of generating a complex-conjugate wave front in the approximation of the given field with respect to pumping without considering absorption and self-stress of waves 1, 2 is described by the truncated equations [26]:

$$\begin{aligned} -dE_4/dz &= iq_1E_4(|E_4|^2+2|E_3|^2);\\ dE_3/dz &= iq_1E_3(|E_3|^2+2|E_4|^2);\\ dE_1/dz &= iq_2E_1(|E_3|^2+|E_4|^2)+i2q_2E_3E_4E_2^*;\\ -dE_2/dz &= iq_2E_2(|E_3|^2+|E_4|^2)+i2q_2E_3E_4E_1^*. \end{aligned} \tag{34}$$

Here $q_1=q_2+q_3$; $q_2=2\pi\omega^2\chi_2/c^2k$; $q_3=4\pi\omega^2\chi_1/c^2k$; $\chi_{1,2}$ are the independent components of the cubic susceptibility tensor. Under the boundary conditions $E_1(0)=E_1^0$, $E_3(l)=0$, $E_3^0=E_3(0)$, $E_4^0=E_4(0)$ system (34) has the solution

$$E_2(0)=\frac{ig}{\zeta}E_1^{0*}\frac{\operatorname{tg}\zeta l}{1-i(\Omega/2\zeta)\operatorname{tg}\zeta l}, \tag{35}$$

where $\zeta=\sqrt{(\Omega/2)^2+|g|^2}$; $\Omega=q_1(E_3^{0*}-E_4^{0*})$; $|g|=2q_2E_3^0E_4^0$.

Introduction of positive feedback (see Figure 15) changes the boundary conditions by $E_1(0)=\sqrt{1-r_1}E_1^0+\sqrt{r_1r_2}E_1(l)$ and $E_2(0)\sqrt{r_1r_2}=E_2(l)$. Here the coefficient r_2 describes the losses in the resonator. The field generated by the WFR system has an amplitude

$$E_2=\frac{ig(1-r_1)\operatorname{tg}(\zeta l)E_1^{0*}}{\zeta\left\{-2\sqrt{r_1r_2}\frac{\cos ul}{\cos\zeta l}\exp\left(-\frac{i\Omega l}{2}\right)+\frac{i\Omega}{2\zeta}\operatorname{tg}(\zeta l)[r_1r_2\exp(-i\Omega l)-1]+[r_1r_2\exp(-i\Omega l)+1]\right\}}, \tag{36}$$

where $ul=q_3(E_3^{0*}+E_4^{0*})l$ is the phase lead of the reflected wave related to nonlinear variation of the index of refraction. In Figure 16 we have the magnitude of the gain in efficiency of the WFR system by comparison with the resonatorless case for different pumping beam intensities given by the parameter $g\ell$ and different losses in the resonator r_2 as a function of the reflection coefficient of the coupling mirror. Curve 1 has a discontinuity which corresponds to the beginning of parametric lasing. From the graphs (see Figure 16) constructed for nonlinearity of the Kerr

type $2\chi_1 = (1/3)\chi_2$, it follows that in order to obtain maximum gain it is necessary to have the parameters r_1, r_2 and $g\ell$ match sufficiently exactly.

It is obvious that the greatest conversion efficiency is achieved for identical intensities of the pumping waves ($\Omega = 0$). In this case the power gain of the reflected wave as a result of using the resonator

$$h = (1-r_1)^2 / [1 + r_1 r_2 - 2\sqrt{r_1 r_2}\cos ul/\cos gl] \qquad (37)$$

can be several orders. In this case, the parametric lasing mode with sharply reduced threshold turns out to be possible:

$$gl = 3\,\mathrm{arctg}\,\sqrt{(1-\sqrt{r_1 r_2})^2 / [2\sqrt{r_1 r_2} + 3\,(1-r_1 r_2)]}. \qquad (38)$$

Setting $r_1 = 1$ in (38), it is possible also to determine the maximum value of the parameter $g\ell$ to obtain the lasing mode for given losses r_2.

The obtained results are valid if the interacting waves are monochromatic or their spectrum coincides with the spectrum of the natural frequencies of the ring cavity. Otherwise a gain in efficiency of the WFR systems will be observed only in individual spectral components of the signal radiation. For large values of the parameter $g\ell$, the self-stress processes can lead to variation of the effective length of the cavity and its natural frequencies.

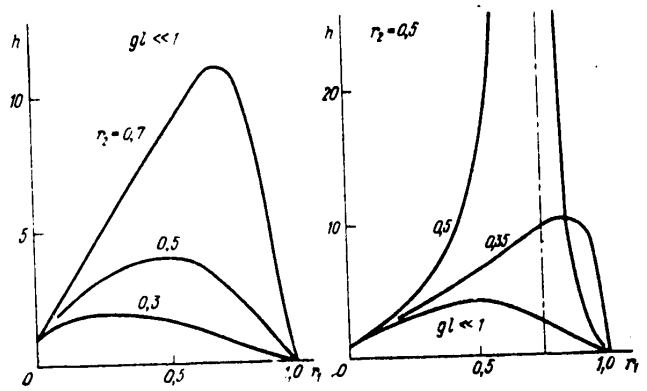

Figure 16. Gain in efficiency of the WFR system by comparison with the resonatorless case.

Analogous arguments can be stated also for degenerate three-photon wave interaction. In contrast to the systems with four-photon WFR, ordinary resonators are also applicable.

Thus, we were able to constuct a mathematical model of the phase distortion compensation system with parametric WFR. The model satisfactorily describes the basic laws of the process of reconstruction of the signal wave front, it permits determination of the maximum possibilities of the method and optimization of the system.

It is of interest that insignificant variations of the standard system theoretically offer the possibility of nonlinear distortion compensation and a significant increase in quantum yield of the system.

BIBLIOGRAPHY

1. B. I. Stepanov, Ye. V. Ivakin, A. S. Rubanov, DAN SSSR (Reports of the USSR Academy of Sciences), No 196, 1971, p 567.

2. B. Ya. Zel'dovich, V. I. Popovichev, V. V. Ragul'skiy, F. S. Fayzullov, PIS'MA V ZHETF (Letters to the Journal of Experimental and Theoretical Physics), No 15, 1972, p 160.

3. A. Yariv, OPTICS COMMS, No 21, 1977, p 49; R. W. Hellwarth, J. OPT. SOC. AMER., No 67, 1977, p 1.

4. OBRASHCHENIYE VOLNOVOGO FRONTA OPTICHESKOGO IZLUCHENIYA V NELINEYNYKH SREDAKH (Optical Radiation Wave Front Reversal in Nonlinear Media), Edited by V. I. Bespalov, Gor'kiy, IPF AN SSSR, 1979.

5. A. Yariv, IEEE J. QF-14, 1978, p 650.

6. N. S. Shiren, APPL. PHYS. LETTS., No 33, 1978, p 299.

7. V. G. Sidorovich, ZHTF (Journal of Technical Physics), No 46, 1976, p 2168; V. I. Bespalov, A. A. Betin, G. A. Pasmanik, PIS'MA V ZHTF, No 3, 1977, p 215.

8. G. V. Krivoshchekov, S. G. Struts, M. F. Stupak, PIS'MA V ZHTF, No 6, 1980, p 428.

9. J. Goodman, VVEDENIYE V FUR'YE-OPTIKU (Introduction to Fourier Optics), Moscow, Mir, 1970.

10. B. Ya. Zel'dovich, V. V. Shkunov, KVANTOVAYA ELEKTRONIKA (Quantum Electronics), No 4, 1977, p 2353.

11. E. S. Voronin, V. V. Ivakhnik, V. M. Petnikova, V. S. Solomatin, V. V. Shuvalov, KVANTOVAYA ELEKTRONIKA, No 6, 1979, p 1304.

12. E. S. Voronin, V. V. Ivakhnik, V. M. Petnikova, V. S. Solomatin, V. V. Shuvalov, KVANTOVAYA ELEKTRONIKA, No 6, 1979, p 2009.

13. Yu. A. Il'inskiy, Yu. A. Yanayt, IZV. VUZOV, SER. RADIOFIZIKA (News of the Institutions of Higher Learning. Radio Physics Series), No 13, 1970, p 37.

14. E. S. Voronin, M. I. Divlekeyev, Yu. A. Il'inskiy, V. S. Solomatin, OPT. I SPEKTR. (Optics and Spectroscopy), No 30, 1971, p 1118.

15. O. Yu. Nosach, V. I. Popovichev, V. V. Ragul'skiy, F. S. Fayzullov, ZHETF, No 16, 1972, p 617.

16. S. G. Obulov, Ye. N. Sal'kova, M. S. Soskin, L. G. Sukhoverkhova, UKR. FIZ. ZHURNAL (Ukrainian Physics Journal), No 23, 1978, p 562.

17. V. V. Ivakhnik, V. M. Petnikova, V. S. Solomatin, V. V. Shuvalov, KVANTOVAYA ELEKTRONIKA, No 7, 1980, p 652.

18. B. Ya. Zel'dovich, V. V. Shkunov, KVANTOVAYA ELEKTRONIKA, No 6, 1979, p 629.

19. Yu. A. Il'inskiy, V. M. Petnikova, KVANTOVAYA ELEKTRONIKA, No 7, 1980, p 439.

20. Ye. V. Ivakin, I. P. Petrovichev, A. S. Rubanov, OPTICHESKIYE METODY OBRABOTKI INFORMATSII (Optical Data Processing Methods), Minsk, Nauka i tekhnika, 1978, p 124.

21. V. V. Ivakhnik, V. M. Petnikova, V. S. Solomatin, V. V. Shuvalov, KVANTOVAYA ELEKTRONIKA, No 7, 1980, p 898.

22. W. Goodman, W. H. Hundley, Ar. D. W. Sacksa, Lehman, APPL. PHYS. LETTS, No 8, 1966, p 311.

23. D. M. Pepper, A. Yariv, OPTICS LETTS, No 5, 1980, p 59.

24. R. Fisher, L. A. Kulevskiy, KVANTOVAYA ELEKTRONIKA, No 4, 1977, p 245.

25. A. Yariv, D. M. Pepper, OPTICS LETTS, No 1, 1977, p 16.

26. B. Ya. Zel'dovich, V. V. Shkunov, OBRASHCHENIYE VOLNOVOGO FRONTA OPTICHESKOGO IZLUCHENIYA V NELINEYNYKH SREDAKH (Optical Radiation Wave Front Reversal in Nonlinear Media), Gor'kiy, IPF AN SSSR, 1979, p 23.

10,845
CSO: 1862/220

UDC 621.386:621.374

PULSED X-RAY TECHNOLOGY

Moscow IMPUL'SNAYA RENTGENOVSKAYA TEKHNIKA in Russian 1981 (signed to press 20 Mar 81) pp 2-5, 110-119

[Annotation, preface, introduction, references and table of contents from book "Pulsed X-Ray Technology", by Stanislav Platonovich Vavilov, Izdatel'stvo "Energiya", 4000 copies, 120 pages]

[Text] The book describes physical principles of producing pulsed x-radiation with duration of 10^{-9}-10^{-6} s. An investigation is also made of the design particulars of equipment for producing bremsstrahlung developed in the Soviet Union and elsewhere. Research results are given on the use of pulsed x-ray technology in different areas of science and engineering: investigation of high-speed processes, flaw detection, in medical research and so on.

For engineers and technicians engaged in the development of pulsed x-ray generators, specialists who use pulsed sources of x-radiation.

Preface

The search for ways to make high-density energy sources has led developers to develop powerful pulsed emitters with maximum intensities. Sources of this kind are electron accelerators and generators of x-ray emission. Their range of application is extremely broad: research, industry, agriculture, medicine.

Problems of producing and using intense electron beams have been dealt with in many surveys and individual papers, whereas questions relating to pulsed x-ray technology have been less well covered.

The pulsed bremsstrahlung generators developed in the late thirties have undergone considerable improvements toward a reduction in pulse duration and increased radiation intensity.

The generation of x-ray pulses in the microsecond and nanosecond ranges is a qualitatively new problem whose solution requires knowledge of many special divisions of high-voltage technology, radiation physics and dosimetry, vacuum and gas electronics.

This book examines the physical principles of various methods of producing x-ray pulses. The structural arrangements and design peculiarities of existing equipment

are examined. A thoery is outlined for the discharge process in a vacuum two-electrode pulsed x-ray tube, and a method is given for calculating the parameters of such a tube.

The author will be grateful for any comments and suggestions by readers, which should be addressed to 113114 Moscow, Shlyuzovaya nab., 10, Energoizdat.

Introduction

The problems considered in this book have begun to form a separate discipline only within the last 10 or 15 years. The first x-ray pulses of short duration (10^{-6} s or less) were produced in the late thirties, and since that time there has been intense accumulation and processing of experimental material. However, the work that has been done has been chiefly of an applied nature. The advances made in the mid-sixties in the formation of intense pulsed electron beams have prepared the ground for a comprehensive study of the physics and engineering of x-ray pulse production. Since that time, many papers have been published dealing with the investigation of different methods of getting x-ray pulses, making pulsed x-ray tubes and their use in science and engineering [Ref. 1, 2].

The first research on pulsed x-ray equipment in the microsecond and nanosecond ranges was done by Kingdon and Tanis [Ref. 3]. A paper by Steenbeck appeared at almost the same time [Ref. 4]. This was followed by a burst of publications.

Vacuum pulsed x-ray tubes were developed in 1939 [Ref. 5, 6], finding application in the study of ballistic and explosive processes. Research started to develop with greatest intensity in the United States, the Soviet Union and Germany. The names of such researchers as V. A. Tsukerman (USSR), Schaafs (Germany) and Slack (United States) became widely known.

Beginning in the late forties there was an expansion in the field of application of x-ray pulses, and papers began to appear on the fine structure of materials as revealed by pulse radiography. The working voltages of tubes rose from 100-150 kilovolts [Ref. 3, 4] to 300-400 kV, and subsequently to 1 MV [Ref. 5].

A theory of field-emission pulsed x-ray tubes was successfully developed in the early fifties, and thoroughgoing research started on the pulsed vacuum discharge with the use of the most modern techniques and equipment [Ref. 6, 7].

The first miniature pulsed x-ray tubes and equipment were developed in the sixties thanks to the work of Soviet scientists: V. A. Tsukerman, N. I. Komyak, Ye. A. Peliks, N. V. Belkin, N. G. Pavlovskaya, E. G.-V. Aleksandrovich, N. Zavada and others [Ref. 1]. Intense bremsstrahlung generators were developed and made in the United States [Ref. 8]. The first papers appeared on nanosecond x-ray analysis [Ref. 9] and on generation of coherent pulses [Ref. 10].

At present, many groups and investigators throughout the world are engaged in research on pulsed x-ray technology and its applications.

REFERENCES

1. Tsukerman, V. A., Tarasov, L. V., Lobov, S. I., "New X-Ray Sources", USPEKHI FIZICHESKIKH NAUK, Vol 103, 1971, pp 319-337.

2. Tomer, G., "X-Ray Pulse Technology" in: "Fizika bystroprotekayushchikh protsessov" [Physics of High-Speed Processes], translated from English, edited by N. A. Zlatin, Moscow, Mir, 1971, Vol 1, pp 336-381.

3. Kingdon, K. H., Tanis, H. E., "Experiments With a Condenser Discharge X-Ray Tube", PHYS. REV., Vol 53, 1958, pp 128-134.

4. Steenbeck, M., "Über ein Verfahren zur Erzeugung intensiver Röntgenlichtblitze", WISS. VERÖFF. SIEMENS-Werke, Vol 17, 1938, pp 363-380.

5. Zelenskiy, K. F., Pecherskiy, O. P., Tsukerman, V. A., "Effects on the Anode of a Pulsed X-Ray Tube Under the Action of Electron Impact", ZHURNAL TEKHNICHESKOY FIZIKI, Vol 38, 1968, pp 1581-1587.

6. Dyke, W. P., Trolan, J. K., "Field Emission: Large Current Densities Space Charge and Vacuum Arc", PHYS. REV., Vol 89, 1953, pp 789-808.

7. Yelinson, M. I., Vasil'yev, G. V., "Avtoelektronnaya emissiya" [Field Emission], Moscow, Fizmatgiz, 1958, 272 pages.

8. Johnston, P. F., "Flash Radiography in Explosive Research", VISUAL, Vol 8, 1970, pp 12-19.

9. Jamet, F., "Recording of X-Rays Diffraction Patterns Using Flash X-Rays in Connection With an Image Intensifier", JOURN. SOC. MOT. PICTURE AND TELEV. ENG., Vol 80, 1971, pp 900-901.

10. Kepros, J. G., Eyring, E. M., Cagle, F. W., William, J., "Experimental Evidence of an X-Ray Laser", PROCEED. NAT. ACAD. SCI., Vol 69, 1972, pp 1744-1745.

11. Slivkov, I. N., "Elektroizolyatsiya i razryad v vakuume" [Electrical Insulation and Vacuum Discharge], Moscow, Atomizdat, 1972, 304 pages.

12. Mesyats, G. A., Proskurovskiy, D. I., "Current Rise in Spark With Pulsed Breakdown of Short Vacuum Gaps", IZVESTIYA VYSSHIKH UCHEBNYKH ZAVEDENIY: FIZIKA, No 1, 1968, pp 81-85.

13. Flynn, P. T. G., "The Discharge Mechanism in the High Vacuum Cold Cathode Pulse X-Ray Tube", PROC. PHYS. SOC., 1956, Vol B69, pp 748-762.

14. Vitkovskiy, I., Bey, P., Faust, U. et al., "Exploding Wires as a Source of X-Radiation", in: "Elektricheskiy vzryv provodnikov" [Electric Explosion of Conductors], translated from English, edited by A. A. Rukhadze and I. S. Shpigel', Moscow, Izdatel'stvo inostrannoy literatury, 1965, pp 108-118.

15. Stenerhag, B., Händel, S. K., Göhle, B., "Effect of Wire Parameters on the Emission of Hard X-Rays From Exploding Wires", JOURN. APPL. PHYS., Vol. 42, 1971, pp 1876-1882.

16. Molchanov, A. G., "Lasers in the Vacuum Ultraviolet and X-Ray Regions of the Spectrum", USPEKHI FIZICHESKIKH NAUK, Vol 106, 1972, pp 165-173.

17. Komyak, N. I., Peliks, Ye. A., "The Kvant, IRA-3 and RINA-1D Portable Pulsed X-Ray Devices", ATOMNAYA ENERGIYA, Vol 32, 1972, pp 520-522.

18. Fursey, G. N., Zhukov, V. M., "Experimental Study of Mechanism of Explosive Emission", ZHURNAL TEKHNICHESKOY FIZIKI, Vol 46, 1976, pp 310-318.

19. Zelenskiy, K. F., Troshkin, I. A., Tsukerman, V. A., "Portable Facilities With Pulse Transformer for Producing Short X-Ray Bursts", PRIBORY I TEKHNIKA EKSPERIMENTA, No 2, 1963, pp 140-144.

20. Dyer, P. E., James, D. J., Ramsden, S. A., Skipper, M. A., "X-Ray Emission From a CO_2 Laser-Produced Plasma", APPL. PHYS. LETT., 1974, Vol 24, pp 316-317.

21. Khmyrov, V. V., Churilov, V. N., "Pulsed Nanosecond Electron Accelerator With High Operating Frequency" in: "Moshchnyye nanosekundnyye impul'snyye istochniki uskorennykh elektronov", edited by G. A. Mesyats, Novosibirsk, Nauka, 1974, pp 128-130.

22. Malozzi, P. J., Epstein, H. M., Jung, R. G. et al., "Laser-Generated Plasmas as a Source of X-Rays for Medical Applications", JOURN. APPL. PHYS., Vol 45, 1974, pp 1891-1895.

23. Chakhlov, V. L., Vavilov, S. P., Pushin, V. S., "Characteristics of Injector With Explosive Cathode", PRIBORY I TEKHNIKA EKSPERIMENTA, No 2, 1975, pp 23-25.

24. Belkin, N. V., Avilov, E. A., "Some Time Characteristics of a Vacuum Device in the Case of Pulsed Voltage Application With Nanosecond Risetime", ZHURNAL TEKHNICHESKOY FIZIKI, Vol 40, 1970, pp 1723-1724.

25. Anisimov, S. I., Imas, Ya. A., Romanov, G. S., Khodyko, Yu. F., "Deystviye izlucheniya bol'shoy moshchnosti na metally" [Action of High-Power Radiation on Metals], edited by A. M. Bonch-Bruyevich and M. A. Yel'yashkevich, Moscow, Nauka, 1970, 272 pp.

26. Pittaway, L. G., Smith, J., Nichols, B. W., "Laser Induced Electron Emission Using a Pulsed Argon Laser", PHYS. LETT., Vol 26A, 1968, pp 300-302.

27. Kolpakov, A. V., Galyamov, B. Sh., Kuz'min, R. N., "Heterodyning of Radiation in the X-Ray Wavelength Range", VESTNIK MOSKOVSKOGO GOSUDARSTVENNOGO UNIVERSITETA, SERIYA FIZIKA, ASTRONOMIYA, Vol 14, 1973, pp 369-370.

28. Tarasova, L. V., Khudyakova, L. N., Loyko, T. V., Tsukerman, V. A., "Fast Electrons and X-Radiation of Nanosecond Pulsed Discharges in Gases at Pressures of 0.1-760 mm Hg", ZHURNAL TEKHNICHESKOY FIZIKI, Vol 44, 1974, pp 564-568.

29. Mesyats, G. A., "Role of Explosive Electron Emission in Electric Discharges in Gas" in: "Sil'notochnaya emissionnaya elektronika, Tezisy vtorogo simpoziuma" [High-Current Emission Electronics, Abstracts of Papers at the Second Symposium], Izdatel'stvo Tomskogo gosudarstvennogo universiteta, Tomsk, 1975, pp 63-64.

30. Gorbachev, V. I., "Kseroradiograficheskiy metod defektoskopii" [Xeroradiographic Flaw Detection Technique], Moscow, Atomizdat, 1973, 128 pp.

31. Kudelin, K. M., "Thermoluminescent Spectrometric Sensor of X-Ray and Gamma Radiation", PRIBORY I TEKHNIKA EKSPERIMENTA, No 2, 1969, pp 200-202.

32. Henkel, S., Higland, V., Sloan, T. et al., "Observation of X-Rays From Spark Discharges in a Spark Chamber", NUCL. INSTR. METH., Vol 44, 1966, pp 345-348.

33. Noggle, R. C., Krider, E. P., Wayland, J. R., "A Search for X-Rays From Helium and Air Discharges at Atmospheric Pressure", JOURN. APPL. PHYS., Vol 39, 1968, pp 4746-4748.

34. Bazhenov, G. D., Mesyats, G. A., Proskurovskiy, D. I., "Cathode Flares During Pulse Breakdown in Vacuum" in: "Proc. IV IS on EIDV", Waterloo, Canada, 1972, pp 116-120.

35. Tarasova, L. V., Khudyakova, L. N., "X-Radiation Accompanying Pulse Discharges in Air", ZHURNAL TEKHNICHESKOY FIZIKI, Vol 39, 1969, pp 1530-1533.

36. Schaafs, W., "Die Erzeugung von Röntgenblitz-Unterferenzen an polykristallinen Material", ZEITSCHR. NATURF., Vol 5A, 1950, pp 631-632.

37. Kremnev, V. V., Kurbatov, Yu. A., "Investigation of X-Radiation From Gas Discharge in High Electric Fields", ZHURNAL TEKHNICHESKOY FIZIKI, Vol 42, 1972, pp 795-799.

38. Mesyats, G. A., Bychkov, Yu. I., Kremnev, V. V., "Nanosecond Pulsed Electric Discharge in Gas", USPEKHI FIZICHESKIKH NAUK, Vol 107, 1972, pp 201-228.

39. Johnson, Q., Mitchell, A. C., Evans, L., "X-Ray Diffraction Study of Single Crystals Undergoing Shock-Wave Compression", APPL. PHYS. LETT., Vol 21, 1972, pp 29-30.

40. Babich, L. P., "Bremsstrahlung of Electrons in Media With External Electric Field", ZHURNAL TEKHNICHESKOY FIZIKI, Vol 42, 1972, pp 1617-1619.

41. Yegorov, L. Ye., Lukashev, A. A., Nitochkina, E. F., Orekin, Yu. K., PRIBORY I TEKHNIKA EKSPERIMENTA, No 2, 1968, pp 200-203.

42. Johnson, Q., Mitchell, A. C., "First X-Ray Diffraction Evidence for a Phase Transition During Shock-Wave Compression", PHYS. REV. LETT., Vol 29, 1972, pp 1369-1371.

43. Andreyeva, M. A., Zezin, S. B., Kolpakov, A. V., Kuz'min, R. N., "Supermonochromatic Radiation in the X-Ray Wavelength Band" in: "Apparatura i metody

rentgenovskogo analiza" [Equipment and Methods for X-Ray Analysis], Leningrad, Mashinostroyeniye, 1970, No 7, pp 80-87.

44. Johnson, "System for Recording Pulse Spectra Emitted by an X-Ray Plasma of Nanosecond Duration", PRIBORY NAUCHNYKH ISSLEDOVANIY, No 2, 1974, pp 47-52.

45. Slabkiy, L. I., Odnovol, L. A., Kozenko, V. P., "X-Radiation Arising Upon Impact of Metallic Bodies", DOKLADY AKADEMII NAUK SSSR, Vol 210, 1973, pp 319-320.

46. Gorazdovskiy, T. Ya., "Effect of Hard Radiation in Shearing Fracture of Solids", PIS'MA V ZHURNAL EKSPERIMENTAL'NOY I TEORETICHESKOY FIZIKI, Vol 5, 1967, pp 78-92.

47. Tsukerman, V. A., Avdeyenko, A. I., "Taking X-Ray Photos With Very Short Exposure Time", ZHURNAL TEKHNICHESKOY FIZIKI, Vol 12, 1942, pp 185-194.

48. Tsukerman, V. A., Manakova, M. A., "Source of X-Ray Flashes for Studying High-Speed Processes", ZHURNAL TEKHNICHESKOY FIZIKI, Vol 27, 1957, pp 391-403.

49. Schörling, O., "X-Ray Flash Spectra of Fe, Ni and Cu", ARK. FYS., Vol 19, 1961, pp 47-67.

50. Baksht, R. B., Yel'chaninov, A. S., "300 keV Source of Pulsed X-Rays" in: "Elektrofizicheskaya apparatura" [Electrophysical Apparatus], Moscow, Energiya, 1970, pp 336-339.

51. Barmasov, V. A., Makeyev, N. G., Rumyantsev, V. G. et al., PIS'MA V ZHURNAL EKSPERIMENTAL'NOY I TEORETICHESKOY FIZIKI, Vol 2, 1976, pp 798-801.

52. Kvartskhava, I. F., Khautiyev, E. V., Ninidze, M. L., "Mechanism of Hard X-Ray and Neutron Emissions of a Plasma Focus", FIZIKA PLAZMY, Vol 2, 1976, pp 40-43.

53. Mel'nik, V. I., Novikov, A. A., "Gas-Discharge Electron Sources With Anode Plasma, and Their Use in Electron-Beam Technology", ELEKTRONNAYA OBRABOTKA MATERIALOV, No 1, 1973, pp 22-28.

54. Blokhin, M. A., "Metody rentgeno-spektral'nykh issledovaniy" [X-Ray Spectral Research Methods], Moscow, Fizmatgiz, 1959, 386 pp.

55. Holzrichter, J. F., Dozier, C. M., McMahon, J. M., "X-Ray Point Source Reflection Photography With a Laser-Produced Plasma", APPL. PHYS. LETT. Vol 23, 1973, pp 687-689.

56. Key, M., Eidman, K., Dorn, C., "Space Resolved X-Ray Measurements on Laser Produced Plasmas", PHYS. LETT., Vol A78, 1944, pp 121-122.

57. Medvedev, Yu. A., Morozov, N. N., Stepanov, B. M., Khokhlov, V. L., "Using Microwave Methods in Dosimetry of Pulsed Ionizing Radiation Fluxes", ATOMNAYA ENERGIYA, Vol 40, No 1, 1976, pp 53-55.

58. Elle, D., "Ein Röntgenblitzrohr mit Kunststoffisolierung und einer Doppelanode", ZEITSCHR. ANGEW. PHYS.,Vol 8, 1956, pp 81-85.

59. Baksht, R. B., Bugayev, S. P., Vavilov, S. P. et al., "Mechanism of Operation of Pulsed X-Ray Tubes" in: "Sovremennoye sostoyaniye i perspektivy vysokoskorostnoy fotografii i kinematografii bystroprotekayushchikh protsessov" [Current State and Outlook for High-Speed Still and Motion-Picture Photography of Rapid Processes], abstracts of the articles, Moscow, Izd. VNIIOFI, 1972, p 174.

60. Vavilov, S. P., "Experimental Study of Pulsed X-Rays With Discharge in Vacuum", author's abstract of dissertation for candidate of technical sciences, Tomsk, 1973, Tomsk Polytechnical Institute.

61. Baksht, R. B., Vavilov, S. P., Urbazayev, M. N., "Duration of X-Radiation Arising Upon Discharge in Vacuum", IZVESTIYA VYSSHIKH UCHEBNYKH ZAVEDENIY: FIZIKA, No 2, 1973, pp 140-141.

62. Vavilov, S. P., "Experimental Study of Pulsed X-Radiation", ZHURNAL TEKHNICHESKOY FIZIKI, Vol 45, 1975, pp 1958-1964.

63. Abramov, V. P., Vavilov, S. P., Gorbunov, V. I. et al., "Flash X-Rays Time and Spectral Characteristics Under Conditions of Vacuum Discharge" in: "Proc. VII IS on EIDV", Novosibirsk, 1976, pp 391-394.

64. Mesyats, G. A., "Generirovaniye moshchnykh nanosekundnykh impul'sov" [Generation of Powerful Nanosecond Pulses], Moscow, Sovetskoye radio, 1973, 225 pp.

65. Freytag, J. P., "Generateurs a rayons X eclair. P. I. Tubes", REV. TECHN. THOMPSON GSF, Vol 1, 1969, pp 553-573.

66. Zelenskiy, K. F., Zavad, N. I., Troshkin, I. A., Tsukerman, V. A., "Powerful Pulse Generator of Short X-Ray Bursts", PRIBORY I TEKHNIKA EKSPERIMENTA, No 4, 1969, pp 177-180.

67. Goldman, M., Goldman, A., "Sur la formation d l'arc electrique dans le vide" JOURN. PHYSIZUE, Vol 24, 1963, pp 303-306.

68. Krmenchugskiy, L. S., Strakovskaya, R. Ya., "Using Pyroelectric Detector for Pulsed Gamma Radiation Monitoring", ATOMNAYA ENERGIYA, Vol 41, 1976, pp 190-194.

69. Garmanov, L. V., Komyak, N. I., Kotsarev, Ye. I., Peliks, Ye. A., "IRA-46/L Three-Channel Pulsed X-Ray Unit", APPARATURA I METODY RENTGENOVSKOGO ANALIZA, No 10, 1972, pp 188-191.

70. Garmanov, L. V., Komyak, N. I., Kotsarev, Ye. I., Peliks, Ye. A., "Pulse X-Ray Unit With Three-Electrode Sharp-Focus Tube for 150 kV", APPARATURA I METODY RENTGENOVSKOGO ANALIZA, No 9, 1971, pp 81-84.

71. Barlet, Fal'k, Khofer et al., "Charge Transfer and Surface Emission Under the Action of Photons", TIIER, Vol 62, No 9, 1974, pp 36-42.

72. Gleyzer, I. Z., Dronova, L. P., Zherlitsyn, A. G. et al., "Tonus High-Current Electron Accelerator", PRIBORY I TEKHNIKA EKSPERIMENTA, No 3, 1974, pp 17-20.

73. Sündström, I., Händel, S. K., Persson, J. E., "Time Resolved Intensity Distribution in an FXR Discharge", ZEITSCHR. PHYS., Vol 200, 1967, pp 499-510.

74. Zyuzin, V. P., Manakova, M. A., Tsukerman, V. A., "Sealed Sharp-Focus Pulse X-Ray Tubes", PRIBORY I TEKHNIKA EKSPERIMENTA, No 1, 1958, pp 84-87.

75. Bychkova, L. G., Bychkov, Yu. I., Vavilov, S. P., Kurbatov, Yu. A., "Generator of Long Pulses of 500 kV Amplitude and Nanosecond Risetime" in: "Elektrofizicheskaya apparatura i elektricheskaya izolyatsiya" [Electrophysical Apparatus and Electrical Insulation], Moscow, Energiya, 1970, pp 92-96.

76. Komyak, N. I., Korobochko, Yu. S., "Optimum Supply Parameters for Pulse X-Ray Units", APPARATURA I METODY RENTGENOVSKOGO ANALIZA, No 4, 1969, pp 95-100.

77. Mesyats, G. A., Bugayev, S. P., Proskurovskiy, D. I., "Explosive Electron Emission", USPEKHI FIZICHESKIKH NAUK, Vol 115, 1975, pp 101-120.

78. Cracknell, A. P., Hall, T. P. P., Twidell, J. W., Whitrow, R. J., "The Determination of the Photon Energy Spectrum of a Flash X-Ray Tube", RADIATION EFFECT, Vol 2, 1970, pp 233-242.

79. Sündström, I., Händel, S. K., Persson, J. E., "Time Resolved Radiation Intensity Distribution in an FXR Discharge", ZEITSCHR. PHYS., Vol 200, 1967, pp 499-500.

80. Aleksandrovich, E. G.-V.. Belkin, N. V., Dron', N. A., Sloyeva, G. N., "Miniature Pulsed X-Ray Tube", PRIBORY I TEKHNIKA EKSPERIMENTA, No 5, 1974, pp 189-190.

81. Aleksandrovich, E. G.-V., Belkin, N. V., Kanunov, M. A., Razin, A. A., "Miniature Pulse X-Ray Tube With Self-Restoring Autocathode", PRIBORY I TEKHNIKA EKSPERIMENTA, No No 6, 1972, pp 198-199.

82. Abramyan, Ye. A., Vasserman, S. V., Dolgushin, V. M. et al., "Generator of Powerful Electron-Beam and X-Ray Pulses (RIUS-5)", PRIBORY I TEKHNIKA EKSPERIMENTA, No 3, 1971, pp 223-224.

83. Grin, "Obtaining X-Ray Diffraction Patterns of Jets Formed by Blasting Shaped Explosive Charges", PRIBORY NAUCHNYKH ISSLEDOVANIY, No 9, 1975, pp 121-125.

84. Yelinson, M. I., "Nenakalivayemyye katody" [Cold Cathodes], Moscow, Sovetskoye radio, 1974, 336 pp.

85. Nögberg, L., Mattsson, A., Nillsson, N. R., Svedberg, A., "An X-Ray Flash Tube With Exchangeable Electrode System", PHYS. SCRIPTA, Vol 1, 1970, pp 197-199.

86. Shall, R., "Detonation Physics" in: "Fizika vysokikh plotnostey energii" [High Energy Density Physics], translated from English, edited by O. N. Krokhin, Moscow, Mir, 1974, pp 258-274.

87. Johnson, Q., Mitchell, A., Keeler, R. N., L. Evans, "Nanosecond X-Ray Diffraction Study of Solids Under Shock Compression", TRANSACT. AMER. CRYST. ASSOC., Vol 4, 1969, pp 133-140.

88. Bykovskiy, Yu. A., Kantsyrev, V. L., Kozyrev, Yu. P., "Using Laser Plasma as a Powerful Pulsed Point Source of Soft X-Rays" in: "Sovremennoye sostoyaniye i perspektivy razvitiya vysokoskorostnoy fotografii i kinematografii bystroprotekayushchikh protsessov", abstracts of the articles, Moscow, Izd. VNIIOFI, 1978, p 110.

89. Killer, R., Roys, Ye., "New Experimental Methods in Shock Wave Physics" in: "Fizika vysokikh plotnostey energii", translated from English, edited by O. N. Krokhin, Moscow, Mir, 1974, pp 158-170.

90. Zelenskiy, K. F., Troshkin, I. A., Tsukerman, V. A. et al., "Portable Pulsed X-Ray Apparatus", USSR Patent No 240868, BYULLETEN' IZOBRETENIY, No 13, 1969.

91. Kurbatov, V. M., Peliks, Ye. A., "IRA-5B Pulsed X-Ray Apparatus", APPARATURA I METODY RENTGENOVSKOGO ANALIZA, No 12, 1973, pp 73-75.

92. Komyak, N. I., Peliks, Ye. A., "IRA-3 and IRA-5 Generators of Nanosecond X-Ray Flashes", DEFEKTOSKOPIYA, No 3, 1971, pp 127-131.

93. Ravary, P., Goldman, M., "Etude sur l'initiation de l'arc dans le vide par l'analyse des temps de commutation" in: "Proc. IV IS on EIDV", 1970, pp 272-275.

94. Mesyats, G. A., "Nanosecond X-Ray Pulses", ZHURNAL TEKHNICHESKOY FIZIKI, Vol 44, 1974, pp 1521-1527.

95. Condith, W. C., Pellinen, D., "Impedance and Spot-Size Measurements on an Intense Relativistic Electron-Beam Device", PHYS. REV. LETT., Vol 29, 1972, pp 263-265.

96. Tolchenov, Yu. M., Chepek, A. V., "Radiation Spectrum of Pulsed X-Ray Tube With Cold Cathode", PRIBORY I TEKHNIKA EKSPERIMENTA, No 4, 1972, pp 233-235.

97. Mühlenpfordt, J., "Verfahren zur Erzeugung kurzeitiger Röntgenblitze", German Patent No 748185, 1939.

98. Komyak, N. I., Peliks, Ye. A., "RINA-1D Pulsed Nanosecond X-Ray Apparatus for Nondestructive Inspection of Materials Under Unsteady Conditions", DEFEKTOSKOPIYA, No 4, 1972, pp 127-131.

99. Bekeshko, N. A., "Electron Delay Generator for Pulsed X-Radiography", PRIBORY I TEKHNIKA EKSPERIMENTA, No 1, 1960, pp 67-68.

100. Tsukerman, V. A., Zelenskiy, K. F., Troshkin, I. A., "Two-Electrode Pulsed X-Ray Tube", USSR Patent No 219704, BYULLETEN' IZOBRETENIY, No 19, 1968.

101. Voytenko, A. Ye., Zherebnenko, V. I., "Explosive Multigap Breaker", PRIBORY I TEKHNIKA EKSPERIMENTA, No 4, 1976, pp 153-155.

102. Fortov, V. Ye., Ivanov, Yu. V., Dremin, A. N. et al., "Explosive Generator of Nonideal Plasma", DOKLADY AKADEMII NAUK SSSR, Vol 221, 1975, pp 1307-1309.

103. Bekturganov, K., Kumanskiy, G. A., "Pulsed X-Ray Tube With Hollow Cathode", PRIBORY I TEKHNIKA EKSPERIMENTA, No 4, 1969, pp 183-184.

104. Ondell, F. A., "The Application of Flash X-Ray Systems to Sports Medicine and Exercise Physiology", JOURN. SPORTS MEDIC., V- 6, 1966, pp 48-54.

105. Zingerman, A. S., Korsunskiy, M. I., Nekrasov, M. S., Eyzenbet, A. A., "Discharge Tube for Pulsed Voltage up to $2.7 \cdot 10^6$ V", ZHURNAL TEKHNICHESKOY FIZIKI, Vol 9, 1939, pp 883-889.

106. Morgovskiy, L. Ya., Peliks, Ye. A., "Investigation of Characteristics of Pulsed X-Ray Sources With Plasma Cathode", APPARATURA I METODY RENTGENOVSKOGO ANALIZA, No 13, 1974, pp 235-238.

107. Oosterkampf, W. J., "X-Ray Photography With Extremely Short Exposure Time", PHILLIPS TECHN. REV., Vol 5, 1940, pp 22-25.

108. Okulov, B. V., Gleyzer, I. Z., Dronova, L. P., "Pulsed Multiemitter Cold Cathode", TRUDY NAUCHNO-ISSLEDOVATEL'SKOGO INSTITUTA YADERNOY FIZIKI PRI TOMSKOM POLITEKHNICHESKOM INSTITUTE, Moscow, Atomizdat, 1974, No 4, pp 22-24.

109. Bichenkov, Ye. I., Polyudov, V. V., Rabinovich, R. L., Titov, V. M., "Pulse Hard X-Ray Device", PRIBORY I TEKHNIKA EKSPERIMENTA, No 3, 1974, pp 208-210.

110. Pikayev, A. K., "Flash Radiolysis of Water and Water Solutions", Nauka, 1955, 286 pp.

111. Al'bikov, Z. A., Veretinnikov, A. I., Kozlov, O. V., "Detektory impul'snogo ioniziruyushchego izlucheniya" [Detectors of Pulsed Ionizing Radiation], Moscow, Atomizdat, 1978.

112. Schaffs, W., "Röntgenblitzrohre zur Untersuchung von schnell ablaufenden Prozessen", MESSTECHNIK, Vol 80, 1972, pp 247-251.

113. Zavada, N. I., Manakova, M. A., Tsukerman, V. A., "Recording Interference of Single Crystals and Polycrystals With Microsecond Exposures", PRIBORY I TEKHNIKA EKSPERIMENTA, No 2, 1966, pp 164-168.

114. Ivanov, Yu. S., Ryukkert, V. V., Sklizkov, G. V., Fedotov, S. I., "Source of X-Radiation for Transilluminating a Laser Plasma", ZHURNAL TEKHNICHESKOY FIZIKI, Vol 42, 1972, pp 1423-1428.

115. Miller, B., "X-Rays Studied for Secure Stationkeeping", AVIATION WEEK, Vol 84, 1966, pp 74-79.

116. Antonenko, L. Ya., Vedyushkina, V. V., Kolosov, N. A. et al., "Flash X-Ray Visualizer", PRIBORY I TEKHNIKA EKSPERIMENTA, No 1, 1972, pp 195-198.

117. Schaafs, W., Krehl, P., "Röntgenblitzuntersuchungen über die Entstehung einer Stosswelle aus einer durch Stosswellenprozesse zur Erstarrung gebrachten Flüssigkeit", ACUSTICA, Vol 23, 1970, pp 99-107.

118. Stepanov, Ye. Ye., "Experimental Study of Time and Energy Characteristics of Semiconductor Detectors in Recording Pulsed X-Rays" in: "Voprosy atomnoy nauki i tekhniki. Yadernoye priborostroyeniye" [Problems of Atomic Science and Engineering. Nuclear Instrument Making], Atomizdat, Moscow, 1976, No 30-31, pp 105-110.

119. Heaton, L. D., ed., "Wound Ballistics", Office of the Surgeon General, Department of the Army, Washington, D. C., 1962, 883 pp.

120. Howieson, J. L., Anderson, R. E., Dyke, W. P., Grundhauser, F. J., "Uses of Flash Radiography in Biodynamic Research", AEROSPACE MEDICINE, Vol 34, 1963, pp 494-496.

121. Kholopin, A. I., Kol'tsov, G. I., Kireyev, P. S., "Pulse Characteristic of Silicon Detector With p-i-n Structure", RADIOTEKHNIKA I ELEKTRONIKA, Vol 17, 1972, pp 132-137.

122. Zavada, N. I., Tsukerman, V. A., "Simple Calorimeter for Measuring Dose of Powerful Flash X-Ray Units", PRIBORY I TEKHNIKA EKSPERIMENTA, No 1, 1976, pp 205-206.

123. Pellinen, "Largest Combined X-Ray Calorimeters", PRIBORY NAUCHNYKH ISSLEDOVANIY, No 8, 1972, pp 115-118.

124. Vavilov, S. P., "Using Flash X-Rays in Flaw Detection", TRUDY NAUCHNO-ISSLEDOVATEL'SKOGO INSTITUTA ELEKTRONNOY INTROSKOPII, Moscow, Atomizdat, No 1, 1978, pp 19-26.

125. Geilring, J. W., "High-Speed Radiographic and Optical Techniques Applied to Hypervelocity Impact Studies", PROC. V IC HSP, Washington, 1962, pp 188-195.

126. Frungel, F., Alberti, H., Thorwart, W., "High-Speed X-Ray Flash Cinematography of Small Objects" in: "Proc. V IC on HSP", N. Y., 1962, pp 170-172.

127. Brewer, W. D., Kassel, P. C., "Flash X-Ray Technique for Investigating Ablative Material Response to Simulated Reentry Environments", INT. JOURN. NONDESTRUCTIVE TESTING, Vol 3, 1972, pp 375-390.

128. Thilo, E. R., "Frankford Arsenal Experience With High-Speed Radiography", ASTM BULLETIN, No 150, 1948, pp 69-72.

129. Zykov, I. K., Baryushchenko, S. B., "Ioniziruyushchiye izlucheniya v aviatsionnoy i kosmicheskoy tekhnike" [Ionizing Radiation in Aerospace Technology], Moscow, Atomizdat, 1975, 128 pp.

130. Iremashvili, D. V., Osepashvili, T. A., "Source of Intense Soft Bremsstrahlung Pulses", PRIBORY I TEKHNIKA EKSPERIMENTA, No 1, 1975, pp 213-214.

131. Pavlovskaya, N. G., Tarasova, L. V., El'yash, S. L., "Soft X-Ray Nanosecond Pulse Source", PRIBORY I TEKHNIKA EKSPERIMENTA, No 5, 1974, pp 190-192.

132. Passner, "Powerful Flash X-Ray Tube With Laser Excitation of Electron Flux", PRIBORY NAUCHNYKH ISSLEDOVANIY, No 11, 1972, pp 88-91.

133. Garnov, V. V., Fedin, Y. D., "Stereoscopic X-Ray Flash Photography of High-Speed Processes", PHOTOGR. KORRESPONDENZ, Vol 104, 1968, pp 21-26.

134. Slack, C. M., Ehrke, L. F., Dickson, D. C., Zavales, C. T., "High-Speed Cine-Radiography", NON.-DESTR. TEST., Vol 7, 1949, pp 7-11.

a35. Charters, A. C., "High-Speed Impact", SCI. AMERICAN, Vol 203, 1960, pp 128-140.

136. Tolchenov, Yu. M., Chepek, A. V., "Working Conditions of Controlled X-Ray Flash Tube With Cold Cathode", PRIBORY I TEKHNIKA EKSPERIMENTA, No 3, 1973, pp 218-219.

137. "X-Ray Equipment for Checking Airline Luggage", ELEKTRONIKA, No 20, 1972, pp 21-22.

138. Vallis, G., Zauer, K., Zyunder, D., "Injecting Intense Relativistic Electron Beams Into Plasma and Gas", USPEKHI FIZICHESKIKH NAUK, Vol 113, 1974, pp 435-462.

139. Didenko, A. N., Grigor'yev, V. P., Usov, Yu. P., "Moshchnyye elektronnyye puchki i ikh primeneniye" [Intense Electron Beams and Their Use], Moscow, Atomizdat, 1977.

140. Bakulin, Yu. D., Diyankov, V. S., Kovalev, V. P. et al., PRIBORY I TEKHNIKA EKSPERIMENTA, No 2, 1979, pp 34-37.

141. Jamet, F., Thomer, G., "Production d'impulsions de rayons X-tres courtes avec tubes a discharge dans le vide due type diode" in: "Proc. VIII IC on HSP", 1969, pp 259-261.

142. Morgovskiy, L. Ya., Kurbatov, V. M., "Particulars of Spectral Makeup of Flash X-Ray Generator Emission", APPARATURA I METODY RENTGENOVSKOGO ANALIZA, No 15, 1975, Leningrad, Mashinostroyeniye, pp 175-179.

143. Ovcharov, A. M., Romanovskiy, V. F., Stepanov, B. M. et al., "RAPS-1 X-Ray Equipment With High-Frequency Electron Acceoerator", DEFEKTOSKOPIYA, No 9, 1980, pp 94-97.

Contents page

6610
CSO: 8144/0162

UDC 621.378

STUDY OF WIDE-APERTURE FLAT RESONATOR FIELDS

Moscow KVANTOVAYA ELEKTRONIKA in Russian Vol 8, No 5 (107), May 81
(manuscript received 3 Sep 80) pp 1037-1044

[Article by V. G. Marchenko]

[Text]

Abstract: Methods of extracting separate monochromatic selfimaging fields in a wide-aperture resonator with amplitude gratings and grating mirrors placed into the cavity are subjected to theoretical and experimental investigation (on a neodymium-doped glass laser). It is shown that the application of the amplitude gratings and grating mirrors in a flat resonator is an effective means of increasing spatial coherence and stable excitation of monochromatic fields with various spatial characteristics. It is noted that by using the gratings it is possible to control the lasing frequency tuning, obtain phase modulation and convert the fields into each other on introducing an additional phase grating into the resonator.

The problem of obtaining coherent radiation from a large volume of active medium is now solved primarily by using unstable resonators [1]. Nevertheless, the development of new ways to solve this problem is of great interest on the theoretical and practical levels. One new solution is considered to be the application of resonators with grating mirrors or introduced gratings, the prospectiveness of which has been discussed in a number of theoretical and experimental studies [2-6]. Formulation of the problem in this way has much in common with the problem of energy output from a resonator through openings in mirrors, which also indicates the urgency of the problem. This paper studies the fields of wide-aperture flat resonators with amplitude gratings.

1. The application of thin wires to suppress undesirable types of oscillations in microwave resonators is a well-known procedure. Analogous experiments have also been performed in the early studies of open resonators [7, 8]. In spite of simplicity and efficiency, this method of controlling fields has not been widely developed. However, it was recently revived [9, 10] in connection with work on phase compensation of emission leaving a stable resonator. Reference [11] presents an experimental study of the influence of grating mirrors simulating metal mirrors with holes for energy output on flat resonator fields. In reference [11] reconstruction

of the periodic structure of the field on a smooth mirror and augmentation of the spatial coherence of the emission were detected. The conclusion was drawn that the grating plays a passive role in the resonator. In connection with the theoretical work [2] experimental studies [3-5] appeared which directly consider the effect of grating mirrors and resonator lengths on the excited fields. Instead of grating mirrors, in [6] a bronze foil grating was used which was installed in direct proximity to a total-reflecting mirror. A number of measures -- a decrease in aperture and area of the shading zones, recording the field from a side of a smooth semitransparent mirror -- permitted excitation of simple, easily interpreted fields in a resonator and study of their dependence on the resonator length. Square gratings with intersecting shading bands were used in both [6] and other papers [3-5, 13]. Therefore we found it interesting to study fields excited in a plane resonator with other types of gratings.

2. The theoretical arguments, which do not claim to sufficient mathematical strictness, but served as a guide in performing the experiments, consisted in the following. As is demonstrated in [12], selfimaging fields in free space and the fields of flat resonators with unlimited ideal mirrors have a common nature. The fields of wide-aperture resonators, the Fresnel numbers of which are many orders greater than one will not differ significantly from the fields of an unlimited resonator. In the scalar approximation monochromatic fields have the form

$$\psi(r, \varphi, z, t) = e^{-i\omega t} \sum_{l=0}^{L} \sin \frac{\pi l z}{d} \sum_{m=-\infty}^{\infty} \Psi_{lm} J_m(\varkappa_l r) e^{im\varphi}, \qquad (1)$$

where r, ϕ, z are a cylindrical coordinate system with origin at one of the mirrors; Ψ_{lm} is the complex amplitude of an electric field which can be nonzero only for $\varkappa_l = [k^2 - (\pi l/d)^2]^{1/2} \ll (D/2d)k$; k is the wave number; d is the resonator length; D is the diameter of its aperture; L is the integral part of the fraction $2d/\lambda$; λ is the radiation wavelength; J_m is a Bessel function of the first kind. In the paraxial approximation this formula includes fields of translational symmetry:

$$\psi(\rho, z, t) = \psi(\rho + a_{mn}, z, t) = \exp[i(kz \mp \omega t)] \times \times \sum_{p,q} \Psi_{pq} \exp\left(-i \frac{b_{pq}^2}{2k} z\right) \exp(i b_{pq} \rho), \qquad (2)$$

where $a_{mn} = ma_1 + na_2$; $b_{pq} = pb_1 + qb_2$; a_1, a_2 and b_1, b_2 are the basis vectors of the field grating and inverse grating, respectively; ρ is the radius vector in the plane XY; m, n, p, q are integers $|b_{pq}| \ll k$. Such fields are selfimaging on satisfaction of the following conditions:

$$2d/\lambda = L; \quad a_1 \sqrt{h_1} = a_2 \sqrt{h_2}; \quad 2\sqrt{h_2/h_1} \cos\alpha = g_2/g_1,$$

where L, h_1, h_2, g_1, g_2 are integers; α is the angle between a_1 and a_2. Here the resonator length will be $d = (g_1 a_1 a_2/\lambda)\sqrt{h_1 h_2} \sin^2\alpha$.

In [12] it is demonstrated that the selfimaging period of fields of translational symmetry can with accuracy to the constant phase be an integral number f times shorter than the exact reconstruction period if the field is formed by a set b_{pq} such that all $N_{pq} = g_1 h_1 p^2 + g_2 h_1 pq + g_1 h_2 q^2$ or (for $b_{pq\ min} \neq 0$) $m_{pq} = g_1 h_1 (p^2 - p^2_{min}) + g_2 h_1$,

$(pq-p_{m_1n}q_{m_1n})+g_1h_2(q^2-q^2_{m_1n})$ have the number f as their greatest common divisor. It is easy to see that expressions (1) and (2) include known modes of a flat resonator [14].

The mechanism of the effect of an absolutely absorbing amplitude grating introduced into a resonator on the fields can be traced in a mechanical analog -- a wire fastened at the ends (Figure 1). Let us assume that at a distance ξ from one of the fastenings, the wire rubs against an infinitely narrow rod. The frictional force is proportional to the derivative of the amplitude with respect to time. Then the equation of motion has the form

$$\frac{\partial^2 y}{\partial t^2}+a\delta(x-\xi)\frac{\partial y}{\partial t}-c^2\frac{\partial^2 y}{\partial x^2}=0.$$

The undisturbed problem (a = 0) has the solution

$$y_n=\sin\left(\frac{n\pi c}{d}t+\alpha_n\right)\sin\frac{n\pi x}{d},$$

where d is the length of the wire; n is an integer. Without solving the disturbed problem, it is possible to state in advance that it will be satisfied by those y_n, the index of which is defined by the ratio $\xi/d = m/n$, that is, the vibrations, one of the nodes of which is located at the point ξ. It is possible to see the validity of what has been stated by direct substitution. The remaining types of vibrations will be damping. If the ratio ξ to d turns out to be irrational, then all of the vibrations will be damping.

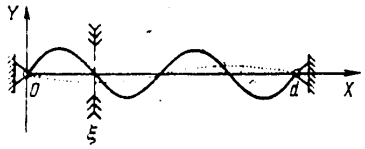

Figure 1. Mechanical model.

The analyzed example provides a basis for assuming that when the grating is placed in the resonator the selfimaging fields, by the topography of the nodes of which the topography of the shading (scattering, absorbing) sections of the grating is selected, remain slightly disturbed. However, in contrast to a one-dimensional wire, three-dimensional fields in the resonator, the dimensions of which are much greater than the wavelength, and the Fresnel numbers are several orders greater than one, can be considered fixed only with respect to one measurement (with respect to the resonator axis) and free with respect to the other two. Therefore in the transverse cross section of the resonator the fields will be simulated by a wire or diaphragm of unlimited dimensions. This means that a grating in a resonator will not require exact installation with respect to the edges of the mirrors, and the spatial harmonics will be phased so that standing waves will be set up in the resonator, the nodes of which match with the shading sections of the grating. The general expression for these standing waves has the form

$$\psi(r, \varphi, z, t) = e^{-i\omega t} \sum_{l=0}^{L} \sin \frac{\pi l z}{d} \sum_{m=-\infty}^{\infty} (A_{lm} \cos m\varphi + B_{lm} \sin m\varphi) J_m(\varkappa_l r).$$

The width of the shading sections of the grating is in practice always finite. This leads to the fact that superposition of different vibrations which, as a result of interference, forms the field null (minimum) in the shading sections, will become energy wise advantageous. However, the field will not become completely extinguished because oscillations with a finite number of small κ_l are excited in a resonator with limited aperture. This determines the additional losses by comparison with resonators without gratings.

3. The experimental setup -- a neodymium-doped glass laser used in the present experiment -- was described previously in [6]. For visual representation of the grating field, the property of selfimaging of resonator fields at a distance 2d was used, as follows from formula (1). Therefore the field was recorded a distance d behind a semitransparent mirror, where the wave traveling along the Z-axis copied the field on the opaque mirror near which the gratings were placed.

Seven types of gratings and grating mirrors were used in the experiments: a one-dimensional grating (parallel wires) with a period of 1 mm and wire diameter of 0.1 mm; four types of square gratings with the same period: a wire grating with wire diameter of 0.1 mm, two of bronze foil with holes 0.5 × 0.5 mm and circular holes of 0.8 mm in diameter, and a grating mirror with nonreflecting "islands" about 0.3 mm in diameter; a hexagonal grating of steel foil with a period of 0.85 mm and width of the shading intervals of 0.25 mm and, finally, a mirror with nonreflecting concentric circles. The grating mirrors were obtained by mechanically damaging a multilayered dielectric coating. Radii r_n of the concentric circles in millimeters were given by the equation $J_0(2\pi r_n) = 0$. The measurements demonstrated that they were sustained with an accuracy to ± 0.06 mm. The nonreflecting rings were about 0.08 mm wide. The deviation of the geometric parameters from the given values did not exceed 0.05 mm. The resonator length varied from 35 to 110 cm. The angular spectrum of the emission was recorded in the focal plane of an objective with F = 100 cm. The experiments were performed in the free-running mode.

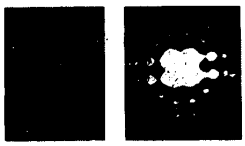

Figure 2. Far zones of laser emission with one-dimensional (a) and two-dimensional (b) gratings in the resonator indicating monocrhomatization of the radiation.

Figure 3. Far emission zone of a laser as a function of the position of the grating in the resonator with identical lasing power.

Experiments were run with the one-dimensional grating which permitted visual comparison of the resonator field with smooth and grating mirrors: the ratio of the

angular dimensions of each lobe of the radiation pattern along and across the grating can be taken as the degree of increase in coherence of the radiation. In our experiments it was 5-7 (Figure 2, a). The fact of monochromatization of the emission was determined in experiments using a square grating with round holes; the far-zone emission was localized on the rings of a Fabry-Perot interferometer (Figure 2, b) inasmuch as a flat resonator is a Fabry-Perot etalon for the field itself.

A square wire grid was used to investigate the excited fields as a function of the position of the grating in the resonator: first the grating was installed in direct proximity to a totally reflecting mirror; in subsequent experiments the distance was increased. The spatial lasing spectrum is presented in Figure 3 for distances (from left to right) of 0.5, 10 and 27 cm. In these experiments the resonator length was 61 cm, the lasing energy was sustained at one level with precision to 10%, and the pumping energy was twice the threshold energy. The results obtained permit the following explanation. When the grating is located in direct proximity to the mirror, a complex single-frequency field is excited in the resonator, the nodes of which are located in the shading sections of the lattice, and the selfimaging period of such a field is equal to a complete pass around the resonator 2d. When the grating is removed from the mirror, the initial complex field can be excited to the point that the depth of focus of the interference pattern formed permits it. With a further increase in distance, the lasing threshold can be lower for fields reconstructed with a complete pass around the two arms of the resonator into which it is divided by the grating. However, it is possible to find a position of the grating where the simplest field $\sin(\pi \ell z/d) \sin k_x x \sin k_y y$ will have minimum excitation threshold for given aperture within broad pumping intervals. The topography of the arrangement of the nodes of this field will not depend on z in the transverse cross section of the resonator. As a result of this fact the losses of such a field on the grating will not depend on the position of the grating in the resonator.

4. Experiments in exciting fields with different gratings were run for different pumping levels and resonator lengths. The angular spectra of the excited fields were distinguished by great variety, in particular when the resonator length was close to the selfimaging halfperiod, and the area of the shading sections was equal to or exceeded the area of the unshaded sections. This can be explained by several causes. First, for this resonator length any set of harmonics described by expression (2) and having field minima in the shading sections is selfimaging. Since there are many such fields having similar losses, the process of exciting them becomes uncontrolled. Secondly the scattering of the field on such gratings can lead to the appearance of a number of additional spatial harmonics, the intensity of which can in individual cases turn out to be comparable to the intensity of the excited field harmonics. However, in the case of good matching of the grating with the field (if necessary, with the application of additional measures such as varying the resonator length or installing an additional grating), the angular lasing spectrum is greatly simplified, the harmonic amplitudes of the scattered field decrease sharply, and the fields become stable in a wide range of pumping energy variation. Images of such fields are presented in Figure 4, in which the used gratings and grating mirrors are presented in column a, the fields on the gratings are presented in column b, and the angular spectra of the fields are presented in columns c-e. Furthermore, we can consider that the X-axis is directed along the rows, and the Y-axis, along the columns.

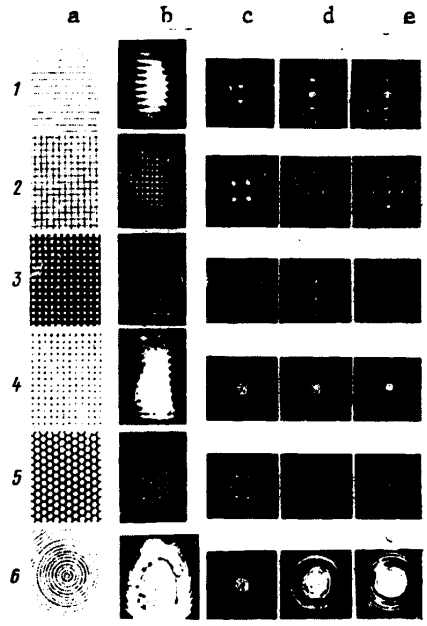

Figure 4. Form of gratings (a) placed in a flat resonator, fields on the gratings (b) and the corresponding Fourier spectra of the radiation (c - e).

Fields excited in a resonator with shading sections in the form of bands (in two-dimensional gratings, in the form of intersecting bands), are subject to a common law: with significant deviation of the resonator length from the selfimaging half-period (from 106 to 80-35 cm) sign-variable fields are excited on the grating. This is indicated by the absence of a central lobe in the far radiation zone (see 1, 3, 5 in Figure 4, c). The absence of an axial spatial harmonic in the given case is explained by the fact that an integral number of halfwaves do not fit in the resonator length. The condition of selfimaging in the paraxial approximation must in this case be satisfied in the form $(k - b_{pq}^2/2k)d = \pi\ell_{pq}$, where ℓ_{pq} is an integer which depends on p and q, at the same time as for the calculated resonator length equal to half the selfimaging period, it breaks down into two equalities: $kd = \pi\ell$ and $(b_{pq}^2/2k)d = \pi N_{pq}$. As the resonator length approaches the calculated length (80-100 cm), fields can be excited which are sign-variable with respect to one coordinate and cophasal with respect to the other, which is indicated by the presence in the radiation pattern of lobes that deviate from the axis only with respect to one coordinate (in Figure 4.2, d, the field is cophasal with respect to the Y-axis and sign-variable with respect to the X-axis; in 3d, the opposite is true). When the resonator length is close to the calculated length (3-5% deviation), cophasal fields are excited (1d, 1e, 2e, 5d). A grating mirror with nonreflecting "islands" (4a) has one noteworthy characteristic consisting of the fact that for dimensions of the shading sections significantly less than the grating period, only cophasal fields are excited in a resonator with this mirror. No less than 80% of the emission

power[1] is contained in the axial spatial harmonic. Cophasal fields were also observed with a grating mirror with shading concentric circles (6a), but with such a mirror it is possible under suitable conditions to hope to obtain the simplest axisymmetric sign-variable selfimaging field, the selfimaging period of which is undefined with accuracy to the phase. In such a field the intensity in the resonator cross section has distribution with respect to a zero-order Bessel function, and the far zone is a circle.

On the whole, it is necessary to note that the lasing threshold with gratings was above the lasing threshold without them, and it depended both on the specific area of the shading sections and the type of field excited in it.

5. It is possible to propose the following interpretions of fields the spatial spectra of which are shown in Figure 4. A field excited on a one-dimensional grating and having a spatial spectrum in the form of two equally intense points symmetric with respect to the projection of the resonator axis (1c) can be expressed on the grating in the form $\psi_{1c} = \sin vy$, where $v = \pi/a$. Cophasal fields are the first two (1d) and three (1e) terms of the cosinusoidal Fourier series. In particular, a field with angular spectrum (1d) can be interpreted as $\psi_{1d} = 1 - \cos 2vy = 2\sin^2 vy$, the zeros of which are located on the wires. The following fields can be placed in correspondence to fields excited in a resonator with square grating:

$$\psi_{2a}=\cos v(x+y)-\cos v(x-y)=\sin vx \sin vy,$$

(a)

$$\psi_{2c}=2\sin vx-\sin v(x+2y)-\sin v(x-2y)=4\sin vx \sin^2 vy,$$

(b)

$$\psi_{2\partial}=2-2\cos 2vx-2\cos 2vy+\cos 2v(x+y)+\cos 2v(x-y)=8\sin^2 vx \sin^2 vy.$$

(c) Key: a. 2c b. 2d c. 2e

Fields, the far zones of which are presented in Figure 4, 3c and 3d, can be interpreted as $\psi_{3c} = \sin^2 vx^3 vy$ and $\psi_{3c} = \sin^2 vx \sin^3 vy$, the Fourier transform of which coincides with the mentioned far zones of the emission. The case 3e obviously is hybrid and is a superposition of fields 2e, 2d and the same 2d, but rotated by 90°:

$$\psi_{3\partial}=\sin vx \sin vy\ (A\sin vx+B\sin vy+C\sin vx \sin vy).$$

(1) Key: 1. 3e

The Fourier spectra presented in Figure 4 (4c and 4d) correspond to the fields

$$\psi_{4a}=2+\cos vx+\cos vy, \quad \psi_{4c}=2+\cos v(x+y)+\cos v(x-y),$$

(1) Key: 1. 4c (2) 2. 4d

and the case 4e also obviously can be interpreted as hybrid. The far zones of the fields excited in a resonator with hexagonal grating are also presented in Figure 4 (5c, 5d and 5e). Analytical expressions for the fields on the grating corresponding to the first two cases can be represented in the form

---

[1] These fields were first observed in [4] on another type of grating mirror which obviously was similar to the one used here as a result of manufacturing technology.

$$\psi_{5a} = 4\sin\frac{vx}{\sqrt{3}}\sin\frac{v}{2}\left(\frac{x}{\sqrt{3}}+y\right)\sin\frac{v}{2}\left(\frac{x}{\sqrt{3}}-y\right) =$$
(a)
$$= -\sin 2\frac{vx}{\sqrt{3}} + \sin v\left(\frac{x}{\sqrt{3}}+y\right) + \sin v\left(\frac{x}{\sqrt{3}}-y\right),$$

$$\psi_{5z} = 4\cos\frac{vx}{\sqrt{3}}\cos\frac{v}{2}\left(\frac{x}{\sqrt{3}}+y\right)\cos\frac{v}{2}\left(\frac{x}{\sqrt{3}}-y\right) =$$
(b)
$$= 1+\cos 2\frac{vx}{\sqrt{3}} + \cos v\left(\frac{x}{\sqrt{3}}+y\right) + \cos v\left(\frac{x}{\sqrt{3}}-y\right).$$

Key: a. 5c b. 5d

In a resonator with a grating mirror 6a fields were excited which can be interpreted as distorted by nonuniform pumping of a field of the type

$\psi_6 = \sum A_i J_0(\varkappa_{L-i} r)$. In particular, $\psi_{6z} = 1 - AJ_0(\varkappa_{L-1} r)$.
(a)

Key: a. ψ_{6d}

6. The experiments demonstrated that the application of gratings and grating mirrors in resonators is an effective method of controlling the fields. In addition to increasing the spatial coherence noted earlier, it was illustrated experimentally that in a flat resonator with a grating monochromatic fields with various spatial characteristics that can be monitored and controlled, can be stably excited.

It is also necessary to note the existing possibility of frequency tuning of a resonator with a grating by varying both its length and the grating period.

The approach developed in [12] and here to the problem of the fields of wide-aperture flat resonators permitted not only explanation of all the peculiarities of the excited fields, but also discovery of the excitation conditions of the most characteristic of them. Thus, in particular, the type of grating mirror depicted in Figure 4 (4a) was theoretically obtained from analysis of possible selfimaging fields. The experiments fully confirmed the conclusion that with this type of losses fields are excited with high energy concentration in the central lobe of the radiation pattern.

Good agreement between theory and experiment, which was demonstrated in this work, offers the possibility of the statement of other propositions with respect to the intraresonator methods of controlling fields. Thus, moving the gratings across the resonator should lead to phase modulation of the fields inasmuch as the nodes of the interference pattern must follow the position of the shading zones. Only such fields can have minimum losses in a resonator with moving grating and, consequently, will have minimum excitation threshold. In addition, using a periodic amplitude grating of defined porosity, it is possible to excite a selfimaging field in the resonator which in some of the resonator cross sections (multiplication planes) will have only phase periodicity, and the amplitude distribution will be close to constant. By installing the corresponding phase grating in the indicated cross section it is possible to achieve equalization of the wave front

leaving the resonator or conversion to another type of field which is selfimaging on passing around a segment of the resonator located behind the phase grating.

I express my sincere appreciation to L. A. Vaynshteyn for useful criticism, valuable advice, great assistance and support in this experiment.

BIBLIOGRAPHY

1. Yu. A. Anan'yev, OPTICHESKIYE RESONATORY I PROBLEMA RASKHODIMOSTI LAZERNOGO IZLUCHENIYA (Optical Resonators and the Problem of Laser Radiation Divergence), Moscow, Nauka, 1979.

2. V. K. Ablekov, V. S. Belyayev, ZHPS (Journal of Applied Spectroscopy), No 23, 1975, p 1110.

3. V. K. Ablekov, V. S. Belyayev, V. M. Marchenko, A. M. Prokhorov, DAN SSSR (Reports of the USSR Academy of Sciences), No 230, 1976, p 1066.

4. V. M. Marchenko, T. M. Makhviladze, A. M. Prokhorov, M. Ye. Sarychev, ZHETF (Journal of Experimental and Theoretical Physics), No 74, 1978, p 872.

5. V. K. Ablekov, V. S. Belyayev, V. I. Vinogradov, V. G. Marchenko, V. M. Marchenko, A. M. Prokhorov, OPTIKA I SPEKTROSKOPIYA (Optics and Spectroscopy), No 44, 1978, p 1208.

6. V. K. Ablekov, V. G. Marchenko, ZHPS, No 29, 1978, p 609.

7. W. W. Rigrod, APPL. PHYS. LETTS., No 2, 1963, p 51.

8. Akira Okaya, TRUDY IIER (Works of the IIER Institute), No 52, 1964, p 1894.

9. L. W. Casperson, N, K. Kincheloe, O. M. Stafsudd, OPTICS COMMS., No 21, 1977, p 1.

10. A. V. Gnatovskiy, N. G. Zubrilin, A. P. Loginov, UKR. FIZ. ZHURNAL (Ukrainian Physics Journal), No 23, 1978, p 1961.

11. Yu. A. Anan'yev, N. I. Grishmanova, N. A. Sventsitskaya ZHTF (Journal of Technical Physics), No 43, 1973, p 1530.

12. V. G. Marchenko, KVANTOVAYA ELEKTRONIKA (Quantum Electronics), No 8, 1981, p 1027.

13. V. K. Ablekov, V. S. Belyayev, V. P. Vasil'yev, A. N. Golovistikov, V. M. Davydov, V. G. Savel'yev, ZHPS, No 28, 1978, p 57.

14. L. A. Vaynshteyn, OKTRYTYYE RESONATORY I OTKRYTYYE VOLNOVODY (Open Resonators and Open Wave Guides), Moscow, Sov. radio, 1966.

10845
CSO: 1862/220

UDC 535.317:621.378

SELFIMAGING FIELDS

Moscow KVANTOVAYA ELEKTRONIKA in Russian Vol 8, No 5 (107), May 81 (manuscript received 3 Sep 80) pp 1027-1036

[Article by V. G. Marchenko]

[Text]

Abstract: Nonmonochromatic and monochromatic fields which selfimage in space are investigated. In the paraxial approximation, fields that are periodic in the transverse cross section and have defined relations between their geometric parameters satisfy the selfimaging condition. Some properties of such fields are investigated. It is demonstrated that the fields of flat resonators are special cases of the investigated selfimaging fields and that in wide-aperture, optical-band resonators the transverse wave numbers have a continuous spectrum of values which has an upper bound in the active resonator as a result of the existence of an excitation threshold. An experimental study was made of some of the characteristic features of monochromatic selfimaging fields and their behavior in the case of aperture restrictions and spatial filtration, that is, for simulation in free space of resonator fields with Fresnel number equal to 100.

The phenomenon of selfimaging fields, that is, obtaining equidistant images of amplitude grids without using optical elements was observed for the first time by Talbot [1] on exposure of a one-dimensional grid to a plane monochromatic wave. This phenomenon is explained as follows. The field after the grid is a sum of plane waves. If the grid has a defined configuration, the orientation of these waves after it is such that the phase lead in some planes parallel to the grid plane — the selfimaging planes -- becomes a multiple of 2π for all waves. Accordingly, the field in the indicated planes repeats the field on the grid. The first theoretical interpretation of this phenomenon was given by Rayleigh [2]. Subsequently, selfimaging fields were rediscovered many times [3, 4], and there was renewed interest in them [5-9].

Selfimaging fields are manifested not only in free space, but also in a space bounded by guide planes. Thus, the focusing effect of a waveguide [10, 11]

formed by plane surfaces is caused by this kind of selfimaging of fields: as a result of multiple reflections from mirror walls in the plane perpendicular to the wave guide axis, a grid of coherent imaginary emission sources arises which is reproduced after defined intervals along the wave guide axis. In the theoretical paper [12], attention was given to the relation of the fields of open plane resonators to the phenomenon of selfimaging of the fields.

This paper is devoted to a theoretical and experimental study of selfimaging fields in free space and the discovery of the peculiarities of the field formation in wide-aperture (Fresnel numbers N >> 1) flat resonators.

1. Let us consider an arbitrary electromagnetic field in free space. It can be represented in the form of a superposition of plane waves which has the following form in scalar approximation

$$\psi(\mathbf{r},t)=\int \Psi(\mathbf{k})\exp i[\mathbf{kr}-\omega(k)t]d\mathbf{k}, \tag{1}$$

where $\Psi(k)$ is the complex amplitude; $\omega(k) = kc$; c is the speed of light, dk is an element of volume in the space of the wave vectors. Let us note that all future calculations are easily generalized to the case of vector fields.

Let us require that the field in space be reproduced with a period z_0 along the Z-axis of the cartesian coordinate system. Then the term k_z can assume only the values $2\pi l/z_0$ ($l = 0, \pm1, \pm2, \ldots$), and instead of the integral (1) we have the expression

$$\psi(x, y, z, t)=\sum_{l=-\infty}^{\infty}\exp\left(i\frac{2\pi lz}{z_0}\right)\int\int_{-\infty}^{\infty}\Psi_l(k_x, k_y)\times \exp[i(k_x x+k_y y-\omega_l t)]dk_x dk_y, \tag{2}$$

where $\omega_l = c\sqrt{k_x^2+k_y^2+(2\pi l/z_0)^2}$.

The selfimaging period of the fields can be less than z_0 if the series (2) turns out to be incomplete. In the case, for example, where the field is formed by a single component with index l, it will be reproduced with a period of z_0/l, and it will not depend on z with accuracy to the phase. If in formula (2) only the terms with values of l having the greatest common divisor f are nonzero, then the selfimaging period will be z_0/f. If the series (2) only has l such that $|l| \geq l_0$, the field period (with accuracy to the phase) will also be f times shorter (here f is the greatest common divisor of the numbers $l - l_0$). Thus, if the field is represented by two terms l_0 and l_1, the selfimaging period is equal to $z_0/(l_1 - l_0)$ with accuracy to the phase.

2. We obtain selfimaging monochromatic fields if we consider in expression (2) that $|k|$ = const must occur or, what amounts to the same thing, ω = const. In this case l varies from -L to +L, where L is the integral part of the fraction z_0/λ, λ is the wavelength, and expression (2) assumes the form

$$\psi(r,\varphi,z,t)=e^{-i\omega t}\sum_{l=-L}^{L}\sum_{m=-\infty}^{\infty}\Psi_{lm}J_m(\varkappa_l r)\exp\left[i\left(m\varphi+\frac{2\pi lz}{z_0}\right)\right], \tag{3}$$

where r, ϕ, z are the cylindrical coordinate system; J_m is a Bessel function of the first kind;

$$\varkappa_l = \sqrt{\omega^2/c^2 - (2\pi l/z_0)^2}; \tag{4}$$

inasmuch as only values of k_x, k_y such that $k_x^2 + k_y^2 = \chi_\ell^2$ are possible for a monochromatic wave in the plane k_x, k_y.

3. Using identities of the type

$$\sum_{m=-\infty}^{\infty} \exp im\varphi J_m(ar) = \exp iay,$$

it is possible to show that expression (3) contains the simplest fields having periodicity in transverse cross section, for example:

$$\psi = \exp(-i\omega t)\exp(i2\pi lz/z_0)\cos k_x x \cos k_y y. \tag{5}$$

However, in connection with the fact that it is impossible to select a series $\varkappa_\ell$ which forms an arithmetic progression, expression (3) cannot define selfimaging periodic (in the z = const cross section) fields of more complex structure.

What has been said pertains to exact selfimaging of fields. However, if the base vectors of the grid a_1 and a_2 are properly selected, periodic fields can be realized which selfimage in the paraxial (parabolic) approximation. Let us consider a monochromatic field

$$\psi = e^{-i\omega t} \sum_{p,\,q} \Psi_{pq} \exp[i(b_{pq}\rho + \beta_{pq} z)], \tag{6}$$

where ρ is a vector with the components x, y, 0; $b_{pq} = pb_1 + qb_2$; $\beta_{pq} = \sqrt{\omega^2/c^2 - b_{pq}^2}$; $|b_{pq}| \leqslant \omega/c$; p, q are integers; b_1, b_2 are base vectors of the inverse grid. If we consider that $|b_{pq}| \ll k$ and set $\beta_{pq} = k - b_{pq}^2/(2k)$ (this includes the paraxial approximation -- we shall limit ourselves to waves propagated at small angles to the Z-axis), then the field

$$\psi(\rho, z, t) = \psi(\rho - a_{mn}, z, t) = \exp[i(kz - \omega t)] \sum_{p,\,q} \Psi_{pq} \exp\left(-i\frac{b_{pq}^2 z}{2k}\right) \times \times \exp(ib_{pq}\rho) \tag{7}$$

(where $a_{mn} = ma_1 + na_2$; m, n are integers) will be selfimaging for

$$(k - b_{pq}^2/2k)\, z_0 = 2\pi l_{pq}, \tag{8}$$

ℓ_{pq} are integers. This condition will be satisfied for any p and q, including for $p = q = 0$. Therefore it is broken down into two conditions:

$$kz_0 = 2\pi L; \quad b_{pq}^2 z_0/2k = 2\pi N_{pq}, \tag{9}$$

where L, N_{pq} are integers.

Thus, in the paraxial approximation the fields having periodicity in the cross section of z = const can in the general case be reproduced only for integral z_0/λ. Within the framework of this approximation the selfimaging effect is manifested after periodic transparencies on diffraction of plane monochromatic waves on them. A theoretical analysis of this effect [5-9] is also based on the indicated approximation.

On the basis of a unique relation between basis vectors a_1, a_2 of the initial grid and b_1, b_2 of the inverted grid [13]

$$\mathbf{b}_1 = 2\pi \frac{\mathbf{a}_2 \times \mathbf{v}}{\mathbf{a}_1 (\mathbf{a}_2 \times \mathbf{v})}, \quad \mathbf{b}_2 = 2\pi \frac{\mathbf{v} \times \mathbf{a}_1}{\mathbf{a}_1 (\mathbf{a}_2 \times \mathbf{v})}, \quad \mathbf{v} = \frac{\mathbf{a}_1 \times \mathbf{a}_2}{|\mathbf{a}_1 \times \mathbf{a}_2|}, \quad \mathbf{a}_i \mathbf{b}_j = 2\pi \delta_{ij}, \; i, j = 1, 2 \tag{10}$$

(δ_{ij} is the Kronecker symbol) from the second condition (9) it is possible to find all the geometric parameters of the grids providing for reproduction. In reference [5] it was demonstrated that the relations $a_1 h_1 = a_2 h_2$, $2h_1 h_2 \times \cos\alpha = h_3$ must be satisfied, where all h_j are integers; α is the angle between a_1 and a_2. In a later paper [9] it was established that the effect must be observed also for h_3 equal to a rational number. Let us show that the class of selfimaging grids is appreciably broader. For this purpose let us expand the second condition of (9) by the scalar product rules:

$$\frac{z_0}{2k} (p\mathbf{b}_1 - q\mathbf{b}_2)^2 = \frac{z_0 b_1^2}{2k} \left(p^2 - 2 \frac{b_2}{b_1} pq \cos\gamma + \frac{b_2^2}{b_1^2} q^2 \right) = 2\pi N_{pq}, \tag{11}$$

where γ is the angle between b_1 and b_2. Assuming that $-2(b_2/b_1)\cos\gamma = g_2/g_1$ and $b_2^2/b_1^2 = h_2/h_1$ are irreducible fractions (the angle γ is obtuse), and considering that (10) implies $b_j = 2\pi (a_j \sin\alpha)^{-1}$ and $\alpha = \pi - \gamma$, we obtain the following relations for the geometric grid parameters and the field selfimaging period:

$$a_1 \sqrt{h_1} = a_2 \sqrt{h_2}^{*}), \quad 2\sqrt{h_2 h_1} \cos\alpha = g_2/g_1,$$
$$z_0 = (2 g_1 a_1 a_2 \sqrt{h_1 h_2} \sin^2\alpha)/(\lambda f) \tag{12}$$

(here f is the greatest common divisor of all $N_{pq} = g_1 h_1 p^2 + g_2 h_1 pq + g_1 h_2 q^2$). Let us note that for f = 1 both conditions of (9) are satisfied, and for f > 1, only the second; therefore reproduction is realized with accuracy to a phase. Considering that the factor $\exp(ikz_0)$ oscillates rapidly for small variations of z_0, at the same time as $\exp[i(-b_{pq}^2 z_0/2k)]$ varies slowly, for f > 1 it is also possible to satisfy the selfimaging condition in the form of (8) with sufficient accuracy for the paraxial approximation if there is insignificant variation of z_0 (within the limits of $|\Delta z_0| \leq \lambda/2$) or the wavelength ($|\Delta\lambda| \leq \lambda^2/2z_0$).

---

*) An analogous relation for the sides of a rectangular waveguide was noted in reference [14].

4. Selfimaging fields which are periodic in the XY plane have a number of remarkable characteristic features: In the cross sections for which $2z/z_0 = \sigma/\tau$ is an irreducible fraction, with grid porosity (period to cell ratio) greater than τ, the field always forms a sharp grid with τ-fold increase in the number of cells per period. Here a shift of the reproduced image with respect to the original for certain σ, τ is possible: the cells of the original are either matched with the cells of the image or or they are shifted along one or both axes such that the projection of the original cells is between the image cells.

For investigation of these properties let us represent the series (7) in the form

$$\psi = \exp[i(kz-\omega t)]\frac{1}{A}\int \chi(\rho-\rho')\,\Delta(\rho', z)\,d\rho';$$
$$\Delta(\rho, z) = \sum_{p,\,q}\exp\left[i\left(\mathbf{b}_{pq}\rho - \pi N_{pq}\frac{2z}{z_0}\right)\right], \qquad (13)$$

inasmuch as $\Psi_{pq} = A^{-1}\int \chi(\rho')\exp(-i\mathbf{b}_{pq}\rho')d\rho'$. Here $\chi(\rho)$ denotes the field distribution with respect to area constructed on the basis vectors $\mathbf{a}_1$ and $\mathbf{a}_2$ by which integration is carried out, and the area of which is equal to A; $d\rho'$ is an element of the area. The second of the expressions in (9) is taken into account in the expression for Δ.

For $2z/z_0 = \sigma/\tau$ (including $\tau = 1$) the expression for Δ can be converted, introducing renormalization of the indices: $p = u\tau + j$; $q = v\tau + s$, where u, v are integers; j, s = 0, 1, 2, ..., $\tau - 1$. Then $\mathbf{b}_{pq} = \tau\mathbf{b}_{uv} + \mathbf{b}_{js}$; $\sigma N_{pq}/\tau = \sigma\tau N_{uv} + \sigma N_{js}/\tau + \sigma g_2 h_1(vj+us) + 2\sigma g_1(ujh_1 + vsh_2)$. The last term of the second equality has no effect on the value of the exponent in view of its evenness. If the next to the last term of this equality is even, then in the expression for Δ summation with respect to u, v and j, s is separated:

$$\Delta\left(\rho, \frac{\sigma}{\tau}\frac{z_0}{2}\right) = C\sum_{u,\,v}\exp[i(-\pi\sigma\tau N_{uv})]\exp(i\tau\mathbf{b}_{uv}\rho), \qquad (14)$$

where

$$C = \sum_{j,\,s=0}^{\tau-1}\exp\left[i\left(-\pi\frac{\sigma}{\tau}N_{js}\right)\right]\exp(i\mathbf{b}_{js}\rho).$$

Thus, the appearance of a sharp grid image in the cross sections $z = \sigma z_0/2\tau$ is the result of evenness of the product of the integers $\sigma g_2 h_1$, and the multiplication phenomenon, that is, τ-fold multiplication of the number of elements per period of the initial grid, is a result of the new spatial frequency τb_{uv}.

For calculation of the shift effect, the sum (14) is reduced to a grid-forming function -- the two-dimensional sum of δ-functions of the type $\sum_{pq}\delta(\rho - \mathbf{a}_{pq})$. This is possible, for the first co-factor under the summation sign is represented in the form

$$\exp(-i\pi\sigma\tau N_{uv}) = \exp[-i\pi g_1\sigma\tau(\pm uh_1 \pm vh_2)] = \exp[-i\tau\mathbf{b}_{uv}(\pm F_1\mathbf{e}_1 \pm F_2\mathbf{e}_2)],$$

where $F_i = 0$ for even and 1/2 for odd $\sigma\tau g_1 h_1$; $\mathbf{e}_i = \mathbf{a}_i/\tau$; and any combination of signs is admissible. The validity of this notion follows from evenness of $\sigma g_2 h_1$,

the equality $a_i b_j = 2\pi\delta_{ij}$ and independence of the value of $\exp[i(\pm\pi n^m)]$ with respect to m for integral $m > 0$ and n. Introducing the notation $\rho_0 = \pm F_1 e_1 \pm F_2 e_2$, let us transform equality (14) to the form

$$\Delta = C \sum_{u,\,v} \exp\left(i\tau b_{uv}(\rho - \rho_0)\right] = C \frac{A}{\tau^2} \sum_{l,\,m} \delta(\rho - \rho_0 - e_{lm}),$$

where $e_{\ell m} = \ell e_1 + m e_2$. Substituting this expression in (13) and performing the integration, we finally obtain

$$\psi\left(\rho, \frac{\sigma}{\tau}\frac{z_0}{2}, t\right) = \exp\left[i\left(k\frac{\sigma}{\tau}\frac{z_0}{2} - \omega t\right)\right] \sum_{l,\,m} C_{lm}\chi(\rho - \rho_0 - e_{lm}),$$

where

$$C_{lm} = \tau^{-2} \sum_{j,\,s=0}^{\tau-1} \exp i\left\{-\frac{\pi}{\tau}\left[\sigma N j_s - 2(lj + ms) + 2(F_1 j + F_2 s)\right]\right\}.$$

From the formula obtained it follows that the number of cells in the image per period of the initial grid increases by τ times, the size and distribution of the field with respect to the cell exactly correspond to the original, and the phase is determined by the coefficient $C_{\ell m}$. For odd $g_1\sigma\tau$ the image is shifted so that the original cells are projected between the image cells with respect to the basis vector for which h is odd. Let us note that the shift vector ρ_0 is defined with accuracy to signs, and therefore it only determines the mutual arrangement of the grid cells of the original and image.

5. Selfimaging fields permit descriptive geometric interpretation. Thus, from the requirement that the field (1) selfimage with a period r_0 in space:

$$\psi(r, t) = \psi(r + n r_0, t),\ n \text{ is an integer},$$

we obtain the condition which the wave vectors of the selfimaging fields must satisfy:

$$k r_0 = 2\pi l,\quad l \text{ is an integer}. \tag{15}$$

In the space of the wave vectors this equation gives a family of equidistant planes (k-planes) perpendicular to r_0 (Figure 1, a) which are a hodograph of the vectors k of the fields that self image with a period r_0 in space. Equation (15) is vector notation for one formula of the Fabry-Perot etalon, the distance between the mirrors in which is equal to the selfimaging halfperiod.

The hodograph of the wave vectors of selfimaging monochromatic fields is obtained by supplementing expression (15) by the equation of a sphere $|k| = \text{const}$. It is a family of circles (Figure 1, b) in the k-planes with radii κ_ℓ. These circles appear in the interferogram of the Fabry-Perot etalon on excitation of it by external diffuse monochromatic radiation.

6. The fields of the natural vibrations in a flat resonator with unlimited mirrors are a special case of selfimaging fields (2). For proof of this let us represent the general solution of the wave equation for fields in a resonator in the form of

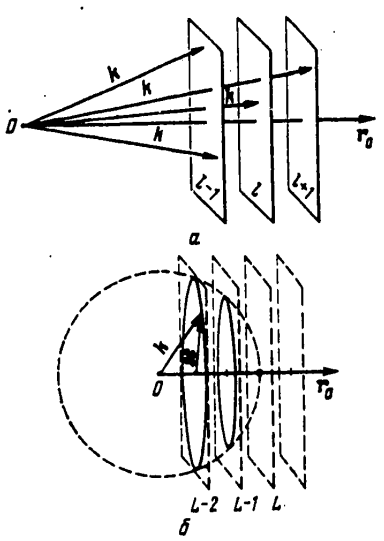

Figure 1. Hodographs of wave vectors of nonmonochromatic (a) and monochromatic (b) selfimaging fields.

superposition of two systems of waves (1) transforming into each other on reflection:

$$\psi(\mathbf{r}, t) = \frac{1}{2i}\int \{\Psi(\mathbf{k}) \exp[i(\mathbf{kr} - \omega t)] + \\ + \Psi'(\mathbf{k}') \exp[i(\mathbf{k}'\mathbf{r} - \omega t)]\} d\mathbf{k}. \tag{16}$$

Considering the mirrors to be ideally reflecting (ψ = 0 for z = 0 and d), we arrive at the following conditions:

$$\Psi(\mathbf{k}) = -\Psi'(\mathbf{k}'), \quad k_x = k'_x, \quad k_y = k'_y, \quad k_z = -k'_z = \pi l/d,$$

where d is the length of the resonator. From the last condition it follows directly that the components k_z and k'_z of the wave vectors assume the same discrete values which they assume in the case of selfimaging fields with selfimaging period equal to twice the resonator length. The boundary conditions lead to the appearance of standing waves along the resonator axis -- expression (16) assumes the form

$$\psi(x, y, z, t) = \sum_{l=0}^{\infty} \sin\frac{\pi l z}{d} \int_{-\infty}^{\infty}\int \Psi_l(k_x, k_y) \exp[i(k_x x + k_y y - \omega_l t)] \times \\ \times dk_x dk_y, \tag{17}$$

at the same time as the terms k_x, k_y remain arbitrary.

Monochromatic fields (3) and (5) also form standing waves with respect to the z-axis under appropriate conditions with respect to the remaining measurements:

$$\psi=\exp(-i\omega t)\sin(\pi lz/d)I_m(\varkappa_l r)\cos m\varphi;$$
$$\psi=\exp(-i\omega t)\sin(\pi lz/d)\cos k_x\cos k_y y,$$

corresponding to the natural vibrations in a flat resonator with circular and rectangular mirrors [15].

Standing waves in the transverse cross section of the resonator are set up for any frequency when mirror reflection from the aperture diaphragms or edges of the mirrors occurs for this frequency. In strict resonator theory [15] it is demonstrated that such reflection will be observed for entirely defined waves if the diaphragms have a sharp boundary. Obviously this fact is realized in the microwave band. In the optical band, as a rule, no special requirements are imposed on the aperture diaphragms; therefore in practice the boundary has roughness exceeding hundreds of wavelengths. In addition, the lateral surface of the active medium usually does not correspond to the requirements imposed on optical surfaces, and frequently it is deliberately frosted or etched, and it is also placed in an immersion oil (for example, in the case of neodymium-doped glass lasers). These facts lead to the appearance of an incoherent diffuse background in the system instead of mirror reflection from the lateral surfaces and diaphragms. Therefore it is natural to assume that in optical resonators, if special measures are not taken, the fields are free in the transverse cross section, that is, k_x, k_y assume continuous values. However, the values k_x, k_y have an upper bound in the active resonator of finite aperture. This is explained by the fact that as a result of dependence of the losses on the angle of inclination of the waves to the resonator axis, waves with larger k_x, k_y do not reach the lasing threshold.

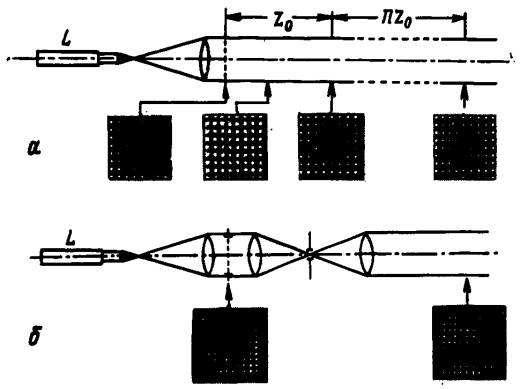

Figure 2. Systems for obtaining monochromatic fields that are selfimaging in space; a -- without spatial filtration; b -- with additional spatial filtration.

Experiments with neodymium-doped glass lasers having angular aperture of 0.14 and Fresnel number greater than 10^3 demonstrated that in the free-running mode the amplitudes of the waves, the transverse wave numbers of which satisfy the inequality

$$\sqrt{k_x^2+k_y^2}\ll\frac{D}{2d}k, \tag{18}$$

where D is the aperture diameter, are nonzero. This means that there no essentially distorted waves in the system. Therefore it is possible to propose that in resonators the geometric dimensions of which are many orders greater than the wavelength, and the Fresnel numbers exceed one by several orders, far from the open edges of the system (distortions are compensated at the edges), the fields will not differ significantly from the fields described by formula (17). Here it is possible to consider that $\Psi_\ell(k_x, k_y)$ are nonzero only for the values of k_x, k_y which satisfy the inequality (18). Of course, the aperture and transverse wave number restrictions are related to each other, but on excitation of many vibrations the angular divergence of the emission is determined by the ratio $\sqrt{k_x^2 + k_y^2}/k$ at the same time as the angular directionality of each vibration is defined by the ratio λ/D.

7. An experimental study of the properties of selfimaging fields was performed on monochromatic fields of translational symmetry in the XY plane. Such fields were formed during diffraction of a plane monochromatic wave on periodic amplitude transparencies (gratings) of three types: square, rectangular and hexagonal. The purpose of the experiments was to check the theoretical conclusions with respect to the properties of selfimaging fields in the planes of the expansion of the elements and a qualitative study of the behavior of the fields with limited aperture of the transparency simulating resonator fields with N = 100.

In the experiments an LG-55, basic-mode He-Ne laser (L) and a beam diverger based on the AKT-400 telescope (Figure 2, a) were used. An amplitude transparency was placed in a collimated beam. A recording of the fields directly on photographic film was placed behind the transparency. The light diameter was about 20 mm.

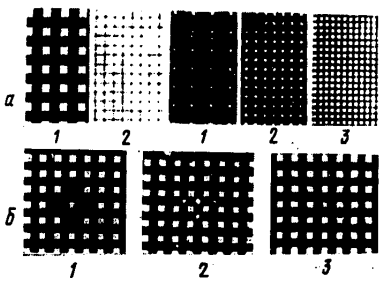

Figure 3. Properties of selfimaging fields of translational symmetry in intermediate cross sections: a -- in the element multiplication planes (1 -- initial fields, 2, 3 -- reconstructed for $\tau = 2$ and 3, respectively); b -- in the shift planes of the reconstructed fields with respect to the initial fields (1 -- fragment of the grid with local defect, 2 -- reconstructed image with shift (central lobe of an isolated element of the grid is projected between image elements; $\sigma = \tau = 1$); 3 -- image without shift ($\sigma = 2$, $\tau = 1$)).

On a square grid ($a_1 = a_2 = a$, $h_1 = h_2 = 1$, $g_1 = 1$, $g_2 = 0$, $f = 1$, $z_0 = 2a^2/\lambda$) with period 1 mm and porosity 20 the formula for the position of the multiplication planes was checked which, in the given case ($\sigma g_2 h_1 = 0$, that is even) assume the form $z = \sigma z_0/2\tau = \sigma a^2/\lambda\tau$. The even grid images in which the number of elements in the initial period reached 12 were recorded. These values of z were realized with high

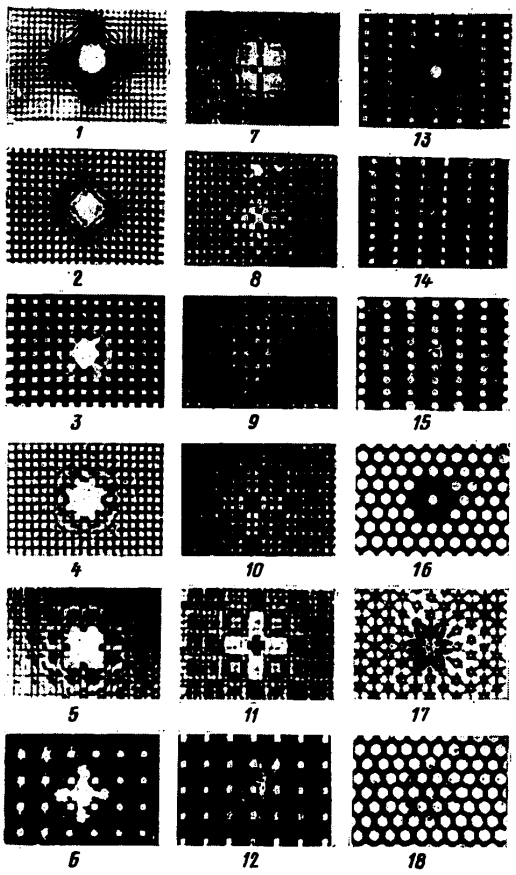

Figure 4. Field reconstruction behind square, rectangular and hexagonal amplitude transparencies: 1-12 — successive images of fields behind a square transparency with porosity 4 at distances $z = \sigma z_0/2\tau$, where σ/τ = 1/4, 1/3, 1/2, 2/3, 3/4, 1, 5/4, 4/3, 3/2, 5/3, 7/4 and 2, respectively (images 2, 6 and 10 have shifts); 13-15 — field behind a rectangular transparency; 13 -- fragment of a transparency with local defect, 14 -- field at a distance $z = z_0/2$ (for $\sigma = \tau = 1$) is shifted horizontally, 15 -- field at a distance z_0 ($\sigma = 2$, $\tau = 1$), shift absence; 16-18 -- field behind a hexagonal transparency; 16 -- fragment of transparency with local defect, 17 -- field for $\sigma = \tau = 1$, image not formed, 18 -- field for $\sigma = 2$, $\tau = 1$, image formed and not shifted.

precision. Preservation of the shape of the cells for $\tau = 2$ and 3 was checked on transparencies of the same type (square grids having porosity 2 and 4 and square cells). Considering the limited aperture and nonuniformity of exposure of the transparency, reconstruction turned out to be satisfactory (Figure 3, a).

In order to check the shift of the reconstructed image with respect to the original, transparencies with local defects were used. These defects were obtained by isolation of one of the grid elements by increasing its diameter or shading out adjacent

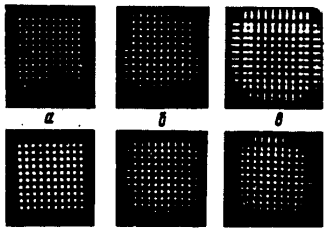

Figure 5. Limited-aperture field reconstruction; a — initial fields; b, c -- fields at distances $z_0/2$ (b) and z_0 (c); upper row — fields behind a transparency without spatial filtration, lower row — with additional spatial filtration.

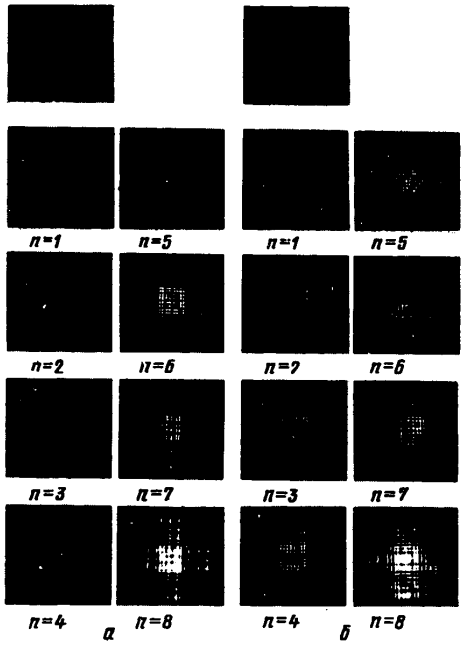

Figure 6. Limited aperture field reconstruction at distances of $nz_0/2$ (n is indicated): a -- behind a transparency without spatial filtration; b -- with spatial filtration; initial fields presented above.

ones or by both methods simultaneously. This made it possible to have the mark of the position of the original cell (the origin of the coordinates) in the reconstruction planes. For a square grid the shift vector acquires the form $\rho_0 = f(\pm e_1 \pm e_2)$, where e_1 and e_2 are mod equal and orthogonal to each other. If the product $\sigma\tau$ is odd, the reconstructed image will be shifted by e/2 in both directions, and the elements of the original in the projection turn out to be between the image elements (2 in Figure 3, b). For $\sigma = 2$, $\tau = 1$, the shift is absent (3 in Figure 3, b). The image shift was also checked on a square grid with porosity 4. In this case the

shift was observed for $\sigma = 1, 3, 5, 7$ and $\tau = 1, 3$ (Figure 4). The dependence of the shift on the parameters h was checked in the experiments with rectangular grid ($h_1 = 1$ and $h_2 = 4$). In this case only the term F_1 was nonzero for $\sigma\tau$ odd; therefore the shift vector assumed the form $\rho_0 = \pm F_1 e_1$ and the shifts could be expected only with respect to e_1. Accordingly, for $\sigma = \tau = 1$ the shift with respect to the indicated direction was recorded experimentally; it was absent for $\sigma = 2$, $\tau = 1$ (see Figure 4).

Another conclusion was checked indicating that the image is formed only in the case where $\sigma g_2 h_1$ is even. For a hexagonal transparency ($a_1 = a_2 = a$, $h_1 = h_2 = 1$, $g_1 = g_2 = 1$, $f = 1$) the value coincides with σ. Figure 4 shows a fragment of a hexagonal transparency with local defect (16), the field for $\sigma = \tau = 1$, where the grid image is not formed (17), and for $\sigma = 2$, $\tau = 1$, when it is formed (18). Inasmuch as the images are observed for even σ, they are never shifted.

Simulation of the resonator fields with Fresnel number equal to 100 was carried out both by irising the transparency to dimensions of 10 × 10 elements and by successive spatial filtration by the scheme depicted in Figure 2, b. As a result of this filtration only the low-frequency spatial harmonics (small k_x, k_y) participated in the formation of the image. The experiments demonstrated that at distances $z \ll Da/\lambda$ the reconstructed fields satisfactorily repeat the initial ones (Figure 5). As the spacing increases, the spatial harmonics diverge, and the image is destroyed (Figure 6). In the first case (without spatial filtration) this takes place for smaller z, for the high-frequency spatial harmonics leave the region of formation of the image faster.

In conclusion, the author considers it his duty to express sincere appreciation to L. A. Vaynshteyn for invaluable support, great assistance and valuable suggestions.

BIBLIOGRAPHY

1. H. F.Talbot, PHIL. MAG., No 9, 1836, p 401.

2. Lord Rayleigh , PHIL MAG., No 11, 1881, p 196.

3. J. M. Cowley, A. F. Moodie, PROC. PHYS. SOC. (LONDON, B70, 1957, pp 486, 497, 505.

4. V. V. Mumladze, N. M. Ramishvili, V. V. Chavchanidze, SOOBSHCHENIYA AN GSSR (Reports of the Georgian SSR Academy of Sciences), No 58, 1970, p 537.

5. J. T. Winthrop, C. R. Worthington, J. OPT. SOC. AMER., No 55, 1965, p 373.

6. R. F. Edgar, OPTICA ACTA, No 16, 1969, p 281.

7. W. D. Montgomery, J. OPT. SOC. AMER., No 57, 1967, p 772.

8. Yu. M. Denisyuk, N. M. Ramishvili, V. V. Chavchanidze, OPT. I SPEKTR. (Optics and Spectroscopy), No 30, 1971, p 1130.

9. A. P. Smirnov, OPT. I SPEKTR., No 43, 1977, p 755.

10. L. A. Rivlin, V. S. Shil'dyayev, IZV. VYZOV. SER. RADIOFIZIKA (News of the Institutions of Higher Learning, Radiophysics Series), No 11, 1968, p 572.

11. Ye. Ye. Grigor'yev, A. T. Semenov, KVANTOVAYA ELEKTRONIKA (Quantum Electronics), No 5, 1978, p 1877.

12. V. K. Ablekov, V. S. Belyayev, ZHPS (Journal of Applied Spectroscopy), No 23, 1975, p 1110.

13. G. Ya. Lyubarskiy, TEORIYA GRUPP I YEYE PRIMENENIYE V FIZIKE (Group Theory and Its Application in Physics), Moscow, Fizmatgiz, 1958.

14. A. T. Semenov, V. S. Shil'dyayev, KVANTOVAYA ELEKTRONIKA, No 3, 1971, p 42.

15. L. A. Vaynshteyn, OTKRYTYYE REZONATORY I OTKRYTYYE VOLNOVODY (Open Resonators and Open Wave Guides), Moscow, Sov. radio, 1966.

10,845
CSO: 1862/220

PLASMA PHYSICS

UDC 533.9.082

HIGH-TEMPERATURE PLASMA DIAGNOSIS METHODS

Moscow METODY DIAGNOSTIKI VYSOKOTEMPERATURNOY PLAZMY in Russian 1980 (signed to press 26 Sep 80) pp 2-5, 200

[Annotation, preface and table of contents from book "High-Temperature Plasma Diagnosis Methods", by Edgard Ivanovich Kuznetsov and Dzholinard Andreyevich Shcheglov, Atomizdat, 1450 copies, 200 pages]

[Text] Some questions associated with non-contact methods of plasma diagnosis are considered. Problems of measuring the main parameters of a high-temperature plasma are analyzed from the standpoint of choosing optimum arrangements of an experiment. Particular emphasis is given to questions of getting the spatial distributions of plasma parameters from integral measurements and measurements of local characteristics. Methods are outlined for studying electric and magnetic fields in plasma. The material and energy balance of plasma is investigated, as well as the influence of impurities and wall processes on plasma behavior (first edition published in 1974). This edition also examines methods of diagnosis used in present-day fusion facilities, including systems for automating diagnostic measurements.

For specialists engaged in the study of high-temperature plasma physics and development of methods for diagnosing high-temperature plasma, as well as those working in related fields. May be used by undergraduate and graduate stuents in physics and engineering physics departments.

Tables 2, Figures 54, references 381.

Preface

Among numerous scientific and engineering problems, one of the most important is the job of achieving controlled nuclear fusion, getting at the enormous reserves of surplus energy stored in the nuclei of light elements that are widely distributed in nature. The paths being taken toward solution of this problem are so intimately related to the main directions of development of plasma physics that research in this field is practically inseparable from the problem of utilizaing the new nuclear fuel--high-temperature plasma of light elements. Present-day experimental fusion facilities have already given us plasma with parameters close to those necessary for power utilization of the thermonuclear reactions that occur in high-temperature plasma. This means that the researcher must deal with plasma heated to tens of

millions of degrees. It is quite natural that there has been an increase in the role of non-contact methods of diagnosis in studies of hot plasma, and that contrariwise some classical methods, such as probe methods, have lost their former significance. Under such conditions many methods of diagnosis that had formerly been of only procedural importance have become basic in measurement of high-temperature plasma parameters. Besides, previously known methods are being perfected, and measurement methods are being borrowed from related branches of physics such as astrophysics and nuclear physics. Finally, new areas are springing up in diagnosis of hot plasma such as the use of laser scattering.

In preparing the new edition of the book, materials were selected and analyzed that supplemented the previously appearing Russian translations of widely known monographs on plasma diagnosis [Ref. 68, 105]. Various procedural problems of high-temperature plasma diagnosis, ideas and suggestions for developing new diagnoses, physical principles of promising but inadequately used methods of measurements--it was with this approximate class of problmes that the reader could become acquainted when the first edition of this book was published in 1974.

The last decade has been a period of intense development of fusion research. There has been an expansion of the range of physical problems with which the experimenter must deal, a considerable rise in the cost of physical facilities, an increase in requirements for accuracy and reliability of measurement results, as well as for the volume of information obtained in a single working cycle. An important place goes to research on designing and building larger, and of course more expensive facilities of the next generation. Designs of such facilities are being developed on the basis of the goals of planned experiments, and in this connection certain requirements arise with respect to the configuration of fittings, placement of equipment, the lines necessary for operation of the diagnosis and so on. From this example alone we can see that the circle of specialists directly or indirectly involved in the problem of high-temperature plasma diagnosis has widened considerably. This is due not only to an increase in the number of methods used, but also to the involvement of specialists in electronics, automation of data gathering and processing, designers, specialists in vacuum technology, in the effects of radiation on structural elements of devices and so on.

In connection with what we have just said, the necessity has arisen for a rather radical change in the structure and thrust of the book, while retaining a certain part of the actual material contained in the first edition. Although this is neither a textbook nor a manual, the authors have decided to include in the first (introductory) chapter a brief overview of diagnostic methods used for measuring the main parameters of high-temperature plasma, with an indication of the parts of the book in which consideration is given to questions relating to the use of specific diagnostic techniques and interpretation of resultant data.

Another distinguishing feature of the book is that the authors have tried to make the presentation of the physical principles of the investigated methods less complicated but more graphic than in the first edition. Considerable attention has been given to the practical consequences stemming from the physical peculiarities of specific diagnoses, and especially to the requirements for placement and interfacing of equipment with the facility, for the design of the facility itself, for factors that dictate restrictions in the use of a given diagnosis and so on.

And finally, a basic feature of the earlier edition, examination of new trends in the development of high-temperature plasma diagnosis and procedural methods, has to a certain extent found reflection in the selection of materials for the second edition. Distribution of materials by chapters has been altered; a brief explanation of the content of individual chapters and the logical relation among them will be found in the first chapter.

Although plasma diagnosis has developed quite rapidly, and surveys at the time of their publication reflect the state of the art several years previously, the authors hope that the book will be of use to those directly involved in studying the physics of high-temperature plasma, or who want to get an idea of the typical problems being solved by methods of hot plasma diagnosis.

Contents page

6610
CSO: 1862/27

MATHEMATICS

UDC 681.015.24

METHOD OF COLLECTIVE RECOGNITION

Moscow METOD KOLLEKTIVNOGO RASPOZNAVIANIYA in Russian 1981 (signed to press 4 Jun 81) pp 2-3, 67-71, 79

[Annotation, preface, conclusion and table of contents from book "Method of Collective Recognition", by Leonard Andreyevich Rastrigin and Roman Khononovich Erenshteyn, Energoizdat, 8500 copies, 80 pages]

[Text] The book examines questions of constructing hierarchical recognition systems. A qualitatively new approach is proposed that yields a whole class of algorithms simulating the process of decision making by a collective. Consideration is given to processes of instructing such a collective, and synthesizing the optimum collective of linear recognition algorithms. Some model problems are solved. The proposed approach is realized for synthesizing the decision of a collective of experts.

For specialists in automatic control theory dealing with problems of pattern recognition as well as undergraduate and graduate students in appropriate fields.

Preface

The enticement (and charm) of the problem of pattern recognition is in its simplicity. Upon first acquaintance with this problem, the researcher is readily drawn into using familiar resources for handling the solution, and sometimes gets a satisfactory result, but more often is in for unpleasant surprises. And only after he has thoroughly analyzed his own specific problem can he manage to solve it. As a rule, the problem of recognition requires an informal approach for solution.

What methods have not been used for solving the recognition problem! Probabilistic methods of regressional and correlational analysis, a variety of approximational approaches involving construction of a hypersurface that separates patterns, a number of set-theory techniques utilizing the apparatus of logic algebra, topological approaches and the like. There is no need to continue this list of the numerous methods of solving the recognition problem, especially as the authors of this book have taken another tack. Rather than inventing a new approach, they have only suggested a method of using approaches that are already known. A wide appeal has been made to analogy with methods of collective decision so effectively used in society. As a result, the authors have, willingly or not, come up with a new method of classification that moves the decision-making problem a level up, i. e. a method is indicated that will be used to decide whether a given situation belongs

to a class. However, the methods themselves are given a priori, and they form a collective whose effectiveness is practically always considerably higher than any of its members.

The collective concept presented in this book can be used in other problems as well, but the recognition problem for which it was originally proposed is the clearest subject for its application.

The authors will be grateful for any comments or suggestions relating to the book.

The authors thank Professor N. A. Andreyev and A. F. Ab for discussing material presented in chapters 4 and 3 respectively.

The authors express sincere gratitude to N. G. Zagoruyko, V. I. Vasil'yev, Ya. A. Gel'fandbeyn, Sh. Yu. Raudis, V. Ye. Golender and B. Y. Kavalerchuk for attentively reading the manuscript and making a number of useful comments that were taken into consideration in the final book, and reviewer V. N. Vapnik, whose advice the authors have done their best to follow. The authors are deeply grateful to E. M. Braverman, now deceased, who suggested writing this book.

The authors

Conclusion

The algorithm that has been considered in this book is an effective pattern recognition algorithm, and therefore it should be correlated with other known methods of recognition. Let us consider how this and other recognition algorithms fit into the general scheme of collective decision making.

Let us begin with such widely used algorithms as those based on the theory of statistical solutions [Ref. 15, 77], local methods [Ref. 15, 53], correlation methods [Ref. 41, 42, 53] and so on. These methods are traditional, and are based on using some sequence of situations (teaching sequence) to find a resolving rule that does not change in the process of arrival of control situations. In the proposed scheme, shown in the figure, a situation of this kind corresponds to the lowest level, where the collective is degenerate, i. e. it consists of only one member, and the weight of this single member of the collective is fixed as a result of teaching.

The next class of algorithms is those in which the weights of the resolving rules--members of the collective--are also fixed, but the number of rules in the collective is greater than unity. Perceptron recognition algorithms [Ref. 3, 47, 55] belong chiefly to this class. Teaching of the simplest perceptron involves adjustment of the weights of A-elements. Each A-element is easily interpreted as an independent resolving rule--collective member. The distinguishing feature of this rule is that it works in some subspace of the initial space of descriptions. The nature of this subspace (its component features) is determined by the relations between elements of the meshwork and the inputs of the given A-element. The decision that we get at the output of the perceptron can be interpreted in turn as the weighted mean decision of a collective consisting of A-elements. The method of potential functions [Ref. 3] is also close to algorithms of perceptron type.

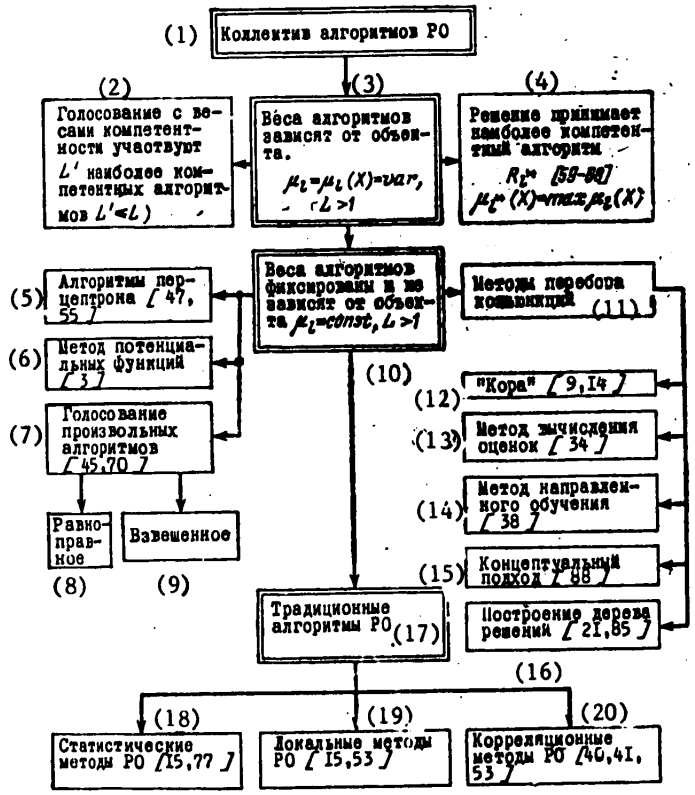

Diagram of generalization of pattern recognition algorithms

KEY:

1--Collective of pattern recognition algorithms
2--Voting with competence weights by the L' most competent algorithms ($L' \leqslant L$)
3--Weights of algorithms depend on the object $\mu_l = \mu_l(X) = var$, $L > 1$
4--Decision made by most competent algorithm R_l^* [Ref. 59-68], $\mu_l^*(X) = \max_l \mu_l(X)$
5--Perceptron algorithms [Ref. 47, 55]
6--Potential function method [Ref. 3]
7--Voting by arbitrary algorithms [Ref. 45, 70]
8--equal
9--weighted
10--weight of algorithms fixed and independent of object, $\mu_l = const$, $L > 1$
11--Conjunction sorting methods
12--"Cortex" [Ref. 9, 14]
13--Estimate calculation method [Ref. 34]
14--Directed teaching method [Ref. 38]
15--Conceptual approach [Ref. 88]
16--Constructing a tree of decisions [Ref. 21, 85]
17--Traditional pattern recognition algorithms
18--Statistical pattern recognition methods
19--Local pattern recognition methods
20--Correlational pattern recognition methods

Attempts have been made to combine several recognition algorithms [Ref. 45, 70]. In this research, like in the perceptron, the solution has been formulated as the weighted mean value of decisions of the algorithms being combined. It should only be noted that in this case the algorithms being combined may also differ in principle, and not just in the type of subspace, as occurs in the perceptron.

In the sense of combining algorithms of the same type, but functioning in different subspaces, still closer to the perceptron is the approach considered by Bongard [Ref. 9]. This approach has engendered a variety of algorithms distinguished essentially by methods of sorting conjunctions [Ref. 9, 14, 21, 25, 32-34, 38, 81, 88], but fitting approximately into the same scheme. Analysis of this class of algorithms should start from the "Cortex" algorithm [Ref. 9, 14]. M. M. Bongard suggested the concept that solution of the problem of pattern recognition should be sought among possible logic functions of the characteristics of description of objects. It can be easily noted that the perceptron also realizes this idea: each A-element is a certain logic function of variables that are connected to the inputs of this A-element. The "cortex" algorithm is based on search for each class of features that are possessed by objects of one class and are not possessed by a single object of another class (or are possessed by a sufficiently small number of objects of this class). The features of the class are conjunctions made up of characteristics of the initial description. In recognition, the number of conjunctions is computed--the features of each class that take on a unit value on a control object. The object is put into the class for which this number is the largest.

Thus, in this algorithm as well we encounter an averaging or voting procedure. Each conjunction can be easily interpreted as an independent resolving rule, and therefore the algorithm fits into the general scheme of the collective of resolving algorithms depicted in Fig. 2 of Chapter 1. The weights of the resolving rules--conjunctions--may be unitary; then we have equal voting. Or they may be determined by a variety of procedures [Ref. 9, 25], in which case we have weighted voting. However, in either event the weights of the conjunctions--resolving rules--are fixed and cannot be changed from one control situation to the next.

Among the various modifications of the method of sorting conjunctions, particular notice should be taken of so-called estimate calculation methods proposed by Yu. I. Zhuravlev. In these methods, an attempt is made to truncate complete sorting [Ref. 34]. We will show that this method as well can be put into the class of collective resolving rules.

On the entire set of features, reference or voting sets are assigned [Ref. 34]--the projections onto subsets selected in a certain way. These projections can be interpreted as individual resolving rules. The control object is projected onto each reference set and is compared with the projections of objects of the teaching sequence. Then the number of coincident projections is computed for both classes to be recognized in each of the reference sets. The number of votes is added, and the object is put into the class that gets the greatest number of votes. The weight of each reference set can be considered as well, in which event the voting becomes weighted.

The directed teaching method proposed by P. Ye. Kunin [Ref. 38] is close to the methods of estimate calculation [Ref. 34] and the "Cortex" algorithm [Ref. 9, 14].

In this algorithm, the resolving rule is induced by the control object. This means that the resolving rule is directionally generated relative to each new object. The only relationships considered are those between the features that are there in the control object. If a conjunction sorting method is used, only those conjunctions that take on unitary values on the control object are sought as the features of each class. Then the decision is likewise made by voting.

The last group of methods that can be put into collective decision-making procedures includes methods of concept formation. These techniques are extensively used in recognition [Ref. 21, 85, 88]. In essence, both the "Cortex" algorithm and the methods of estimate calculation can be put into this class. A survey of methods of concept formation is given in Ref. 21. Special algorithms of concept formation are V. V. Chavchanidze's conceptual method [Ref. 88], and methods based on constructing a tree of decisions [Ref. 21, 88]. In these methods, each control object has its own corresponding path on the tree of decisions. This path is induced by the presence or absence of some feature in the given object. It terminates at a certain vertex that is put into correspondence with the index of one of the classes to be recognized. A path on the tree of decisions can also be readily interpreted as some conjunction of variables and their negations. In the "Cortex" algorithm, the decision is determined in the process of voting between conjunctions, whereas in this approach the decision is completely determined by one conjunction, the weight as a resolving rule being fixed a priori. In the conceptual approach, the decision is determined by the object having some concept that is defined as an aggregate of features, which may be both qualitative and quantitative in the general case. In the latter two methods, the collective decision is determined by the resolution of one of the rules--conjunction or concept--although the choice is made only with respect to values of a feature in the control object, and not by the qualitative characteristics of the rule that is chosen. This completes analysis of the second level of the diagram.

In considering methods based on the ideas of the perceptron and methods of conjunction sorting, it has already been pointed out that in this case the member of a collective is a rule defined either as an A-element connected with a number of features, or as a conjunction of several features. In other words, the nature of the rules themselves does not change; it is only the subspace in which these rules operate that changes. It turns out that if the approach proposed in this book is applied to rules of this kind, we can get efficient and fairly simple recognition systems.

In the diagram, a place on the upper level is given to the approach proposed in our book. This is the case where the weights of the algorithms--members of the collective--vary depending on the specific control situation, and are interpreted as coefficients of competence of the algorithms. On this level, we can consider two cases: The simplest case where the decision of the collective is determined by the decision of the rule with maximum competence coefficient for the given object, and the general case where the rules vote with competence weights for decision making. In such voting, all the resolving rules--members of the collective--may take part, or only the first L' most competent rules. In the second case, we can define some most competent coalition, specifically one that is made up of only a single rule.

The approach considered in this book applies not only to the problem of pattern recognition. Actually, in typical problems of behavioral synthesis, choice of an optimum solution, designation of the best plan and so forth, the difficulty as a rule is in selecting the algorithm for solution of the problem that is best in some sense among the available choice of algorithms. The invention of a new algorithm in this situation is inadvisable, and in any case is not economical.

Living organisms have learned to handle this job effectively, and in standard situations they construct behavior by combining algorithms already known to them.

Let us consider the following quite prevalent situation. Let there be some (finite or infinite) set of problems of the same type $\{X_i\}$, $i = 1, 2, \ldots, I$. These problems are coded by n parameters $x_1, x_2, \ldots, x_n$ so that each problem in space Ω^n is represented by point $X_i = (x_1, x_2, \ldots, x_n)$, and the entire set of problems forms region Ξ $X_i \in \Xi$, $i = 1, 2, \ldots$

Let there also be a finite set of algorithms $\{R\} = (R_1, R_2, \ldots, R_L)$ for solution of problems $X_i \in \Xi$. Each of these algorithms R_l, $l = 1, 2, \ldots, L$, does or does not solve problem X_i. The effectiveness of the solution is defined by some given criterion Q that puts X_i and R_l into correspondence with the number

$$q = Q(X_i, R_l), \tag{1}$$

characterizing the workability of algorithm R_l in solving problem X_i.

Let us give examples of problems of this type: 1) the problem of pattern recognition already discussed: X is the specific recognition problem, {R} is the set of recognition algorithms, such as Bayes methods, potential functions, perceptron, etc., q is the criterion of recognition efficiency; 2) the problem of determining a root, where X is the specific function whose root is to be determined, {R} is a set of algorithms for determining the root, such as methods of tangents, chords, dichotomy and so forth, and q is the number of iterations necessary for reaching the ε-neighborhood of the root; 3) the problem of search optimization, where X is the situation that arises in the process of optimzation, {R} is a set of search algorithms such as the methods of the gradient, random search, etc., and q is the average increment in the function to be optimized or the number of unsuccessful steps; 4) the problem of forecasting or extrapolation, where X is the situation whose future state is to be predicted, {R} is a set of algorithms for prediction or extrapolation, including formal and informal techniques (methods of expert estimates), and q is the relative error of prediction.

The selection of the optimum algorithm for solution of problem X thus reduces to solution of the extremum problem

$$Q(X_i, R_l) \to \underset{l = 1, \ldots, L}{\text{extr}} \Rightarrow R_{l*}, \tag{2}$$

where R_{l*} is the best of the available algorithms for solving problem X_i.

The algorithms proposed in this book in slightly modified form can be used to solve these diverse problems. The modification of the algorithm depends on the type of problem to be solved. The given approach enables solution of problem (2),

bypassing complete sorting of algorithms. Since the solution of optimization problem (2) involves a once-through solution of problem X_i, the choice of optimum algorithm in the case of complete sorting becomes meaningless as the problem has already been solved.

As already stated, living organisms handle problem (2) fairly well. Therefore the given approach can be used as a model for understainding processes of behavioral selection of organisms in standard situations. In this case, the course of study is obvious: it is necessary to describe the space of problems Ω^n to be solved by the organism, to distinguish a set of problems Ξ and a set of algorithms of behavior {R}, and then by observing behavior in different situations, i. e. in the solution of problems of set Ξ, to isolate the region of competence of each behavioral algorithm R_l. If these regions do not intersect, there is every reason to assume thqt the living organism realizes the algorithm described above in selecting behavior.

To go one step farther, the idea of a collective of algorithms in the social world long ago found application in the concept of division of labor. There is no doubt as to the optimality of this kind of organization. The authors hope that they have successfully defended the idea of the collective in the non-social world as well, and specifically in handling pattern recognition problems.

Contents page

6610
CSO: 1862/22

- END -